

VANADIUM-REDOX FLOW AND LITHIUM-ION BATTERY
MODELLING AND PERFORMANCE IN WIND ENERGY
APPLICATIONS

By

John A. Chahwan

B.Eng. (McGill University, Montreal, Quebec)

Thesis submitted to the McGill University Department of Electrical and Computer
Engineering in partial fulfillment of the requirements of the degree of Master in
Engineering

Department of Electrical and Computer Engineering,

McGill University,

Montréal, Québec, Canada

May 2007

© John A. Chahwan, 2007



Library and
Archives Canada

Published Heritage
Branch

395 Wellington Street
Ottawa ON K1A 0N4
Canada

Bibliothèque et
Archives Canada

Direction du
Patrimoine de l'édition

395, rue Wellington
Ottawa ON K1A 0N4
Canada

Your file *Votre référence*
ISBN: 978-0-494-38480-0
Our file *Notre référence*
ISBN: 978-0-494-38480-0

NOTICE:

The author has granted a non-exclusive license allowing Library and Archives Canada to reproduce, publish, archive, preserve, conserve, communicate to the public by telecommunication or on the Internet, loan, distribute and sell theses worldwide, for commercial or non-commercial purposes, in microform, paper, electronic and/or any other formats.

The author retains copyright ownership and moral rights in this thesis. Neither the thesis nor substantial extracts from it may be printed or otherwise reproduced without the author's permission.

AVIS:

L'auteur a accordé une licence non exclusive permettant à la Bibliothèque et Archives Canada de reproduire, publier, archiver, sauvegarder, conserver, transmettre au public par télécommunication ou par l'Internet, prêter, distribuer et vendre des thèses partout dans le monde, à des fins commerciales ou autres, sur support microforme, papier, électronique et/ou autres formats.

L'auteur conserve la propriété du droit d'auteur et des droits moraux qui protègent cette thèse. Ni la thèse ni des extraits substantiels de celle-ci ne doivent être imprimés ou autrement reproduits sans son autorisation.

In compliance with the Canadian Privacy Act some supporting forms may have been removed from this thesis.

Conformément à la loi canadienne sur la protection de la vie privée, quelques formulaires secondaires ont été enlevés de cette thèse.

While these forms may be included in the document page count, their removal does not represent any loss of content from the thesis.

Bien que ces formulaires aient inclus dans la pagination, il n'y aura aucun contenu manquant.


Canada

Abstract

As wind energy penetration levels increase, there is a growing interest in using storage devices to aid in managing the fluctuations in wind turbine output power. Vanadium-Redox batteries (VRB) and Lithium-Ion (Li-Ion) batteries are two emerging technologies which can provide power smoothing in wind energy systems. However, there is an apparent gap when it comes to the data available regarding the design, integration and operation of these batteries in wind systems. This thesis presents suitable battery electrical models which will be used to assess system performance in wind energy applications, including efficiency under various operating conditions, transfer characteristics and transient operation. A design, sizing and testing methodology for battery integration in converter based systems is presented. Recommendations for the development of operating strategies are then provided based on the obtained results.

Résumé

La récente croissance en utilisation d'énergie éolienne augmente le besoin en systèmes de stockage d'énergie pour diminuer les fluctuations de puissance produite par le vent qui est de nature variable. Les batteries Vanadium-Redox (VRB) et Lithium-Ion (Li-Ion) sont deux technologies émergentes qui peuvent être utilisées afin de réduire les fluctuations éoliennes dans la production d'énergie. Cependant, l'information disponible concernant la conception, l'implémentation et l'opération de ces types de systèmes est insuffisante. Ce rapport présente une méthodologie pour la modélisation de batteries afin de déterminer leur performance, incluant la fonction de transfert, le comportement transitoire et le rendement. De plus, une méthodologie pour la conception et l'essai de systèmes de batteries dans des systèmes d'éoliennes basés sur des convertisseurs statiques est présentée. Des recommandations qui ont trait à l'optimisation des systèmes de commande sont faites.

Acknowledgements

I would like to sincerely thank my thesis supervisor and friend Dr. Géza Joós for his guidance and support throughout my undergraduate and master's studies at McGill University. His insightful perspective on the engineering profession has helped me make the right decisions with respect to my career and studies. Under his guidance, I was able to challenge myself by setting higher objectives and fulfilling greater personal achievements, while extending my technical knowledge.

I would like to extend my thanks to Chad Abbey for his continued help and guidance throughout my research project. I would also like to thank my peers in the McGill University power engineering department including Kyriakos Gogas, Jean Morneau, Wei Li, Jose Restrepo, Xiaopeng Liu, Ping-Kwan Keung and Dr K. El Arroudi for forming a strong and friendly power engineering community, as well as always being available to help.

I would also like to thank Melanie Chamberlain and Neeraj Gupta from NRC for their appreciated contributions.

The financial support from "Le Fonds Québécois de la recherche sur la nature et les technologies" is gratefully acknowledged.

Table of Contents

CHAPTER 1	INTRODUCTION.....	1
1.1	Wind Energy Storage.....	1
1.2	Storage Research.....	2
1.2.1	<i>Types of Storage</i>	2
1.2.2	<i>Common Batteries</i>	3
1.2.3	<i>Wind Storage Research</i>	4
1.3	Battery Modelling.....	5
1.3.1	<i>Battery Performance</i>	5
1.3.2	<i>Battery Modelling Overview</i>	5
1.3.3	<i>Model Evaluation</i>	6
1.3.4	<i>Model Validation</i>	7
1.4	Existing Models.....	8
1.4.1	<i>NiH₂ Model</i>	8
1.4.2	<i>Lead Acid Model</i>	8
1.4.3	<i>Lithium-Ion Battery Models</i>	9
1.4.4	<i>VRB Models</i>	10
1.5	Research Objectives.....	12
1.5.1	<i>Problem Definition</i>	12
1.5.2	<i>Identifying the Gaps</i>	12
1.5.3	<i>Research Goals</i>	13
1.5.4	<i>Claim of Originality</i>	14
1.6	Thesis Outline.....	14
CHAPTER 2	MODEL DEVELOPMENT.....	16
2.1	Introduction.....	16
2.2	Model Requirements.....	16
2.3	VRB Model Characteristics.....	17
2.3.1	<i>Model Specifications</i>	17
2.3.2	<i>Internal Voltage and Temperature Considerations</i>	18
2.3.3	<i>R_{internal} and R_{parasitic}</i>	19
2.3.4	<i>State of Charge Modeling</i>	20

2.3.5	<i>Transient Operation</i>	20
2.4	Lithium-Ion Battery Model Characteristics	21
2.4.1	<i>Model Specifications</i>	21
2.4.2	<i>Internal Voltage and Losses</i>	22
2.4.3	<i>State of Charge Modeling</i>	23
2.4.4	<i>Transient Operation</i>	23
2.5	SIMULINK Implementation.....	24
2.6	Conclusions.....	24
CHAPTER 3 MODEL VALIDATION AND PERFORMANCE		26
3.1	Introduction.....	26
3.2	VRB Model Validation.....	26
3.2.1	<i>Static Operation</i>	26
3.2.2	<i>Dynamic Charge and Discharge Cycles</i>	28
3.2.3	<i>Energy Storage</i>	30
3.2.4	<i>VRB Model Discussion</i>	31
3.3	Li-Ion Model Validation.....	32
3.3.1	<i>Cell Voltage</i>	32
3.3.2	<i>Dynamic Charge and Discharge Cycles</i>	33
3.4	Standardized Profile for Experimental Tests	35
3.4.1	<i>Typical Wind Profile</i>	35
3.4.2	<i>Charge-Discharge Profile</i>	37
3.5	VRB Performance.....	39
3.5.1	<i>VI Transfer Characteristic</i>	39
3.5.2	<i>System Efficiency</i>	39
3.5.3	<i>Dynamic Response</i>	43
3.6	Lithium-Ion Performance.....	44
3.6.1	<i>VI Transfer Characteristic</i>	44
3.6.2	<i>System Efficiency</i>	44
3.6.3	<i>Dynamic Response</i>	47
3.7	Li-Ion and VRB Performance Comparison	47
3.8	Conclusions.....	48

CHAPTER 4	WIND ENERGY STORAGE SYSTEM DESIGN	49
4.1	Introduction.....	49
4.2	Battery Sizing.....	49
4.3	Scaling the VRB Model.....	51
4.3.1	<i>System Requirements</i>	51
4.3.2	<i>Modeling a 42 kW Industrial VRB</i>	51
4.3.3	<i>VRB Thevenin Equivalent</i>	53
4.3.4	<i>Multiple Stacks</i>	53
4.3.5	<i>252 kW VRB System</i>	55
4.4	Battery Converter Interface.....	56
4.4.1	<i>Buck-Boost dc-dc Converter</i>	56
4.4.2	<i>Inductance Design</i>	56
4.4.3	<i>Converter Controls</i>	58
4.4.4	<i>VRB dc efficiency</i>	59
4.5	Conclusions.....	61
CHAPTER 5	WIND ENERGY STORAGE SYSTEM IMPLEMENTATION	63
5.1	Introduction.....	63
5.2	Storage Schemes	63
5.3	DFIG Detailed System Model	65
5.3.1	<i>Model Operation without Storage</i>	65
5.3.2	<i>Controlling the Battery System</i>	66
5.3.3	<i>Wind System Operation</i>	68
5.4	DFIG Average System Model	71
5.4.1	<i>Operation without Storage</i>	71
5.4.2	<i>Controlling the Battery System</i>	71
5.4.3	<i>System Operation</i>	73
5.5	DFIG Simple Model for Real-Time Simulation.....	76
5.5.1	<i>Centralized storage</i>	76
5.5.2	<i>Real-Time System Implementation</i>	76
5.5.3	<i>Experimental Setup</i>	76
5.5.4	<i>Configuration and Validation of Control Systems</i>	78
5.5.5	<i>Experimental Results</i>	78

5.6	DFIG System Performance with VRB storage	83
5.6.1	<i>Battery Energy Management</i>	83
5.6.2	<i>System Overall Efficiency</i>	83
5.6.3	<i>Impact on Grid</i>	84
5.7	Conclusions	84
CHAPTER 6 CONCLUSIONS AND FUTURE WORK		86
6.1	Summary	86
6.1.1	<i>Battery Models</i>	86
6.1.2	<i>Integration into Wind Systems</i>	86
6.2	Conclusions	87
6.2.1	<i>Modelling</i>	87
6.2.2	<i>Operating Considerations</i>	88
6.2.3	<i>Design Considerations</i>	88
6.2.4	<i>A Methodology for the Study of Wind Storage Systems</i>	90
6.3	Future Research	90

List of Figures and Tables

Table 1: Available Power Storage Technologies	2
Table 2: Main Battery Storage Technologies	3
Fig. 1.1: Li-Ion impedance model [25]	9
Fig. 1.2: Li-Ion dynamic model [27]	10
Fig. 1.3: VRB simple model [17]	12
Fig. 2.1: Proposed VRB model	18
Fig. 2.2: Proposed Li-Ion model	22
Fig. 2.3: VRB model in SIMULINK	25
Fig. 2.4: Li-Ion battery model in SIMULINK	25
Fig. 3.1: Static operation of a 3.3kW VRB at fixed 20% SOC	27
Table 3: Comparison of Results for Static Simulation	27
Fig. 3.2: VRB full discharge cycle (Initially 80% SOC, $P_{out} = 3.3 \text{ kW}$)	28
Fig. 3.3: VRB full charge cycle (Initially: 20% SOC, $P_{in} = 3.3 \text{ kW}$)	29
Fig. 3.4: Complete cycle for 3.3 kW 3 hour VRB	30
Fig. 3.5: 3.3 kW VRB discharge at 69.9 A for 3 hours (209 Ah)	31
Fig. 3.6: Li-Ion battery cell voltage versus SOC	33
Fig. 3.7: 40 Ah Li-Ion battery discharge at 40 A for 1 hour (100% initial SOC)	34
Fig. 3.8: 40 Ah Li-Ion battery charge at 40 A for 1 hour (0% initial SOC)	34
Fig. 3.9: Typical wind profile for storage device	37
Fig. 3.10: Typical VRB output power profile	38
Fig. 3.11: 3.3 kW VRB VI characteristic	39
Fig. 3.12: 3.3 kW VRB charge efficiency versus input currents	40
Fig. 3.13: 3.3 kW VRB discharge efficiency versus input currents	41
Table 4: Charge Efficiency for Various Operating Conditions	42
Table 5: Discharge Efficiency for Various Operating Conditions	42
Fig. 3.14: Worse case charge to discharge transition (80 A currents)	43
Fig. 3.15: Li-Ion VI characteristic	44
Fig. 3.16: Li-Ion battery charge efficiency versus current	45
Fig. 3.17: Li-Ion battery discharge efficiency versus current	46
Fig. 3.18: Worse case charge to discharge transition (Initially 50% SOC, 80 A currents)	46
Fig. 4.1: 42 kW VRB model VI characteristic (Various SOC)	52
Table 6: Battery Steady State Thevenin Equivalent	53
Fig. 4.2: Two VRB models in series	54

Fig. 4.3: 252 kW battery bank	56
Fig. 4.4: Dc chopper implementation for VRB	57
Fig. 4.5: Charging and discharging the 42 kW VRB using a dc chopper	58
Fig. 4.6: Dc-dc chopper PI control	59
Fig. 4.7: 42 kW VRB current control using the dc chopper	59
Fig. 4.8: Discharge efficiency versus current for VRB-Chopper	60
Fig. 4.9: Charge efficiency versus current for VRB-Chopper	61
Fig. 5.1: Local DFIG storage system	64
Fig. 5.2: Centralized storage system	65
Fig. 5.3: DFIG system power reference controls	66
Fig. 5.4: Power output response (DFIG detailed model, 252 kW VRB)	67
Fig. 5.5: Power output response time (DFIG detailed model, 252kW VRB)	67
Fig. 5.6: Overall control system	68
Fig. 5.7: Power output after sudden wind drop (DFIG detailed model, 252 kW VRB)	69
Fig. 5.8: VRB system after sudden wind drop (DFIG detailed model, 252 kW VRB)	69
Fig. 5.9: Power output after sudden wind rise (DFIG detailed model, 252 kW VRB)	70
Fig. 5.10: VRB system after sudden wind rise (DFIG detailed model, 252 kW VRB)	70
Fig. 5.11: Power output response (DFIG average model, 252 kW VRB)	72
Fig. 5.12: Power output response time (DFIG average model, 252 kW VRB)	72
Fig. 5.13: Wind profile	73
Fig. 5.14: Turbine output power without storage (DFIG average model, 252 kW VRB)	73
Fig. 5.15: Turbine output power with storage (DFIG average model, 252 kW VRB)	74
Fig. 5.16: Battery SOC (DFIG average model, 252 kW VRB)	75
Fig. 5.17: Storage system power response (DFIG average model, 252 kW VRB)	75
Fig. 5.18: RTS experimental setup	77
Fig. 5.19: Storage system power reference (Centralized storage, RTS)	79
Fig. 5.20: Storage system response experimental results (Centralized storage, RTS)	79
Fig. 5.21: Turbine output power without storage (Centralized storage, RTS)	80
Fig. 5.22: Turbine output power with storage experimental results (Centralized storage, RTS)	80
Fig. 5.23: Storage system power flow experimental results (Centralized storage, RTS)	81
Fig. 5.24: Battery SOC (Centralized storage, RTS)	81
Fig. 5.25: Dc voltages experimental results (Centralized storage, RTS)	82
Fig. 5.26: Dc bus current experimental results (Centralized storage, RTS)	82
Fig. 6.1: Methodology for the study and design of wind storage systems	91

Chapter 1

Introduction

1.1 Wind Energy Storage

The motivation for developing and implementing electrical equivalent models for batteries comes from an interest in studying their application in wind energy systems. As wind energy penetration levels increase, there is a growing interest in using short and long-term storage devices to aid in managing the fluctuations in wind turbine output power. Advantages of using these devices include:

- Short-term (seconds), medium-term (minutes) and possibly long-term (hours) management of wind power fluctuations;
- Smoothing of large power output swings from wind farms;
- Providing real and reactive power for local voltage support during transmission system short-circuits and large transients;
- Meeting peak-load demands without interruption and without increase in generation: maximizing wind plant capacity;

Wind is by nature unpredictable. However, in an electrical system, load demands must be instantaneously met. Storage systems can act to smooth out wind energy variations and play a role in stabilizing the wind farm and local grid. The importance of detailed models can thus not be overemphasized, as they help to dictate what is reasonable as well as the constraints imposed upon the operating strategy.

In systems like Doubly-Fed Induction Generator (DFIG) wind turbines, energy storage has been demonstrated to provide smooth output power by acting as a real power source or sink. Furthermore, it provides improved transient and dynamic responses, and a potential to aid frequency and voltage regulation [1], [2], [3], [4], [5], [6].

Energy storage systems can be used within a remote off-grid power system as well as grid connected wind parks. In remote hybrid systems, there is an interest in increasing wind penetration, reducing the diesel fuel consumption costs, as well as avoiding voltage and frequency variations [7]. In interconnected power system wind parks, the focus is on improving power quality and stability for a larger power range [8].

1.2 Storage Research

1.2.1 Types of Storage

There are several ongoing studies related to the use of energy storage in power systems. Many authors have seen new potential in short and long-term storage devices based on the latest developments in storage technologies [9], [10], [11], [12], [13].

Table 1: Available Power Storage Technologies

STORAGE TECHNOLOGY	ADVANTAGES	DISADVANTAGES	ROUND TRIP EFF.	TIME SCALE
Pumped Hydroelectric	High efficiency Long term storage Widely used	Large capital cost Significant land area Specific topography	70-80%	Hours – Days
Compressed Air	High reliability Long term storage	Polluting (Uses fuel) Large capital cost Operating costs	85%	Hours - Days
Batteries	High flexibility Non-polluting Quick response	Efficiency dependent on electrochemistry High capital cost	60-80%	Minutes - Hours
Super Capacitor	Long cyclic life Small volume	Short term storage Limited power range	86%	Seconds - Minutes
Flywheel	Very high efficiency Commercial success	Short term storage Large capital cost Large size	89%	Seconds - Minutes
SMES	Quick response	Refrigeration needs Large capital cost Low overall efficiency	21 %	Seconds

Storage options include Pumped Hydroelectric, Super-Capacitor Energy, Compressed Air Energy, Battery Storage (Vanadium-Redox, Lead Acid, and Lithium-Ion), Superconducting Magnetic Energy and Flywheel Energy. Table 1 summarizes the characteristics of these technologies.

1.2.2 Common Batteries

There are several battery technologies that are available for energy storage [14], [15], [16] as shown in Table 2 below. Batteries offer flexibility in terms of sizing, while providing a quick response.

Table 2: Main Battery Storage Technologies

STORAGE TECHNOLOGY	LIFETIME	ROUND TRIP DC-DC EFF.	TIME SCALE	COMMENTS
Vanadium-Redox Flow Battery	10.000 cycles	80%	Minutes-Hours	Highly scalable, Cost effective, Medium and long term applications
Lithium-Ion (Li-Ion)	3000 cycles	Near 100%	Seconds-Minutes	High cost, Limited to lower power range, Short term applications, Quick response
Lead Acid	3000 cycles	85%	Seconds-Minutes	High cost and maintenance requirement, Short term applications
Sodium-Sulfur (NaS)	2250 cycles	89%	Minutes-Hours	Temperature sensitive, Combined use for power quality and peak shaving
Zinc-Bromine Flow Battery	> 5000 cycles	75%	Minutes-Hours	Highly scalable, Medium and long term applications

1.2.3 Wind Storage Research

Vanadium-Redox Batteries (VRB) and Lithium-Ion (Li-Ion) batteries in particular appear to have potential for wide-scale implementation in wind energy systems.

VRB technology has many advantages including operation over a wide range of power outputs, high storage efficiency, rapid response, low maintenance costs and long lifecycle [17], [18]. Operation under rapidly changing conditions is possible without impact on efficiency, because the integrated pump ensures the availability of electrolyte at all times near the electrodes. The State of Charge (SOC) of a VRB is also directly dependent on the amount of charged electrolyte in the tanks, and is thus easy to track.

Furthermore, the power and voltage ranges of a VRB depend on the cell stack, while the energy capacity depends on the tank size and volume of electrolyte [12]. This independence between energy and power ratings provides high flexibility in terms of design. These characteristics make VRB technology well suited for wind energy applications. There are ongoing projects that look at the integration of VRB in wind systems [12].

Large capacity Li-Ion batteries are also emerging in fields such as satellites, space stations and launch vehicles [19]. Recent research for the use of Li-Ion batteries as backup sources in large scale power systems has also been undertaken [20]. Li-Ion batteries have several characteristics that make them attractive for large power applications, such as excellent high-rate discharge performance, operation through a wide range of temperatures, easy charge controllability and low self-discharge. Additional advantages include long life performance as well as small size.

In order to study various aspects of battery storage in wind energy applications, fast and accurate battery models are needed. These models could then be used within complete wind-energy system simulations in order to obtain valid results on their benefits and limitations, from both technical and economical perspectives.

1.3 Battery Modelling

1.3.1 Battery Performance

Battery performance needs to be evaluated when comparing these various technologies. The obtained data can then be used to determine how each battery should be operated, and whether it meets the design requirements. Battery performance data [14], [21], [22] includes the following:

- Dc charge and discharge efficiency: this corresponds to the efficiency from the dc bus, and includes the dc-dc chopper which controls the battery.
- Ac charge and discharge efficiency: this corresponds to the efficiency from the ac bus, through a dc-ac converter. Converter losses are usually 5% round-trip.
- Discharge time, energy capacity and energy density
- Transient response time
- VI transfer characteristic
- Rated and maximum power
- Cycle life and temperature effects

1.3.2 Battery Modelling Overview

Batteries have a series of characteristics that dictate their behaviour. These physical characteristics would ideally all be taken into account in a perfect model. They include: lifetime, capacity, stability, charge-discharge behaviour as well as efficiency of the charge-discharge process. Several types of battery models exist, for different applications and with varying accuracy. These include physical, empirical, abstract and mixed models [22].

Physical models are the most complex and accurate models. Due to the complexity of such models, simulations can take hours to days, and are primarily used by battery designers.

Empirical models such as Peukert's law [22] approximate a certain behavior of the battery based on a simple mathematical formula. Parameters are determined by fitting the expression to available experimental data. They often have limited accuracy and insight.

Mixed models use high-level representation of battery. The analytical expressions are based on physical laws and experimental data determines the parameters. These models have comparable accuracy to the physical models and give a high insight into the current state of a battery. What they lose in accuracy, they gain in computational speed.

Abstract models provide an equivalent representation of the battery. The level of analytical insight will depend on each model and the number of variables used, however there is a tradeoff between accuracy and simulation speed. Examples of such models include discrete-time models, stochastic models and electric circuit models.

1.3.3 Model Evaluation

A model is characterized by the following ([22], [23], [24], [25], and [26]):

- Type (physical, empirical, abstract, mixed)
- Variables of interest and total number of parameters
- Computational complexity and simulation time
- Accuracy, analytical insight and assumptions
- In-depth battery knowledge requirement (chemistry)
- Performance and apparent tradeoffs

Therefore, a model's pertinence can be validated with respect to a proposed application, based on these characteristics. In general, an ideal model should allow the optimum representation of real battery characteristics with a minimum set of parameters

1.3.4 Model Validation

Battery models need to be validated. This is accomplished by evaluating the simulation results of a model against measured experimental data. The scope of the experimental data required is thus determined by what the proposed model claims to represent.

For battery model validation, we are interested in a series of current and voltage measurements. The data required for model validation, based on models reviewed ([17], [22], [23], [24], [25] and [26]) can include the following:

- Voltage versus capacity at different temperatures
- Cycle life (discharge capacity versus cycle number)
- Load change transient response
- Performance under demanding conditions
- Input charging currents for varying available power
- Pulse and frequency response measurements
- Tafel voltage curves (voltage versus current for several SOC) [26]
- Battery voltage dynamics (fast switch from charge to discharge)
- Constant current discharge and discharge idle time
- Constant current charge, constant voltage charge and charge idle time

1.4 Existing Models

In order to develop accurate battery models that meet the requirements for wind energy applications, ongoing research in battery modelling will first be reviewed in this section.

1.4.1 NiH2 Model

The Nickel-Hydrogen (NiH₂) battery complex electrochemical dynamic model represents dc non-linear behavior and transient dynamics [26]. The math model consists of the sum of two electrochemical process dc currents, which depend on the battery terminal voltage. These are the Nickel plate charging current and the parasitic overcharge reaction current.

This model is useful for dc analysis, low and mid-frequency stability and dynamic analysis (dynamic transient effects). The dynamic elements and electrochemical model parameters are all handled as programmable variables. Good model accuracy is demonstrated using pulse and frequency response measurements, Tafel voltage curves [26] and battery voltage dynamics.

1.4.2 Lead Acid Model

The mathematical Lead-Acid battery model [18] takes into account self-discharge, battery storage capacity, internal resistance, over-voltage and environmental temperature. The model is tested and validated experimentally. The system consists of a data acquisition system, a controller rack, and two temperature-controlled chambers. Current controlled sources are used for testing.

The tests are done at different temperatures, voltage ranges as well as rates of charge and discharge. The tests include constant current discharge, discharge idle time, constant current charge, constant voltage charge and charge idle time. The experimental results are closely correlated with simulation results.

1.4.3 Lithium-Ion Battery Models

The Lithium-Ion battery is one type of storage device of high interest for wind energy systems. It appears to be well suited for small wind installations, such as the ones found in remote communities.

The PSPICE macro-model [24] incorporates cell voltage, state of charge, rate dependence and thermal characteristics. The model is developed based on ICR-18650 Lithium-Ion cells data. The parameter coupling is dependent on lookup tables created from data measurements. Battery characteristics modeled include state of charge, degradation of cells over time, rate dependence, electrochemical delays, cell impedance as well as thermal properties.

Model validation is accomplished by comparing measurement and simulation curves. These curves include “voltage versus capacity” at different temperatures, cycle life and load step transient response. The model is found to be accurate with errors of less than 5% error for cycle life, and less than 12% for thermal performance. Load response accuracy on the other hand could be improved by including more than one time constant.

The Li-Ion impedance model [25] on the other hand employs Electrochemical Impedance Spectroscopy (EIS) to obtain physical-based non-linear equivalent circuit models of super capacitors describing Li-Ion batteries. Voltage response and dc currents are measured as ac current flows in the device, and the impedance spectrum is obtained.

The model, shown in figure 1.1, takes into account impedance dependence on temperature and state of charge. Parameters are defined with respect to battery nominal current and the number of battery cells connected in series.

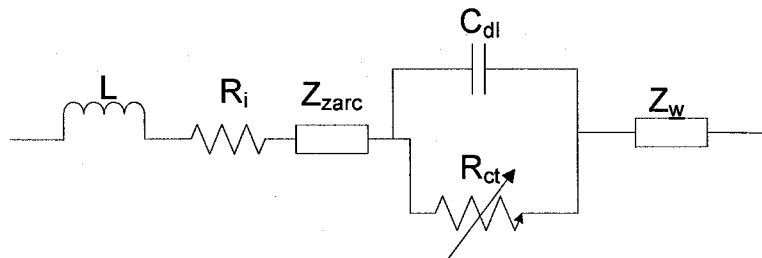


Fig. 1.1: Li-Ion impedance model [25]

Comparing simulation results to measured data in the time domain validates the model. Validation data also includes voltage and current responses at certain SOC and room temperatures. The accuracy obtained is excellent because Li-Ion batteries are suited for this kind of model.

The dynamic lithium battery model [27], which is shown in figure 1.2, represents the battery by a simple electrical circuit. The transients are represented by a capacitor, while the losses are separated into two internal resistances. The internal voltage source, representing the equilibrium potential, is expected to vary based on the SOC. The model parameters are found by curve fitting, based on data obtained from manufacturers.

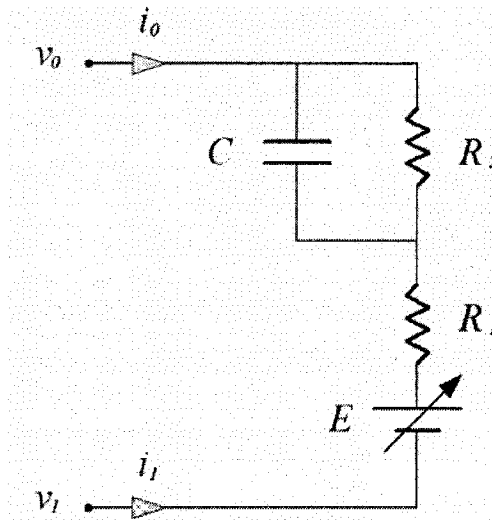


Fig. 1.2: Li-Ion dynamic model [27]

1.4.4 VRB Models

VRB technology uses a controlled pump to induce flow, which improves battery performance and efficiency. These storage devices can be used with large wind installations and other distributed generation, such as photovoltaic systems [28]. In contrast with a Li-Ion battery, the main differences are:

- Large scale storage using electrolyte tanks
- Use of controller and pump for circulation

- Use of an ion exchange membrane, which can result in a larger fraction of the internal resistance being constant
- Independence between power and energy rating
- Longer lifetime

It has been shown experimentally that various VRB losses can be modeled using constant resistive values [29]. The simple flow battery model [17], as shown in figure 1.3, takes into account internal resistance and parasitic resistance. The total energy storage of the system depends on the SOC and amount of active chemicals in the system. The total power available is related to total electrode area within the cell stacks. The model also accounts for system energy content and transient responses.

The internal resistance accounts for losses due to reaction kinetics, mass transport resistance, membrane resistance, solution resistance, electrode resistance and bipolar plate resistance. Parasitic resistance accounts for power consumption by recirculation pumps, the system controller, and power loss from cell-stack by-pass currents.

In order to validate the model, various operating cases were examined, including normal and extreme conditions. Some additional model assumptions are made for the pumping energy estimation:

- Pump and impeller efficiencies assumed constant
- System pressure drop increases with flow
- DC pump and simple resistive voltage controller
- Simple pump control algorithm

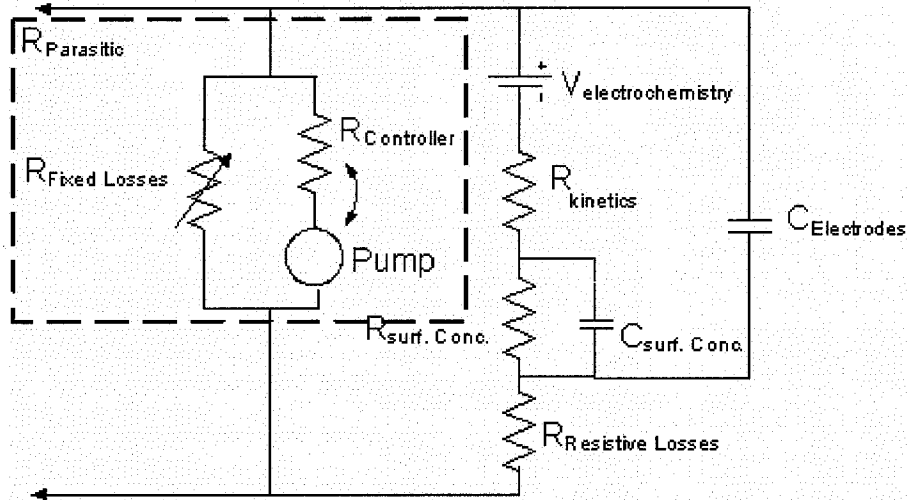


Fig. 1.3: VRB simple model [17]

1.5 Research Objectives

1.5.1 Problem Definition

The large-scale problem that needs to be solved is determining the technical and economical advantages and limitations of VRB and Li-Ion battery storage devices in wind energy systems. The study of the appropriate battery models and their integration within DFIG wind systems will provide the insight needed for system design assessment and optimization.

1.5.2 Identifying the Gaps

There is an apparent gap when it comes to the design, integration and operation of large scale VRB and Li-Ion batteries in wind systems. Crucial information regarding the batteries is not readily available, including efficiency under various operating conditions, design and sizing methodologies as well as short, medium and long-term operating strategies. This is due to an evolving technology and a competitive market in which information is kept confidential by the manufacturers. Therefore, accurate generic (not manufacturer specific) models are thus needed, since they will provide generic information without requiring on-site testing.

The purpose of this research project is thus to develop suitable benchmark VRB and Li-Ion electrical models and to implement them into simulation software such as SIMULINK. These models will be based on existing mathematical models that will be modified and improved for the purpose of the research. The models will then be validated mathematically and experimentally.

Wind energy storage system design also needs to be examined. The VRB model will be integrated into a DFIG wind system, as well as incorporated into a real-time OPAL-RT simulation. It will provide insight on how to design and operate the storage system efficiently. These results will be used to demonstrate the pertinence of battery storage integration in wind energy systems, as well as to provide recommendations with respect to design and operating strategies.

1.5.3 Research Goals

The research goals are as follows:

1. Develop, improve, implement and validate electrical VRB and Lithium-Ion battery models based on physical and mathematical principles.
2. Examine battery sizing issues and model scalability for large scale applications.
3. Develop a DFIG storage system by integrating a VRB within the wind system, using simple, average and detailed DFIG models.
4. Develop a real-time simulation system using OPAL-RT, which combines real and simulated components in order to experimentally validate the system design methodology.
5. Develop a typical wind profile which can be used as a standard to experimentally test and compare different batteries in wind systems.
6. Use the obtained performance data to draw conclusions on the operation of battery storage systems within a wind energy context. Provide recommendations to facilitate the design of short-term and long-term control algorithms.

1.5.4 Claim of Originality

To the best of the author's knowledge, the thesis provides new ideas in the field of wind energy storage by:

- Developing and implementing an electrical VRB model with unique features suitable for wind energy study.
- Developing and implementing an electrical Li-Ion battery model with unique features suitable for wind energy study.
- Obtaining detailed performance data regarding the transfer characteristic, transient operation and efficiency of VRB and Li-Ion battery technology under various operating conditions.
- Demonstrating the operation of a DFIG-VRB system using the developed VRB model within various DFIG systems (offline and real-time).
- Providing a methodology for the design of battery systems for wind energy integration.
- Providing recommendations for the development of control algorithms.
- Developing a battery sizing approach.
- Developing a model scalability methodology.

1.6 Thesis Outline

In Chapter I, existing literature on the topics of wind energy storage and battery modeling is reviewed. The role of storage in wind energy applications is examined. The requirements for suitable models are then discussed.

Chapters II focuses on the development of suitable VRB and Li-Ion models. The various elements that make up the models and their relation to the physical characteristics of batteries are discussed.

In Chapter III, the models are validated through typical charge and discharge simulations. They are used to obtain battery performance, including transfer characteristic, efficiency under various operating conditions as well as transient operation. VRB and Li-Ion battery performance is then compared. A tentative wind profile is also presented, which can be used as a standard to testing wind-storage systems.

In Chapter IV, issues related to VRB design for a DFIG system are discussed. This includes battery sizing, model scalability as well as battery interface. A dc-dc converter interface is developed and used to control the battery. The impact of the converter on battery performance is examined.

The VRB system is then integrated within a wind system in Chapter V. This is done for both a detailed DFIG model, as well as an average DFIG model in SIMULINK. The system is also implemented in a real-time experimental setup using OPAL-RT I/O technology as well as real converters. The results show how the battery acts to smooth out a DFIG wind turbine output under varying wind conditions.

Chapter VI concludes the thesis by reviewing the methodology developed, and assessing the effectiveness of battery storage in wind energy systems. Recommendations for the development of wind storage operating strategies are provided. This sets the ground for future research on the topic of battery design and modeling in wind energy applications.

Chapter 2

Model development

2.1 Introduction

It was determined that accurate electrical models are needed for wind energy storage system studies. In this chapter, model requirements are discussed. VRB and Li-Ion models are presented. Various battery characteristics are examined, including the power rating, cell stack voltage, pump losses, internal and parasitic resistance losses, state of charge representation and transients.

2.2 Model Requirements

The model needed requires specific characteristics. In terms of analytical insight, it should produce results related to the storage efficiency of the process, transient response and output transfer function. The model should consider how much energy can be extracted given an amount of energy stored, and should include the impact on the charge-discharge current. Furthermore, different levels of simulation time scales are needed, and thus the model should be adaptable to various DFIG system models.

In terms of complexity, the model must be accurate yet manageable in larger system simulations. There must be a reasonable tradeoff between complexity and computational time. In terms of scale, the model should be adaptable to typical power and voltage levels encountered in various wind energy applications.

The battery capacity and discharge behavior need to be modeled appropriately taking into account dependence on transient effects, temperature effects and the state of charge (SOC).

2.3 VRB Model Characteristics

In a VRB, the total energy storage of the system depends on the SOC and amount of active chemicals in the system. The total power available is related to the electrode area within the cell stacks. The power and Energy are thus not related, and this allows for easy scaling of the battery specifications as required.

The model to be implemented in SIMULINK takes into account previous research related to VRB modeling [29], as well as VRB modeling data provided by Natural Research Council Canada (NRC) [17]. It will improve on an existing mathematical model, shown in figure 1.3, by filling the appropriate gaps. These gaps include pump losses, SOC dynamics and scalability issues. The proposed model has the following unique properties:

- The state of charge, which represents the amount of active chemicals in the system, is modeled as a variable that is dynamically updated.
- The stack voltage is modeled as a controlled voltage source. The power flow through this source impacts the changes in the SOC.
- The variable pump losses are modeled as a controlled current source.

The model also includes internal resistance and parasitic resistance. The internal resistance accounts for losses inside the cell stack due to reaction kinetics, mass transport resistance, membrane resistance, solution resistance, electrode resistance and bipolar plate resistance. Parasitic resistance accounts for power consumption by re-circulation pumps, the system controller, and power loss from cell-stack by-pass currents [17]. Figure 2.1 below shows the proposed model.

2.3.1 Model Specifications

The model to be implemented will be based on a 3.3 kW-3 hour 48 V residential VRB system. The step-by-step procedure for deriving the parameters should be easily repeatable for different sized VRB systems.

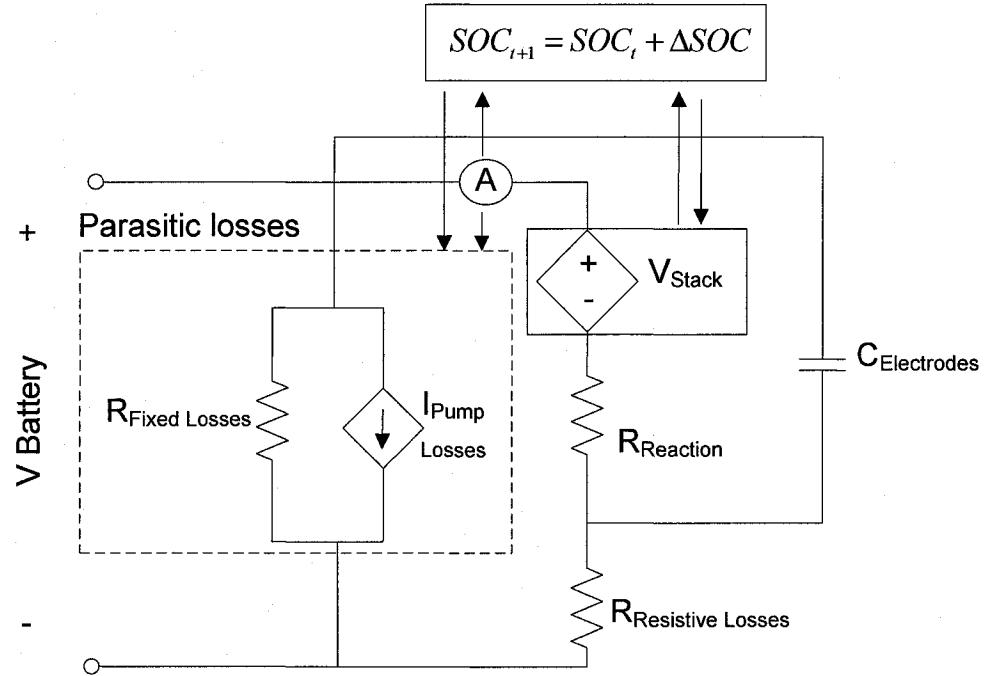


Fig. 2.1: Proposed VRB model

The calculations are based on estimating losses to be 15% internal, and 6% parasitic in the worse case operating point (end of cycle discharge), for a minimum voltage of 42 V, and a current of 78.6 A. Thus for the battery to be able to provide 3.3 kW with 21% losses, the cell stack internal power should be:

$$P_{stack} = \frac{3300}{1 - 0.21} = 4177 \text{ W} \quad (1)$$

2.3.2 Internal Voltage and Temperature Considerations

The battery individual cell voltage is directly related to the state of charge of the battery based on the Nernst equation [17]:

$$V_{cell} = V_{equilibrium} + 2 \frac{RT}{F} \ln \left(\frac{SOC}{1 - SOC} \right) \quad (2)$$

In the Nernst equation, $V_{equilibrium}$ is defined as the cell potential at a SOC of 50%, F is defined as the Faraday constant equal to 96485 C/mole and R is defined as the

universal gas constant equal to 8.314510 J/(K.mole). The temperature impact on battery operation is reflected by 'T'.

The internal stack voltage (or open-circuit battery voltage) V_{Stack} is modelled as a controlled voltage source which depends on both the number of cells and the SOC. For 'n' cells, V_{Stack} would be equal to $n \cdot V_{cell}$ as shown in equation (3). In this case, 39 cell stacks are needed.

$$V_{Stack} = n \cdot \left(V_{equilibrium} + 2 \frac{RT}{F} \ln \left(\frac{SOC}{1 - SOC} \right) \right) \quad (3)$$

The battery output voltage $V_{battery}$ will thus depend on both the open circuit voltage, as well as the operational losses. In steady state, if I_{stack} is defined as the input stack current, then $V_{battery}$ can be expressed as follows:

$$V_{battery} = V_{Stack} + I_{stack} \cdot (R_{reaction} + R_{resistive_losses}) \quad (4)$$

2.3.3 $R_{internal}$ and $R_{Parasitic}$

Typically, internal resistance values for batteries are variable due to over-potential issues [29]. However, in the case of a VRB, a larger fraction of internal resistance is constant. This allows estimating $R_{internal}$ to be constant. $R_{internal}$ is set to 0.101 Ω , which is derived by estimating 15% losses at a maximum current of 78.6 A.

The parasitic losses are separated into fixed and variable losses [17]. The fixed losses are represented as a fixed resistance and the variable losses as a controlled current source. The losses are as follows:

$$P_{parasitic} = P_{fixed} + k \left(\frac{I_{stack}}{SOC} \right) = 84 + 42.5 \left(\frac{I_{stack}}{SOC} \right) \quad (5)$$

The parasitic and pump losses are derived as follows:

$$R_{fixed} = \left(\frac{42^2}{84} \right) = 21 \Omega \quad (6)$$

$$I_{pump} = \left(\frac{42.5 \left(\frac{I_{stack}}{SOC} \right)}{42} \right) = 1.011 \left(\frac{I_{stack}}{SOC} \right) \quad (7)$$

The pump losses are modeled as a controlled current source that is dependent on the stack current and state of charge, in parallel with the fixed parasitic resistance.

2.3.4 State of Charge Modeling

The system state of charge can be defined as:

$$\text{State of Charge} = \frac{\text{Current Energy in Battery}}{\text{Total Energy Capacity}} \quad (8)$$

SIMULINK discrete simulations compute all variables at each time step. Therefore one way to keep track of the state of charge is to update the SOC variable from one time step to the next, based on the power that goes through the cell stack. The SOC is computed each cycle based on the previous SOC, using a fixed step simulation. The change in SOC is modeled as follows:

$$SOC_{t+1} = SOC_t + \Delta SOC \quad (9)$$

$$\Delta SOC = \frac{\Delta E}{E_{capacity}} = \frac{P_{stack} \times TimeStep}{E_{capacity}} = \frac{I_{stack} \times V_{stack} \times TimeStep}{P_{rating} \times Time_{rating}} \quad (10)$$

2.3.5 Transient Operation

An important issue in battery modeling is transient behavior. The ability of the system to respond quickly to fast changes is especially important for power smoothing applications. In a VRB, the transient effects are related to electrode capacitance, as well as concentration depletion of active vanadium species near the felt fiber electrode.

The model will focus on transient behavior related to electrode capacitance, as shown in figure 2.1. $R_{internal}$ is divided into $R_{reaction}$ (0.061 Ω) and $R_{resistive}$ losses (0.04 Ω).

$C_{\text{electrodes}}$ is estimated to be 0.15 F for a 39 cell stack, where each cell has a 6 F series capacitance. Concentration depletion is less of an issue for VRB technology, depending on the pump system used.

2.4 Lithium-Ion Battery Model Characteristics

Li-Ion battery systems consists of a series of cells, each capable of storing a fixed amount of energy. The energy capacity of a Li-Ion battery is expressed in Ah, which corresponds to its discharge capacity at the rated current, for 1-hour. The total power available is thus dependent on the rated output voltage and current.

The model to be implemented in SIMULINK is based on previous research related to Li-Ion battery modeling ([27], [30], and [31]). The model is based on an existing mathematical model, shown in figure 1.2. Figure 2.2 below shows the proposed model which takes into account the following Li-Ion properties:

- The State of Charge, which represents the amount of active chemicals in the system, is modeled as a variable that is dynamically updated.
- The operating losses are modeled using resistances, separated into resistive and reaction losses. This accounts for the finite conductivities of electrodes and separators, concentration gradients of ionic species near the electrodes and limited reaction rates at the electrode [27].
- The stack voltage is modeled as a controlled voltage source, dependent on the number of cells and the SOC. The power flow through this source controls the changes in the SOC.
- Transient effects are modeled using a capacitance across R_{reaction} .

2.4.1 Model Specifications

For comparison purposes with the VRB model, the Li-Ion battery model to be implemented will have roughly the same power rating. It will use 30 cells rated at 40 Ah, which will produce an output power of 3300 W for an output voltage of 82.5 V. The

internal voltage will vary between 81 V and 125 V depending on the SOC. Li-Ion batteries are constructed using a series of cells which makes them easily scalable.

2.4.2 Internal Voltage and Losses

The battery internal stack voltage varies between 2.7 V and 4.2 V. It is related to the state of charge of the battery based on the following formula:

$$V_{cell} = V_{equilibrium} + k \cdot \ln\left(\frac{0.9 \times SOC}{100 - 0.9 \times SOC}\right) \quad (11)$$

$$V_{Stack} = n \cdot V_{cell} \quad (12)$$

This equation is obtained by estimating the Li-Ion cell voltage characteristic based on manufacturer data [27]. $V_{equilibrium}$ was found to be 3.797. The k factor was approximated to be 0.1829 for regular room temperature.

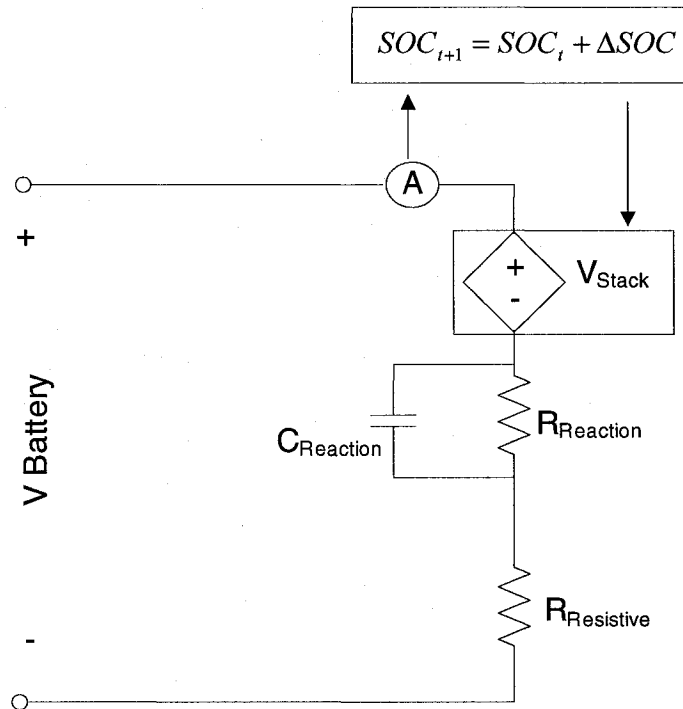


Fig. 2.2: Proposed Li-Ion model

During steady state, V_{battery} can be expressed as:

$$V_{\text{battery}} = V_{\text{Stack}} + I_{\text{stack}} \cdot (R_{\text{reaction}} + R_{\text{resistive}}) \quad (13)$$

Based on typical manufacturer data, losses of up to 5% can arise under worse case conditions [30]. Thus R_{internal} will be estimated to account for 5% losses at a 40 A rated current, for a fully depleted battery. The internal voltage in that case would be 81 V. At a constant current of a 40 A, an internal resistance of 101 m Ω will produce 5% losses.

R_{internal} is then divided into two-thirds $R_{\text{resistive}}$ and one-third R_{reaction} , which amounts to 67.33 m Ω and 33.66 m Ω respectively. These values agree closely with the ones proposed in [27].

2.4.3 State of Charge Modeling

Similarly to the VRB model, the state of charge is defined as:

$$\text{State of Charge} = \frac{\text{Current Energy in Battery}}{\text{Total Energy Capacity}} \quad (14)$$

The same approach is used to keep track of the SOC as was described in section 2.3.4: The SOC is computed each cycle based on the previous SOC, using a fixed step simulation. The change in SOC for a Li-Ion battery is modeled as follows:

$$SOC_{t+1} = SOC_t + \Delta SOC \quad (15)$$

$$\Delta SOC = \frac{\Delta E}{E_{\text{capacity}}} = \frac{I_{\text{stack}} \times \text{TimeStep}}{I_{\text{rating}} \times \text{Time}_{\text{rating}}} \quad (16)$$

2.4.4 Transient Operation

The transient effects in Li-Ion batteries are related to double-layer formation at the electrode/solution interface, capacitance due to purely electrical polarization and capacitance from diffusion limited space charges. They will be approximated as a first

order transient response [27], and modeled using a single 4F capacitor per cell, across R_{reaction} . This amounts to a total C_{reaction} of 0.133 F for 30 cells in series.

2.5 SIMULINK Implementation

The developed models were implemented using SMULINK (SimPowerSystems toolbox), as shown in figures 2.3 and 2.4. The following approach was used in both cases:

- The internal battery voltage is implemented using a controlled voltage source 'Vec'. The voltage is controlled by the 'Stack Voltage' block.
- The 'Stack Voltage' block computes the battery voltage according to equations (3) and (11). It takes into account the 'SOC' variable, as well as the number of cells (set by the 'cells' constant).
- The 'SOC' block dynamically computes the SOC at each time step according to equations (9) and (14). The change in energy content between each time step ΔE is computed as the product of the power flowing through 'Vec' by the time step.
- The battery total energy capacity is defined initially in the 'SOC' block.
- The VRB and Li-Ion battery resistive and capacitive parameters are implemented using elements from the SimPowerSystems library.
- In the VRB case, the pump losses current is implemented as a controllable current source. The current is computed according to equation (6).

2.6 Conclusions

Simple VRB and Li-Ion models were developed based on battery physical and mathematical properties, as well as existing battery modelling data. They were implemented in SIMULINK. They accounted for various battery characteristics including operating losses, transient operation and energy storage. The next step is to validate the models, and use them to obtain insight on battery performance including efficiency, transfer characteristic and transient response.

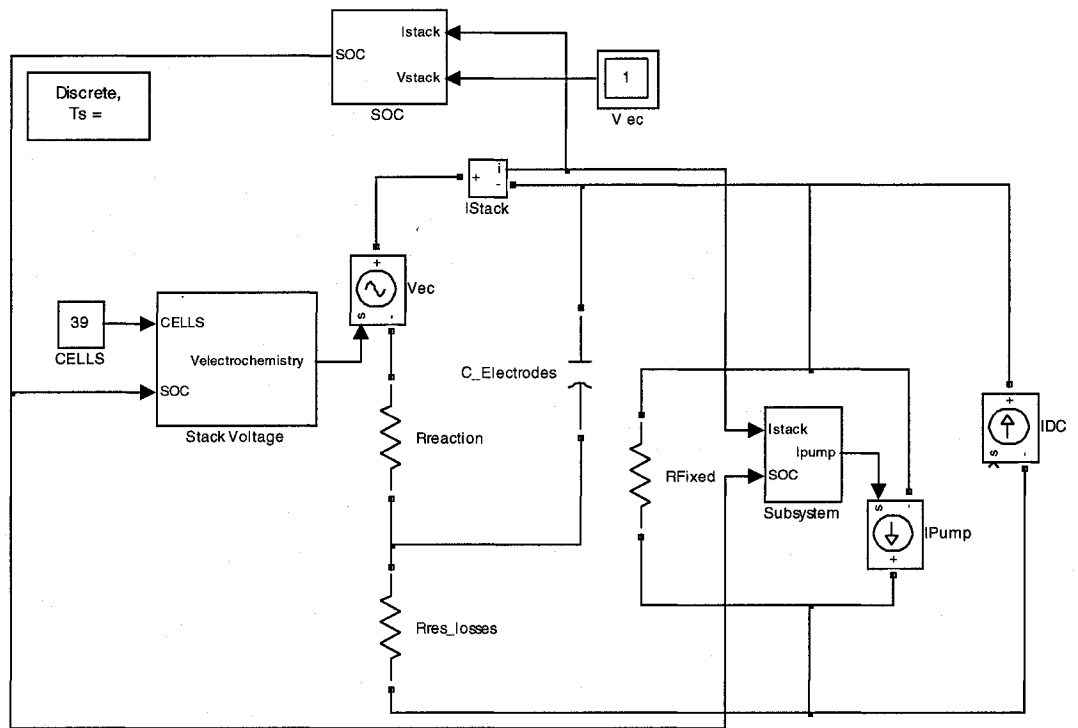


Fig. 2.3: VRB model in SIMULINK

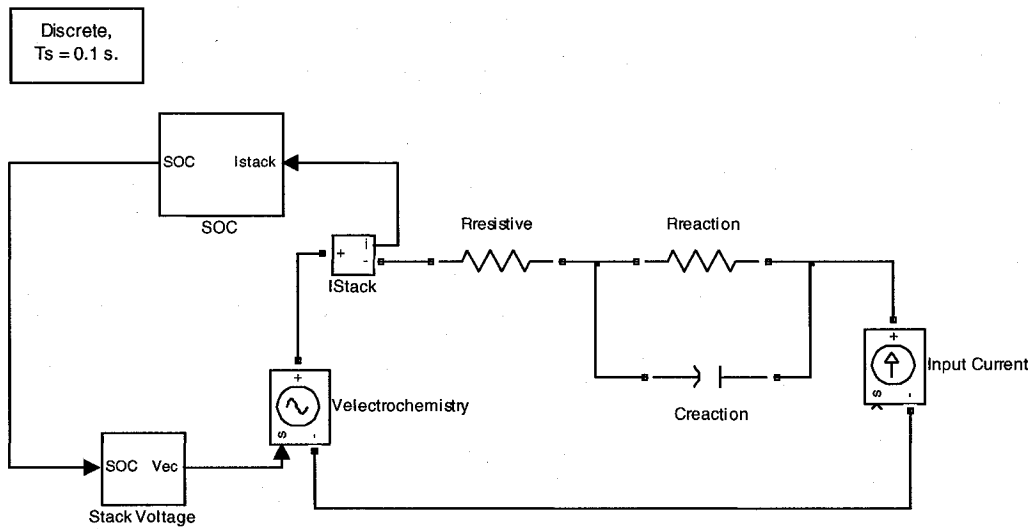


Fig. 2.4: Li-Ion battery model in SIMULINK

Chapter 3

Model Validation and Performance

3.1 Introduction

VRB and Li-Ion models which meet the project requirements were developed in the previous section, based on battery physical and mathematical properties. Battery models need to be validated against simulation and experimental results. A series of possible tests was indicated in section 1.3.4. However, there are currently no published standards or procedures for testing batteries specifically for wind energy applications. Such data would include typical charge and discharge profiles that can be used to compare various battery technologies.

In this chapter, the models will be validated by running typical charge and discharge simulations. Experimental validation is then discussed, and a standard wind profile developed for testing. Finally, the models are used to obtain insight on the battery performance, including efficiency, transfer characteristic and transient response. This data will be used to compare VRB and Li-Ion technologies and their suitability for wind energy applications.

3.2 VRB Model Validation

3.2.1 Static Operation

First, the model is validated by comparing simulated results against the results presented in [17] for a state of charge of 20%, and an output voltage of 43.5 V.

The obtained results can be seen in figure 3.1 and table 3. The largest error obtained is of 3%. Note that in order to be able to provide a rated output power of 3313 W we need an internal stack power of 4270 W to compensate for operating losses.

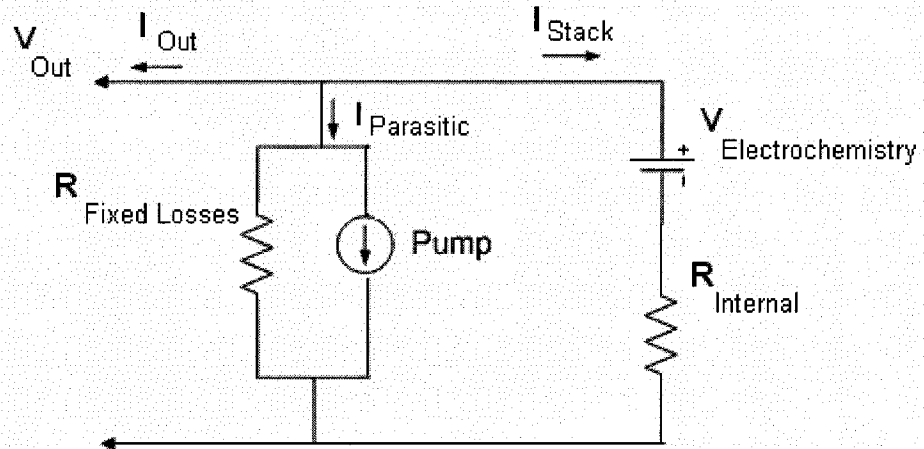


Fig. 3.1: Static operation of a 3.3kW VRB at fixed 20% SOC

Table 3: Comparison of Results for Static Simulation

Parameter	Results according to [11]	SIMULINK simulation	Error
V_{stack}	51.8 V	51.82 V	>1%
I_{stack}	81.9 A	82.4 A	>1%
$V_{internal}$	8.6 V	8.32 V	3%
$P_{internal}$	681 W	685.9 W	>1%
$I_{parasitic}$	6.1 A	6.238 A	2%
$P_{parasitic}$	265 W	271.3 W	2%
I_{out}	75.8 A	76.2 A	>1%
P_{out}	3300 W	3313 W	>1%

3.2.2 Dynamic Charge and Discharge Cycles

The dynamic behaviour is examined by looking at the charging and discharging of a 3.3 kW 3 hour (9.9 kWh) rated battery. In practice, operation is limited between 20% and 80% SOC due to over voltage and under voltage issues.

3.2.2.1 Full Discharge Cycle

The discharging of a charged battery (SOC = 80%) at a constant output power of 3.3 kW is first considered. In this example, a dc current source sets the output current based on the output voltage, keeping the output power at 3.3 kW. It is assumed that 9.9 kWh of stored energy can be used effectively. The simulation is executed in SIMULINK for 3 hours, with a time step of 1second. The results can be seen in figure 3.2.

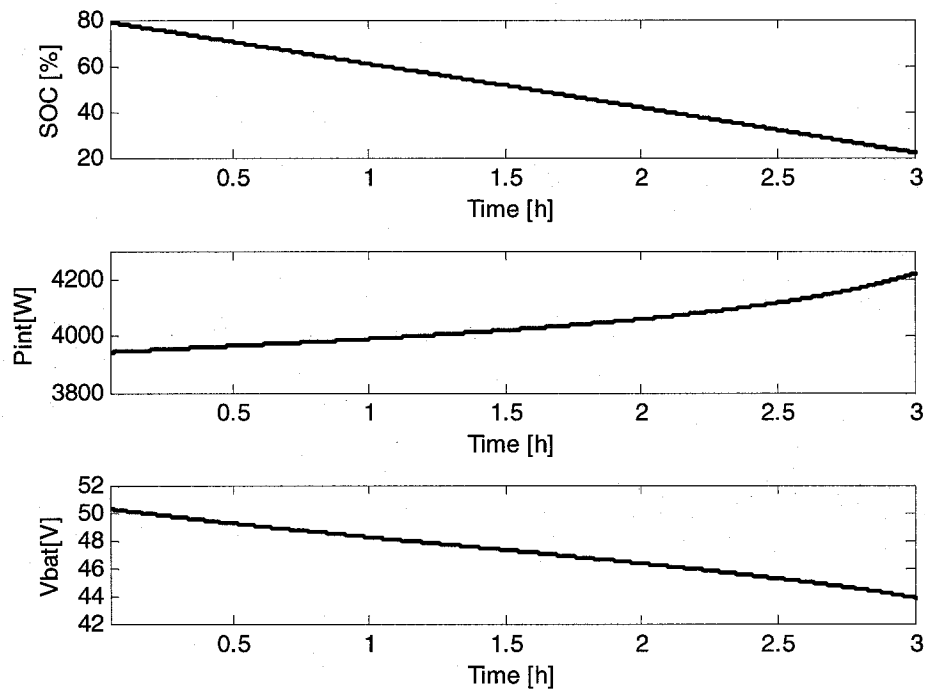


Fig. 3.2: VRB full discharge cycle (Initially 80% SOC, P_{out} = 3.3 kW)

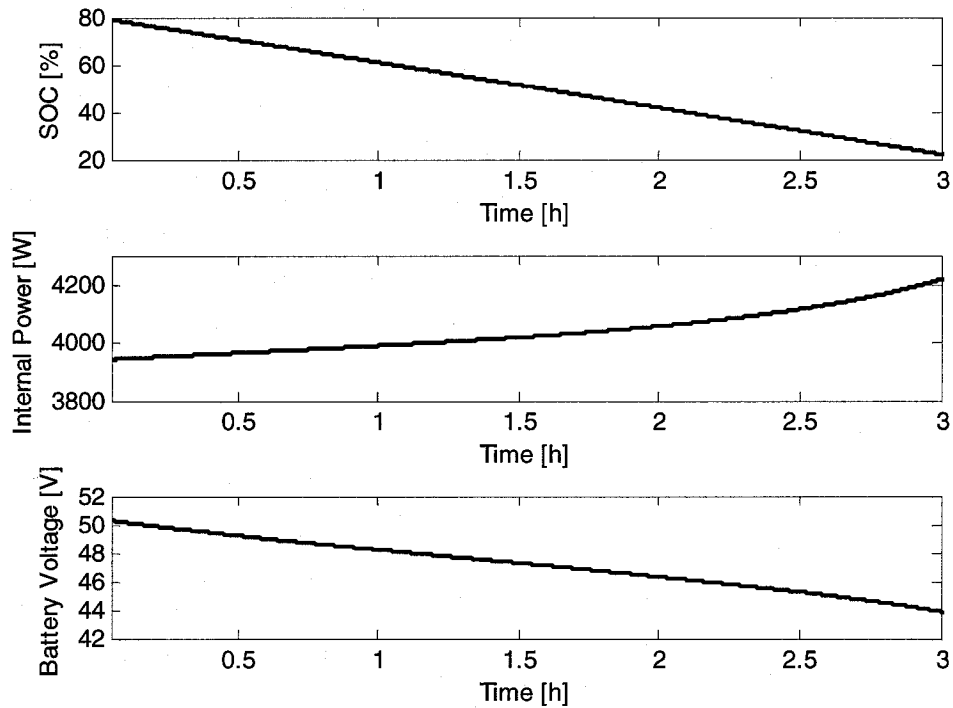


Fig. 3.3: VRB full charge cycle (Initially: 20% SOC, P_{in} = 3.3 kW)

The internal discharge power is kept constant close to 4100 W. This ensures that the output power will be 3.3 kW after losses. The voltage does in fact vary linearly in the 20% to 80% SOC. The battery model meets the requirements in terms of discharge voltage and SOC profiles.

3.2.2.2 Full Charge Cycle

The charging of a discharged battery (SOC = 20%) at a constant input power of 3.3 kW is then considered. The simulation is executed in SIMULINK for 4 hours, with a time step of 1second. The results can be seen in figure 3.3.

The charging power is kept close to 3.3 kW. The voltage varies linearly as well in the 20% to 80% SOC region. Due to the losses, the actual power getting stored varies between 2850 W and 2700 W at that current. Therefore, the battery must be charged at 3.3 kW for more than 4 hours to reach 80% SOC. The battery model does however meet the requirements in terms of charge voltage and SOC profile.

3.2.2.3 Full Cycle at Constant Current

Figure 3.4 shows a full charge-discharge cycle. The voltage and battery output power can be observed as the SOC varies between 10% and 90%. The charging current of 65 A is followed by a discharging current of 65 A.

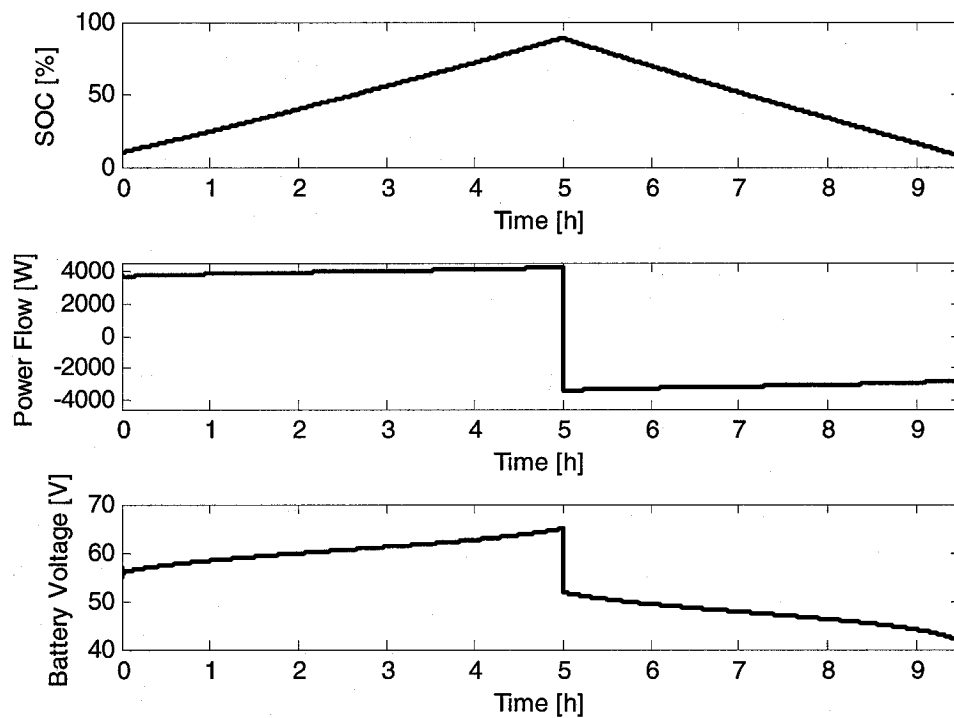


**Fig. 3.4: Complete cycle for 3.3 kW 3 hour VRB
10 to 90% SOC, 65 A**

3.2.3 Energy Storage

Another approach that is used to validate the model is to compare the rate of discharge proportionality factor. The value according to [17] is of 0.283 %SOC/Ah. The energy content of the system is therefore evaluated in terms of Ah.

For an input average voltage of 47.2 V, and a discharge power of 3.3 kW, there is a current of 69.9 A. Thus, for 3 hours of operations, 209 Ah of energy is expected. This is verified by discharging the battery at 69.9 A for 3 hours. Figure 3.5 below shows the SOC drop from 80% to 23%.

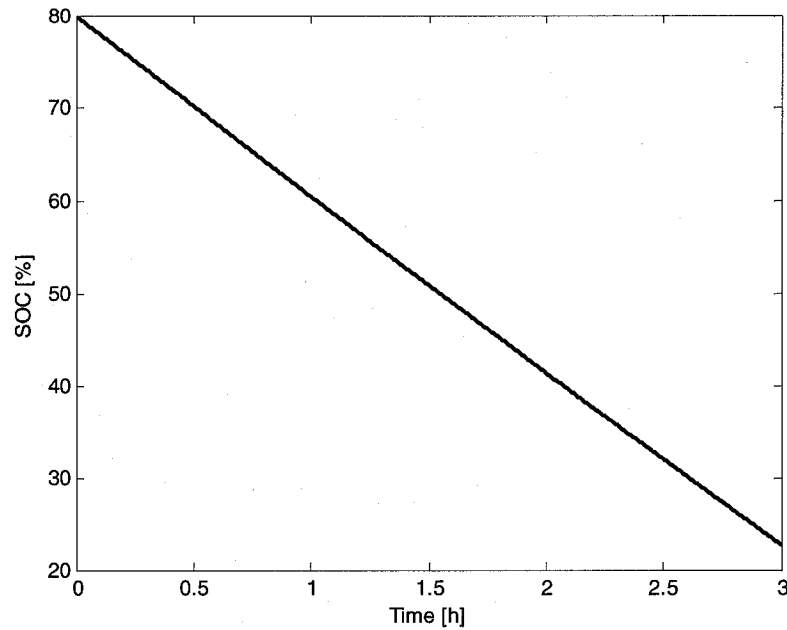


Fig. 3.5: 3.3 kW VRB discharge at 69.9 A for 3 hours (209 Ah)

The rate of discharge is thus:

$$\text{Rate of Discharge} = \frac{0.57 * 100}{209} = 0.272 \%SOC / Ah \quad (17)$$

The system energy content is therefore close to 209 Ah, as the VRB is discharged from 80% to 23% in 3 hours.

3.2.4 VRB Model Discussion

The following issues need to be considered in battery modeling: battery discharge behaviour, rate-dependent capacity [21], temperature effects and capacity fading.

The developed battery model does a good preliminary job at capturing the discharge behaviour and temperature effects of a VRB. Rate-dependence on the other hand is less of an issue when dealing with flow batteries, as the role of the flow pump is to ensure that the electrode surface is in contact with the maximum concentration of

active species during charge and discharge. Capacity fading, which is mainly an issue for Lithium-Ion batteries, is not modeled either.

This VRB model has several advantages. It accounts for a large number of battery operating losses in a simple manner which makes it computationally efficient yet accurate, and thus well suited for short-term as well as long-term simulations. This also allows for accessibility and scalability. Its computational simplicity also allows its integration in real-time simulations, which can combine real and simulated elements to provide experimentally validated results. Furthermore, this model also accounts for thermal effects, transients and dynamic SOC behaviour.

However, its limitations lie in the fact that chemical reactions and life-cycle issues are not represented. Furthermore, current limits and saturations are not modeled. It is thus left to the user to take into account what is reasonable in terms of maximum power operation, as well as battery life-time.

In this research project, we are interested in studying the battery's behavior and efficiency within a wind system. The developed model appears to meet these requirements. However additional experimental data is required in order to fully validate the model.

This is not a major issue since the battery software implementation can be easily updated to reflect any changes to the model at a later stage. What is more important is the methodology applied in this project to determine, integrate and analyze the battery model. That approach, which is covered in this report, can then be repeated for different types of batteries and models, as they become available.

3.3 Li-Ion Model Validation

3.3.1 Cell Voltage

Figure 3.6 shows the individual internal cell voltage against the SOC, which varies between 2.7 V and 4.2 V. The curve matches the Li-Ion data found in [27], [30] and [31].

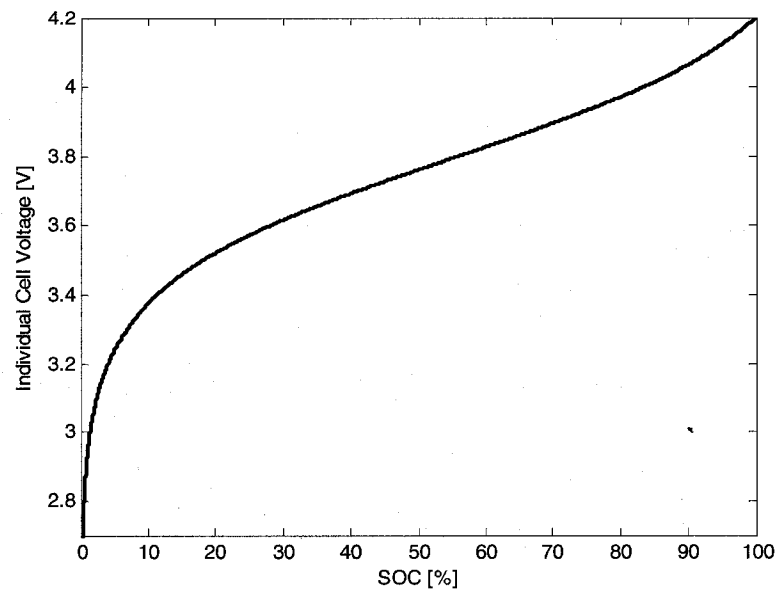


Fig. 3.6: Li-Ion battery cell voltage versus SOC

3.3.2 Dynamic Charge and Discharge Cycles

The dynamic behavior is examined by looking at the charge and discharge of a 30 cell 40 Ah rated Li-Ion battery. The Li-Ion battery can be operated between 0% and 100% SOC (also referred to as discharge capacity).

3.3.2.1 Full Discharge Cycle

Figure 3.7 shows a Li-Ion full discharge cycle, at a constant current of 40 A. The voltage and battery output power can be observed as the SOC varies between 100% and 0%. The results agree with Li-Ion data found in [27], [30] and [31].

3.3.2.2 Full Charge Cycle

Figure 3.8 shows a Li-Ion full charge cycle, at a constant current of 40A. The voltage and battery output power can be observed as the SOC varies between 0% and 100%. The results agree with Li-Ion data found in [27], [30] and [31].

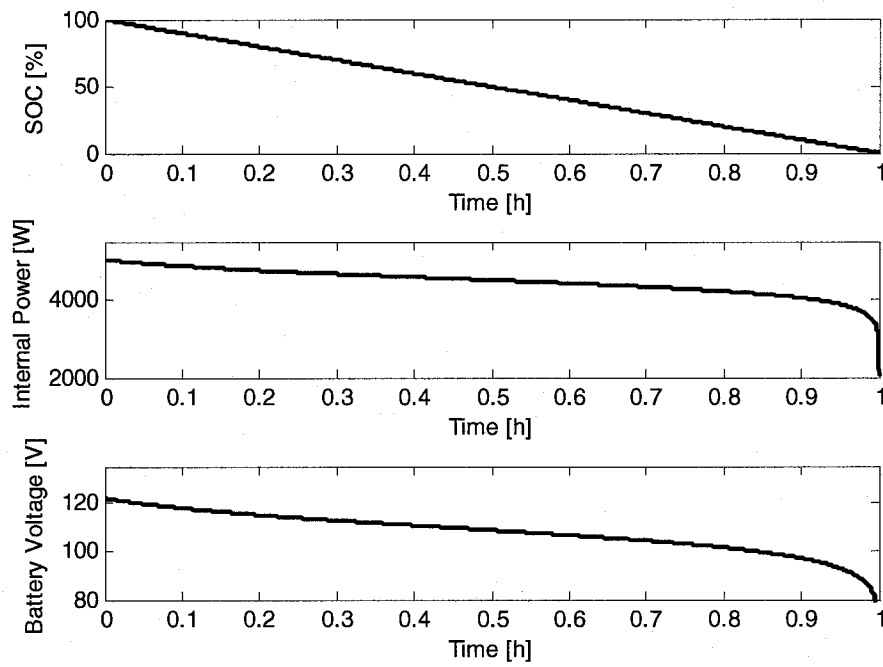


Fig. 3.7: 40 Ah Li-Ion battery discharge at 40 A for 1 hour (100% initial SOC)

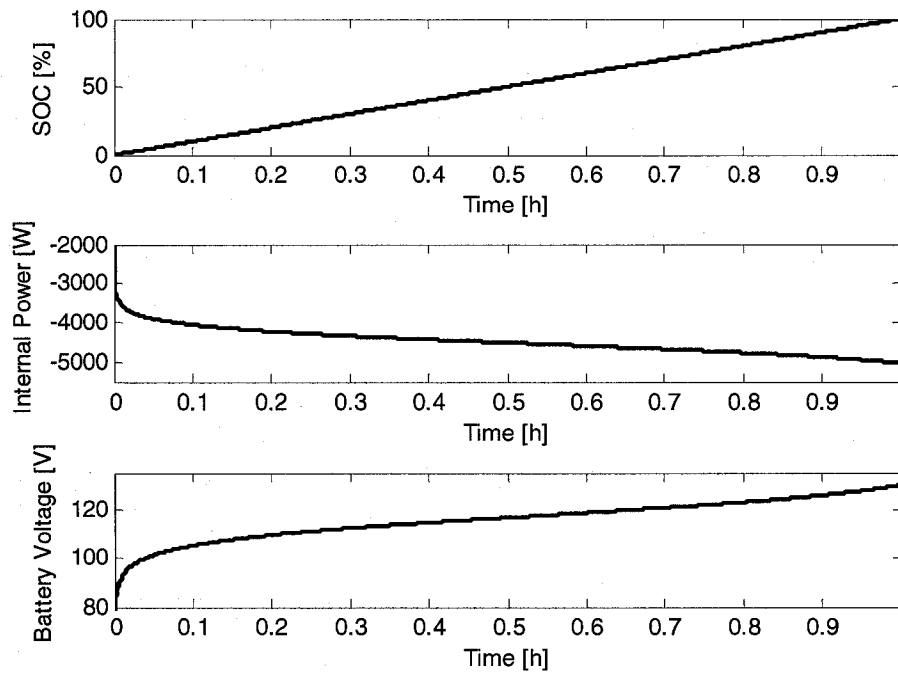


Fig. 3.8: 40 Ah Li-Ion battery charge at 40 A for 1 hour (0% initial SOC)

3.4 Standardized Profile for Experimental Tests

A test system should be used for model validation, battery performance assessment and technology comparison. It should allow for voltage and current measurements in time and frequency domain. Tests should include effects of temperature on the model, and therefore some type of climate control around the battery would be required. The test equipment should allow readings of the SOC and available energy. Some tests will also require fast changes in the load, and fast switching between charge and discharge, and therefore the appropriate controls are needed. A series of possible tests for battery validation was indicated in section 1.3.4.

However, there are currently no published standards for testing battery models in wind applications. A standardized test profile would provide a methodological approach to validating battery models. Furthermore, it could be used to evaluate battery performance within a wind system, as well as to compare various battery technologies. A typical charge-discharge profile will thus be developed in this section.

Wind characteristics need to be examined in order to determine how they impact wind turbine operation. This will allow the development of a typical wind profile that covers all basic operating conditions related to storage in wind energy applications. It will be used subsequently to provide a possible charge-discharge profile to test a 3.3kW Industrial VRB.

3.4.1 Typical Wind Profile

Wind is characterized by availability, speed (instantaneous and mean), direction, density, turbulence, shear as well as gust. The geographical location is also important, as wind behaviour depends on the local geographical setting (e.g.: plains, mountains, etc.). In this case, the wind direction is of little interest since the wind data is considered in a single dominant direction. Similarly, the wind shear, which corresponds to the change in wind speed based on height, will not play a role in a typical wind profile, since the wind data is examined at a fixed height.

Wind gust corresponds to the sudden changes in wind speed with respect to the average wind speed. Thus a highly turbulent wind will have higher gusts, at a higher frequency. In a wind-storage system, the battery operation is mainly affected by the wind speed and its variations. However, very high frequency variations will not affect the turbine response, as they are typically filtered out through the turbine's mechanical inertia.

In defining a tentative "typical wind profile", wind data will cover the following situations:

- High mean wind speed: the mean wind speed will be considerably higher than the rated turbine wind speed. In this case, the battery is expected to mostly charge and store the excess power which would be otherwise lost.
- Low mean wind speed: the mean wind speed will be considerably lower than the rated turbine speed, but above the cut-in speed which will allow the turbine to stay operational. In this case, the battery is expected to mostly discharge and compensate for the lack of power.
- High turbulence: the wind will be highly turbulent and the speed will vary considerably. In this case, the battery will have to often switch between charge and discharge operation. This evaluates its capability to respond quickly.
- Geographical location: we also need to look at typical wind profiles obtained from different geographical classifications. In this example, we consider two landscapes: "Rolling hills, bushes and small trees" as well as "flat landscape, open fields and meadows".

Based on these criteria, the following wind profile is defined, as shown in figure 3.9. The profile is based on real wind data obtained from the Database on Wind Characteristics, developed by the RISO national laboratories. The data was obtained at two locations: San Gorgonio in California, U.S. and Tjare in Denmark. San Gorgonio is classified as a Hill/Scrub site, at a 539 m altitude, while Tjare is classified as a flat/pastoral site, at an altitude of 4 m.

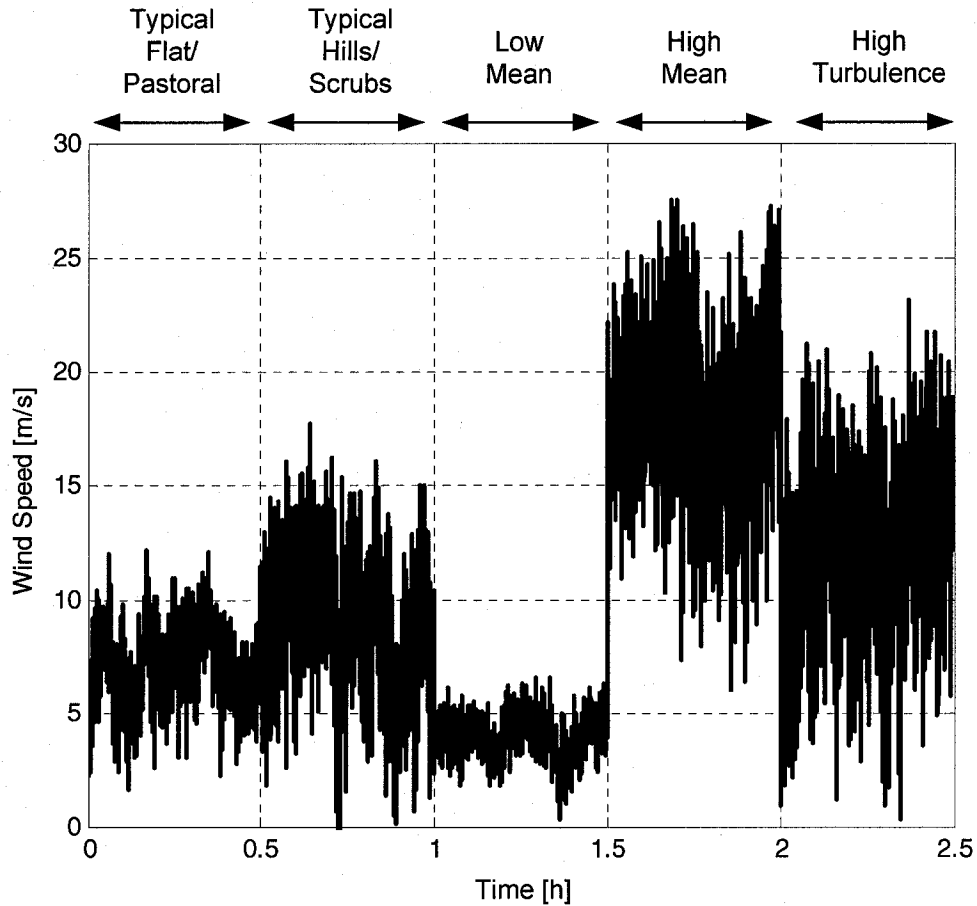


Fig. 3.9: Typical wind profile for storage device

3.4.2 Charge-Discharge Profile

In a wind-storage system, the battery acts to smooth out the output power of the wind turbine by charging and discharging accordingly. In order to provide test data for batteries in wind energy systems, we propose a typical charge-discharge profile, based on the typical wind profile presented in figure 3.9. The power output profile is obtained based on a simple DFIG model for a 2 MW (maximum power) turbine, and a simple control scheme. Since the power output varies between 0 and 2 MW, if we want the output power to be constant at 1 MW, the battery needs to be able to provide or absorb 1 MW power.

These values are all scaled down accordingly for experimental testing using a 3.3 kW VRB. The following charge-discharge profile is thus obtained, as shown in figure 3.10. The battery profile covers 2.5 hours, at a 2 second sample rate.

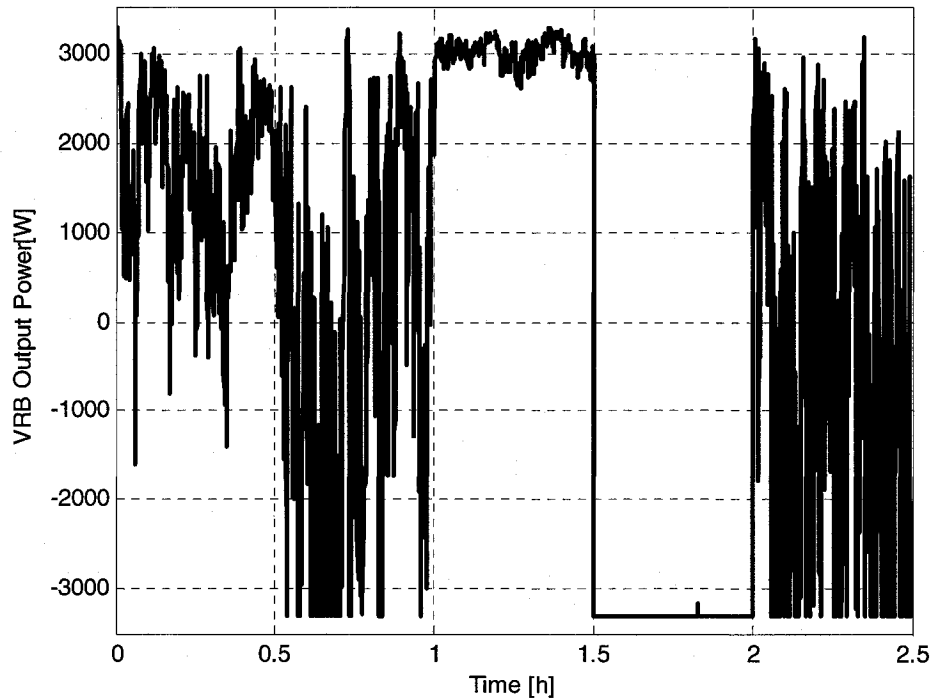


Fig. 3.10: Typical VRB output power profile

The following steps summarize battery model experimental validation using standardized wind profiles such as the one proposed in this section:

- Apply the standard wind profile to wind generator model and develop a storage power profile, based upon the operating algorithm.
- Apply the profile to both the battery and the model, acquiring SOC, current, and other relevant parameters.
- Compare the experimental and model results and determine whether the realization is representative or not, based on some predefined specifications.
- If revision is required, modify the model parameters accordingly.

3.5 VRB Performance

The VRB performance is obtained in this section using the developed model, for a 3.3 kW 3 hour system.

3.5.1 VI Transfer Characteristic

The 3.3 kW VRB VI transfer characteristic is shown in figure 3.11 for various SOC. The battery rated current is 40 A. The battery can potentially be operated for short periods of time at a maximum current of 80 A.

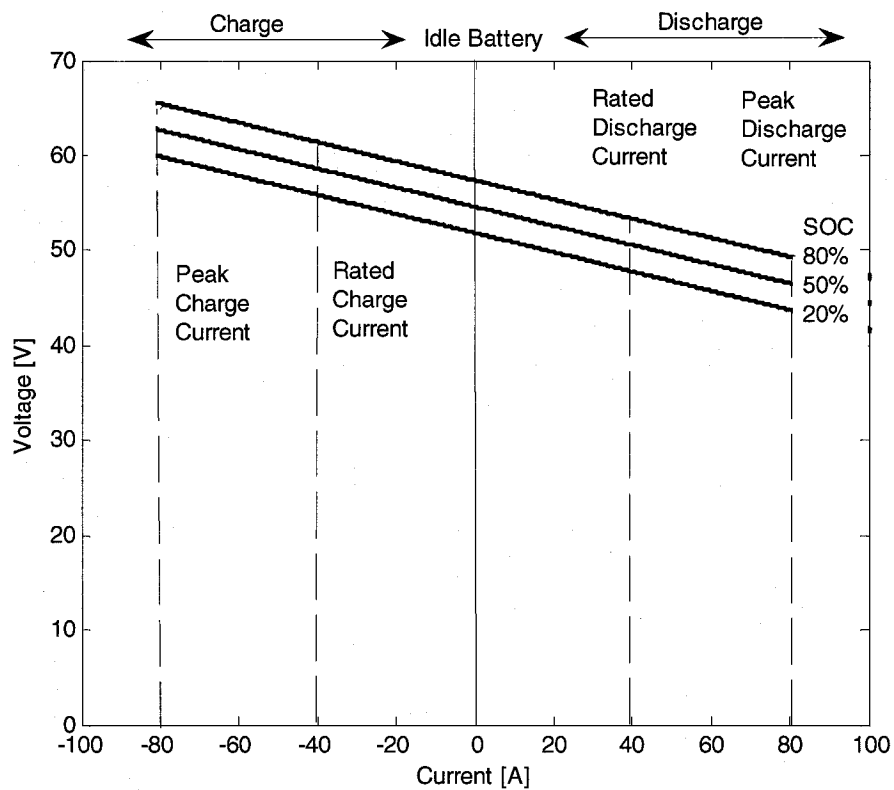


Fig. 3.11: 3.3 kW VRB VI characteristic

3.5.2 System Efficiency

The efficiency will depend on both the SOC as well as the input current. Information regarding battery efficiency under various operating conditions can be used to determine efficient operating control strategies. Both charging and discharging efficiencies are discussed.

3.5.2.1 Charge

The system dc efficiency during charging operation is defined as:

$$\eta_{charge} = \frac{P_{Input}}{P_{Stored}} \quad (18)$$

The efficiency of the battery is obtained for different input currents and SOC, as shown in figure 3.12 below. The most efficient region is between 35 and 45 A, and varies slightly depending on the SOC. This is the region in which the battery should ideally be operated. As the current increases or decreases beyond this region, there is a notable drop in efficiency.

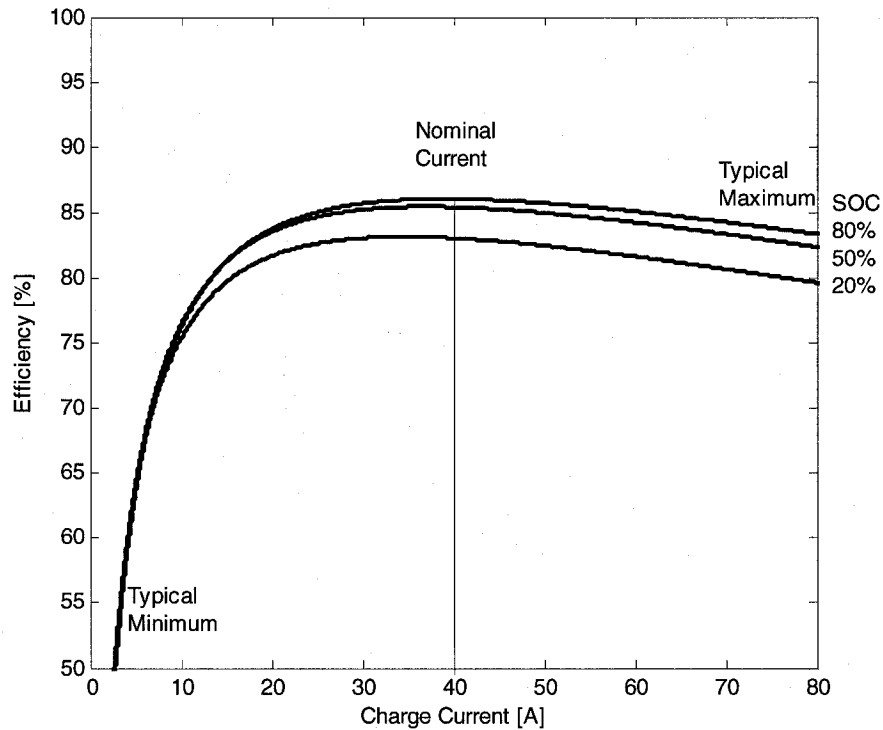


Fig. 3.12: 3.3 kW VRB charge efficiency versus input currents

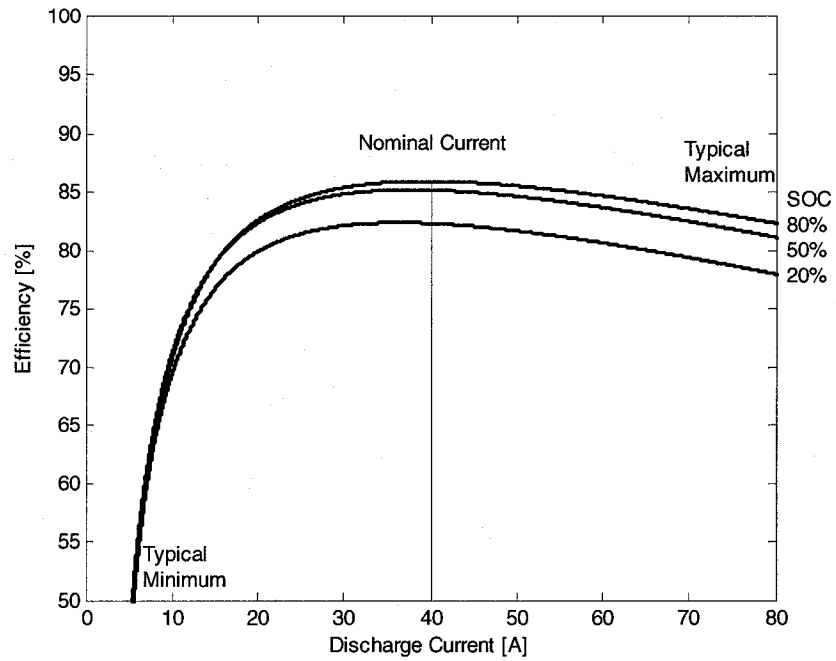


Fig. 3.13: 3.3 kW VRB discharge efficiency versus input currents

3.5.2.2 Discharge

The battery dc discharging efficiency is then considered, which is defined as follows:

$$\eta_{discharge} = \frac{P_{Electrochemistry}}{P_{Output}} \quad (19)$$

Similarly to 3.5.2.1, the efficiency of the system is considered for various SOC and currents. The result is shown in figure 3.13. The most efficient region in this case is also identified to be between 35 and 45 A. Similarly, the system efficiency drops for higher and lower currents.

3.5.2.3 Efficiency for Various Operating Conditions

Tables 4 and 5 below present the various efficiencies of a 3.3 kW VRB for its full range of SOC and power conditions, for both charge and discharge cases. The charge and discharge powers are provided in p.u. Note that this refers to the power at the output

of the battery, rather than at the cell stack. The efficiency varies similarly in both charge and discharge cases, with respect to the SOC and power.

Table 4: Charge Efficiency for Various Operating Conditions

P (p.u.)	2	1.5	1	0.9	0.8	0.7	0.6	0.5	0.4	0.3	0.2	0.1
P (W)	6600	4950	3300	2970	2640	2310	1980	1650	1320	990	660	330
SOC												
0.95	0.829	0.847	0.861	0.862	0.861	0.859	0.854	0.844	0.826	0.79	0.712	0.46
0.9	0.825	0.844	0.859	0.861	0.861	0.859	0.855	0.847	0.83	0.79	0.723	0.485
0.85	0.822	0.842	0.858	0.86	0.861	0.86	0.856	0.848	0.832	0.801	0.73	0.5
0.8	0.819	0.84	0.857	0.859	0.86	0.859	0.856	0.849	0.834	0.803	0.735	0.51
0.75	0.817	0.838	0.856	0.858	0.859	0.859	0.856	0.849	0.835	0.805	0.738	0.519
0.7	0.815	0.836	0.855	0.857	0.858	0.858	0.856	0.849	0.835	0.807	0.741	0.527
0.65	0.812	0.834	0.854	0.856	0.857	0.857	0.855	0.849	0.836	0.808	0.744	0.533
0.6	0.81	0.833	0.852	0.855	0.856	0.857	0.854	0.849	0.836	0.809	0.746	0.539
0.55	0.808	0.83	0.85	0.853	0.855	0.855	0.854	0.848	0.835	0.809	0.748	0.544
0.5	0.805	0.828	0.849	0.851	0.853	0.854	0.852	0.847	0.835	0.81	0.749	0.549
0.45	0.802	0.826	0.846	0.849	0.852	0.852	0.851	0.846	0.834	0.809	0.75	0.554
0.4	0.799	0.822	0.844	0.847	0.849	0.85	0.849	0.844	0.833	0.809	0.751	0.559
0.35	0.795	0.819	0.841	0.844	0.846	0.847	0.846	0.842	0.831	0.808	0.752	0.563
0.3	0.79	0.814	0.836	0.84	0.842	0.844	0.843	0.839	0.829	0.806	0.751	0.567
0.25	0.784	0.808	0.831	0.834	0.837	0.838	0.838	0.834	0.825	0.803	0.75	0.571
0.2	0.776	0.8	0.823	0.826	0.829	0.831	0.831	0.827	0.818	0.797	0.746	0.573
0.15	0.763	0.787	0.81	0.813	0.816	0.818	0.819	0.816	0.807	0.788	0.739	0.574
0.1	0.739	0.763	0.786	0.79	0.793	0.795	0.795	0.793	0.785	0.767	0.722	0.568
0.05	0.681	0.702	0.723	0.727	0.73	0.732	0.733	0.731	0.725	0.709	0.671	0.538

Table 5: Discharge Efficiency for Various Operating Conditions

P (p.u.)	-2	-1.5	-1	-0.9	-0.8	-0.7	-0.6	-0.5	-0.4	-0.3	-0.2	-0.1
P (W)	-6600	-4950	-3300	-2970	-2640	-2310	-1980	-1650	-1320	-990	-660	-330
SOC												
0.95	0.732	0.801	0.847	0.853	0.857	0.86	0.86	0.855	0.844	0.821	0.771	0.644
0.9	0.714	0.791	0.843	0.85	0.855	0.859	0.86	0.856	0.847	0.825	0.778	0.654
0.85	0.7	0.784	0.84	0.847	0.853	0.858	0.859	0.857	0.848	0.827	0.782	0.661
0.8	0.689	0.778	0.837	0.845	0.852	0.856	0.858	0.857	0.848	0.829	0.784	0.665
0.75	0.678	0.773	0.834	0.843	0.85	0.855	0.857	0.856	0.849	0.83	0.786	0.669
0.7	0.668	0.768	0.832	0.841	0.848	0.854	0.856	0.856	0.849	0.83	0.788	0.672
0.65	0.657	0.763	0.829	0.838	0.846	0.852	0.855	0.855	0.848	0.831	0.789	0.674
0.6	0.646	0.758	0.826	0.836	0.844	0.85	0.854	0.854	0.848	0.831	0.79	0.677
0.55	0.635	0.752	0.823	0.833	0.842	0.848	0.852	0.853	0.847	0.831	0.791	0.678
0.5	0.622	0.746	0.819	0.83	0.839	0.846	0.85	0.851	0.846	0.83	0.791	0.68
0.45	0.607	0.74	0.816	0.826	0.836	0.843	0.848	0.849	0.844	0.829	0.791	0.681
0.4	0.588	0.733	0.811	0.822	0.832	0.84	0.845	0.847	0.842	0.828	0.79	0.682
0.35	0.564	0.724	0.805	0.817	0.827	0.836	0.841	0.843	0.84	0.826	0.789	0.683
0.3	0.523	0.713	0.798	0.811	0.821	0.83	0.836	0.839	0.836	0.823	0.787	0.683
0.25	0	0.699	0.789	0.802	0.813	0.823	0.829	0.832	0.83	0.818	0.784	0.681
0.2	0	0.68	0.776	0.79	0.802	0.812	0.819	0.823	0.821	0.81	0.777	0.678
0.15	0	0.65	0.755	0.77	0.783	0.794	0.802	0.807	0.806	0.797	0.766	0.671
0.1	0	0.59	0.715	0.732	0.746	0.758	0.768	0.775	0.776	0.768	0.741	0.652
0.05	0	0	0.598	0.62	0.638	0.654	0.668	0.677	0.682	0.68	0.66	0.587

These results are useful when developing operating strategies for wind energy storage systems. The matrices need to be taken into account, and the operating strategy optimized to make sure that charge and discharge operations are done at the most efficient operating points when possible. This data also needs to be taken into account when sizing the battery.

3.5.3 Dynamic Response

In order to assess the battery dynamic performance, the worse case transition is considered: the operation is switched from a charging current of 80 A to a discharging current of -80 A. Figure 3.14 shows that the battery output voltage takes 52 ms to reach steady state when switching from charge to discharge. It takes 47 ms to reach steady state when switching from discharge to charge. The transition time is not dependent on the SOC.

The impact of the electrode capacitance is noticeable when observing the battery voltage. The transients could thus impact the battery operation at variation rates of 19 Hz and above. However, the mechanical inertia in a DFIG wind system will typically play a major role in damping the impact of rapid wind fluctuations, by acting as a low pass filter.

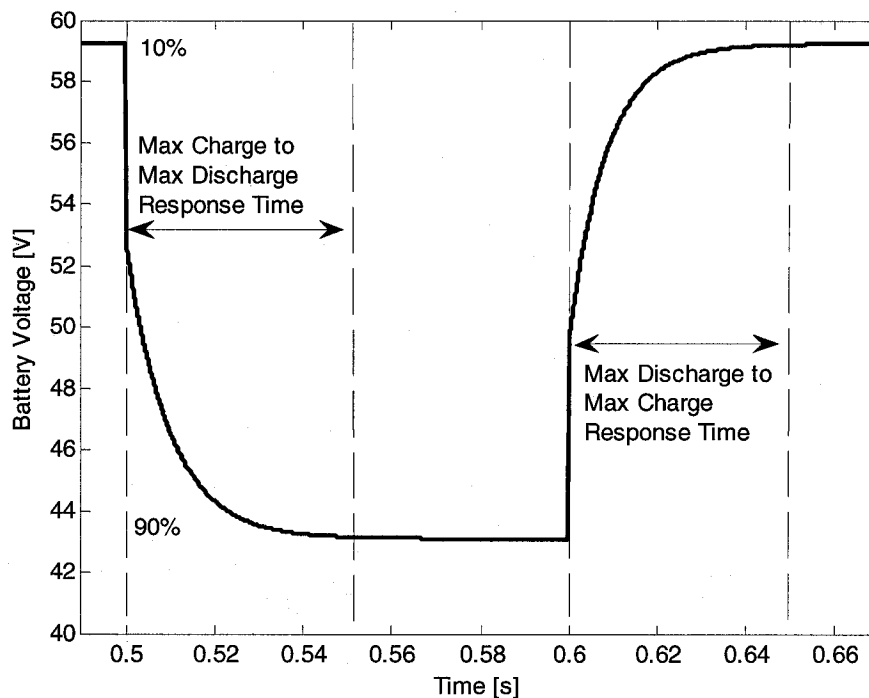


Fig. 3.14: Worse case charge to discharge transition (80 A currents)

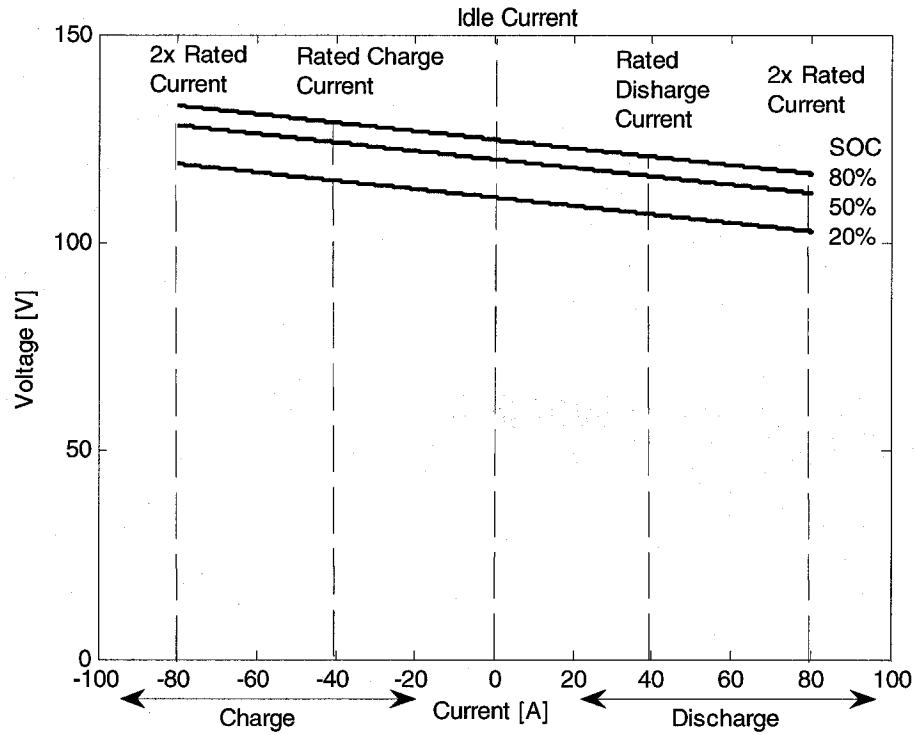


Fig. 3.15: Li-Ion VI characteristic

3.6 Lithium-Ion Performance

The Li-Ion battery performance is obtained in this section using the developed model.

3.6.1 VI Transfer Characteristic

The 40Ah Li-Ion battery VI transfer characteristic is shown in figure 3.15 for various SOC.

3.6.2 System Efficiency

In this section, both charging and discharging efficiencies are obtained, as a function of current and SOC.

3.6.2.1 Charge

The system dc efficiency during charge is defined as:

$$\eta_{charge} = \frac{P_{Input}}{P_{Stored}} \quad (20)$$

The efficiency curves are shown in figure 3.16. The battery efficiency is found to be 97% for the rated current. It drops linearly as the current increases.

3.6.2.2 Discharge

The system dc efficiency during charge is defined as:

$$\eta_{discharge} = \frac{P_{Electrochemistry}}{P_{Output}} \quad (21)$$

The efficiency curves are shown in figure 3.17. The efficiency for discharge is similar to the efficiency during charge, increasing with the current amplitude. It is also found to be 97% at the rated current.

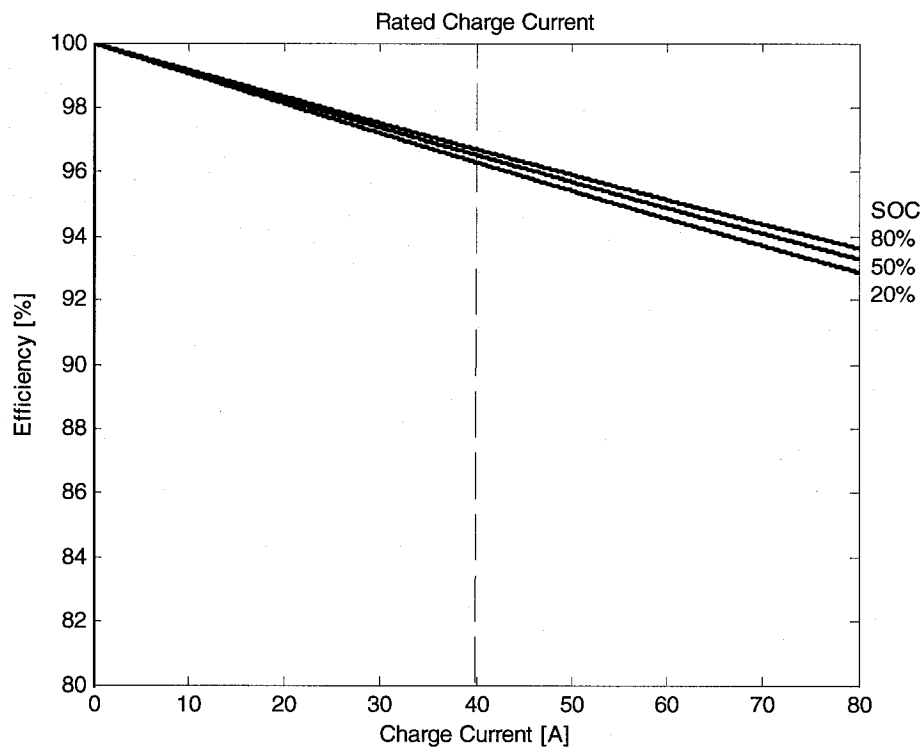


Fig. 3.16: Li-Ion battery charge efficiency versus current

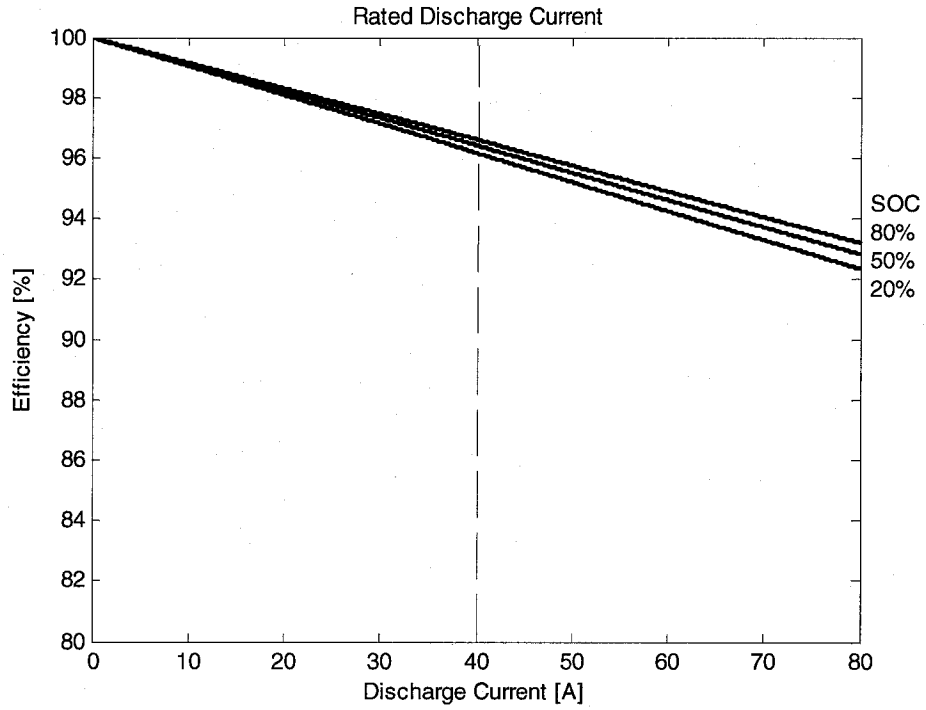


Fig. 3.17: Li-Ion battery discharge efficiency versus current

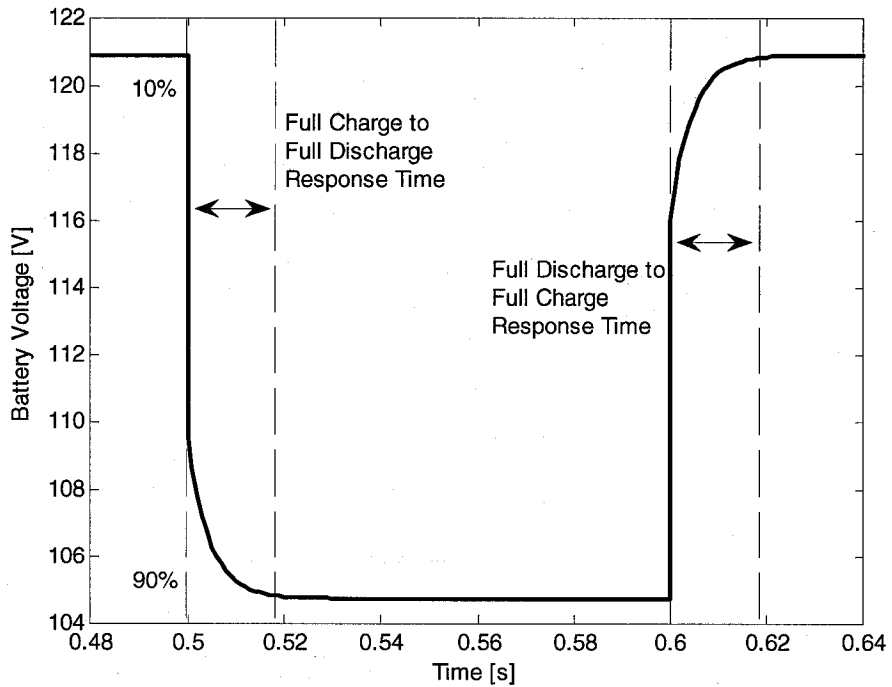


Fig. 3.18: Worse case charge to discharge transition (Initially 50% SOC, 80 A currents)

3.6.3 Dynamic Response

The worse case transition is considered: the operation is switched from a charging current of 80 A to a discharging current of -80 A. Figure 3.18 shows that the battery output voltage takes 19 ms to reach steady state when switching from charge to discharge. It also takes 19 ms to reach steady state when switching from discharge to charge. The dynamic response is not dependent on the SOC.

3.7 Li-Ion and VRB Performance Comparison

The battery models were validated and the battery performance was obtained, including the VI transfer characteristic, the efficiency and the dynamic response. In terms of technical performance, the Li-Ion battery demonstrated better results, including:

- Higher efficiency: 97% Li-Ion battery efficiency compared to 86% VRB efficiency during charge and discharge at the rated currents.
- Faster dynamic response: 19 ms response time for the Li-Ion battery compared to 54 ms for the VRB.
- SOC operating region: Similar to the VRB output voltage, the Li-Ion battery output voltage is linear for a SOC range of 20% to 80%. Both batteries should be operated in this range in wind energy applications, to avoid overcharge or undercharge issues.

The VRB advantages over the Li-Ion include better scalability, longer lifetime, and better economical performance potential (including reduced cost per kWh for larger systems). The increased performance of the Li-Ion battery might justify its use in certain situations where very high efficiency is needed, however the VRB appears to be better suited for large scale applications.

3.8 Conclusions

VRB and Li-Ion battery models were developed and implemented in SIMULINK. A systematic approach towards battery modeling and validation was presented. The batteries performances were studied and the VI transfer characteristics as well as transient responses were determined. Furthermore, data regarding the operating efficiency under various conditions was obtained. This provided insight on how to optimize the operation of these batteries, as well as a basis for comparing the two battery technologies.

The next step will consist of looking at the design of wind-energy storage systems. The VRB, which so far seems better suited for large-scale applications, will be integrated into large wind energy DFIG systems. VRB storage design and integration for DFIG systems will be examined using the developed model. Model scalability will also be considered.

Chapter 4

Wind Energy Storage system design

4.1 Introduction

A VRB model has been developed and validated. It was subsequently used to assess the battery performance, including transient operation, transfer characteristic and efficiency. The battery integration in a wind energy system will now be discussed. There are two main issues that need to be considered in wind-storage design, which are the battery sizing and the battery interface.

Battery sizing issues will first be considered. The model scalability for integration with a large wind turbine (>1 MW) is then discussed. Finally a dc-dc chopper interface is developed to control the flow of the current in and out of the battery. Its impact on battery performance is also considered.

4.2 Battery Sizing

Battery sizing for wind energy applications is a major issue, because it directly affects the economics of the project. A well sized battery can be the difference between a feasible and non-feasible project. The advantage of having an accurate battery model is that it can be used for system testing in specific applications over a desired timescale. This allows the validation of the battery system design parameters. When designing a VRB system, there are 3 sizing parameters that need to be considered: the *battery rated power*, the *battery maximum power* and the *battery energy capacity*.

The battery sizing will be dependent on the operating needs of the battery. A battery will play two roles in power systems: output power smoothing (short-term) and load leveling (medium and long-term). Typically, other flow batteries such as NaS will have a power rating of 80% of the wind farm capacity they are associated with.

The battery cell rating, as defined by the manufacturer, is the power at which the battery cell will be operated at its most efficient point. However, under contingencies, the

Chapter 4: Wind Energy Storage System Design

battery needs to be operated at higher than normal power for a short period of time (seconds), defining the maximum battery power. The energy capacity on the other hand will depend on the maximum amount of energy stored. The following are some of the issues that need to be taken into consideration in wind energy battery sizing:

- The battery system should play a role in both load leveling and power smoothing applications, in order to maximize the system benefits.
- The battery system must be able to displace the needed energy from low-demand periods to high-demand periods.
- There is a large capital cost associated with a VRB, however the cost per kWh decreases as the energy storage capacity increases;
- The battery needs to be optimized so as to reduce size and cost. On the other hand, larger capacity allows more day-ahead purchases of balancing power, which in return avoids expensive spot purchases.
- The battery system must be able to provide, at any given time, enough energy to allow the startup of backup generators such as diesel. Thus, operation at above rated currents in some transition cases must be possible for short periods of time.
- Typically, VRB size varies between 15% and 25% of the wind farm rated capacity.

In particular, in remote wind-diesel systems, the system should be optimized so as to reduce emissions and operating costs related to diesel generation. In other words, the diesel system should be shut down when possible. The battery however must also ensure that the diesel system has enough start-up time when the wind resource becomes scarce, without any electrical interruption to the local community.

Diesel system operation should be avoided below 45% of its capacity, where it becomes very inefficient. The wind-battery system must be designed, along with the control algorithms, to either allow the diesel generator to run at near-full capacity, or allow it to shut down.

Based on typical sizing in recent projects [17], the integration of a 250 kW VRB system will be examined for a wind turbine in the 1 MW range.

4.3 Scaling the VRB Model

4.3.1 System Requirements

The VRB will be integrated on the dc bus of a 1 MW DFIG wind turbine. Since the 3.3 kW model efficiency and output curves agree with results found for a 42 kW VRB [17], it will be scaled up accordingly. The VRB will have a nominal output voltage of 120 V, and thus a 100 cell stack will be needed. A system of six 42 kW VRB batteries will be used, for a total power of 0.252 MW (0.504 MW peak).

4.3.2 Modeling a 42 kW Industrial VRB

The 42 kW VRB model is derived using the same method covered in chapter 2. Similarly, the calculations are based on the worse case operating point at the end of the discharge cycle. The losses are divided into 15% internal and 6% parasitic. At that point, a minimum voltage of 105 V is reached. The maximum discharge current is 400 A. Thus for the battery to be able to provide 42 kW with 21% losses, the cell stack output power should be:

$$P_{stack} = \frac{42000}{1-0.21} = 53164.55 \text{ W} \quad (22)$$

4.3.2.1 $R_{internal}$ and $R_{Parasitic}$

$R_{internal}$ accounts for 15% of the losses, which corresponds to 7974.7 W. At an operating current of 400 A, $R_{internal}$ is found to be 0.0498 Ω . The parasitic losses are separated into fixed and variable losses, as follows:

$$P_{parasitic} = P_{fixed} + k \left(\frac{I_{stack}}{SOC} \right) = 1063.3 + 2126.6 \left(\frac{I_{stack}}{SOC} \right) \left(\frac{20}{400} \right) \quad (23)$$

The parasitic fixed and variable losses are obtained as follows:

$$R_{fixed} = \left(\frac{105^2}{1063.3} \right) = 10.37 \Omega \quad (24)$$

$$I_{pump} = \left(\frac{106.33 \left(\frac{I_{stack}}{SOC} \right)}{105} \right) = 1.0126 \left(\frac{I_{stack}}{SOC} \right) \quad (25)$$

4.3.2.2 Transient Parameters

$R_{internal}$ can now be divided into $R_{reaction}$ (0.03 Ω) and $R_{resistive}$ (0.0197 Ω), using the same proportions as in section 2.3.5. $C_{electrodes}$ is determined to be 0.06 F for a 100 cell stack, where each cell has a 6 F capacitance.

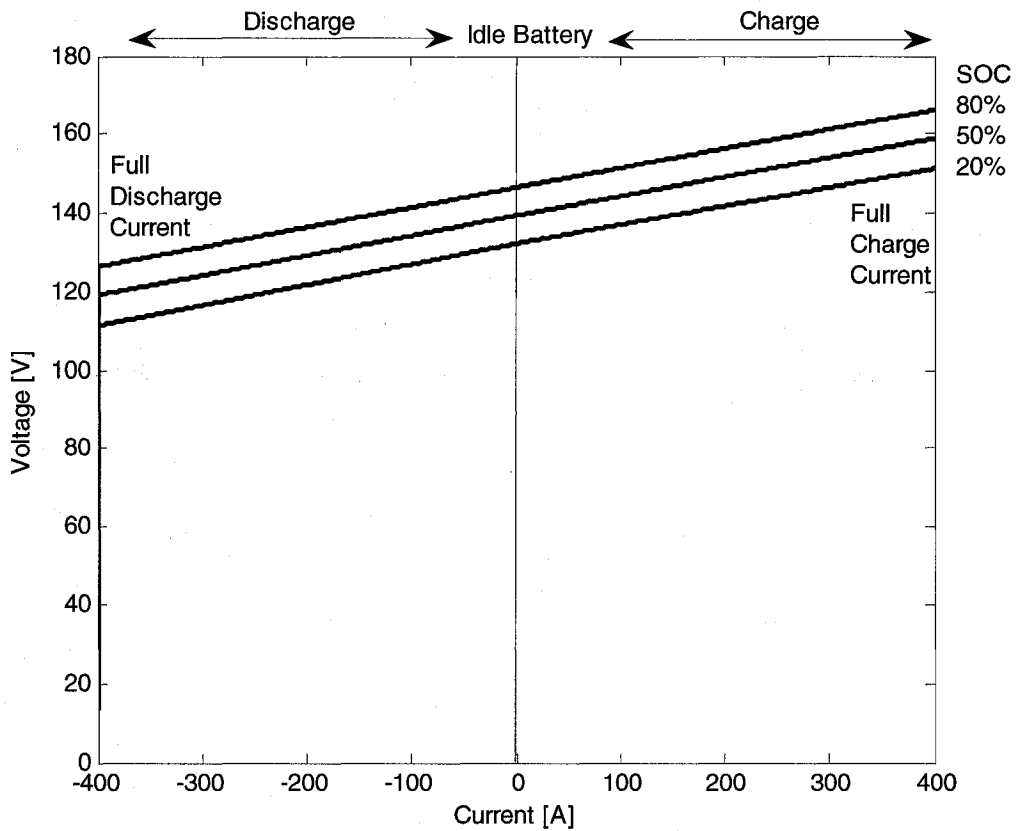


Fig. 4.1: 42 kW VRB model VI characteristic (Various SOC)

4.3.2.3 Model Implementation

The new values for R_{reaction} , $R_{\text{resistive}}$, $C_{\text{electrodes}}$ and R_{Fixed} are integrated into the initial SIMULINK VRB model. We also modify I_{Pump} , the number of cells as well as the time and power ratings. Figure 4.1 shows the 42 kW battery transfer characteristic for various SOC values.

4.3.3 VRB Thevenin Equivalent

The battery model steady state Thevenin equivalent can be obtained for various SOC. The R_{Thevenin} value corresponds to the slope of the VI transfer characteristic, while the V_{Thevenin} value can be obtained from the open circuit voltage, corresponding to idle battery operation. Table 6 shows the Thevenin equivalent parameters, for a SOC of 20%, 50% and 80%.

Table 6: Battery Steady State Thevenin Equivalent

SOC	R_{Thevenin}	V_{Thevenin}
20%	0.05	132 V
50%	0.05	139 V
80%	0.05	146 V

4.3.4 Multiple Stacks

A 42 kW battery is not sufficient for a 1 MW DFIG, where there might be a need to inject or extract up to 500 kW at any time. One possible solution which has been tested previously is to use six 42 kW VRB stacks in series [17] in order to build a 252 kW system.

In terms of modelling, there are two options: scaling up one model to 252 kW or using several 42 kW models in series. The second alternative offers better insight because, typically, separate stacks can have varying efficiency (up to 3% [17]). Having

several stack models allows the consideration of these various efficiencies. Figure 4.2 below shows an example of two stacks in series.

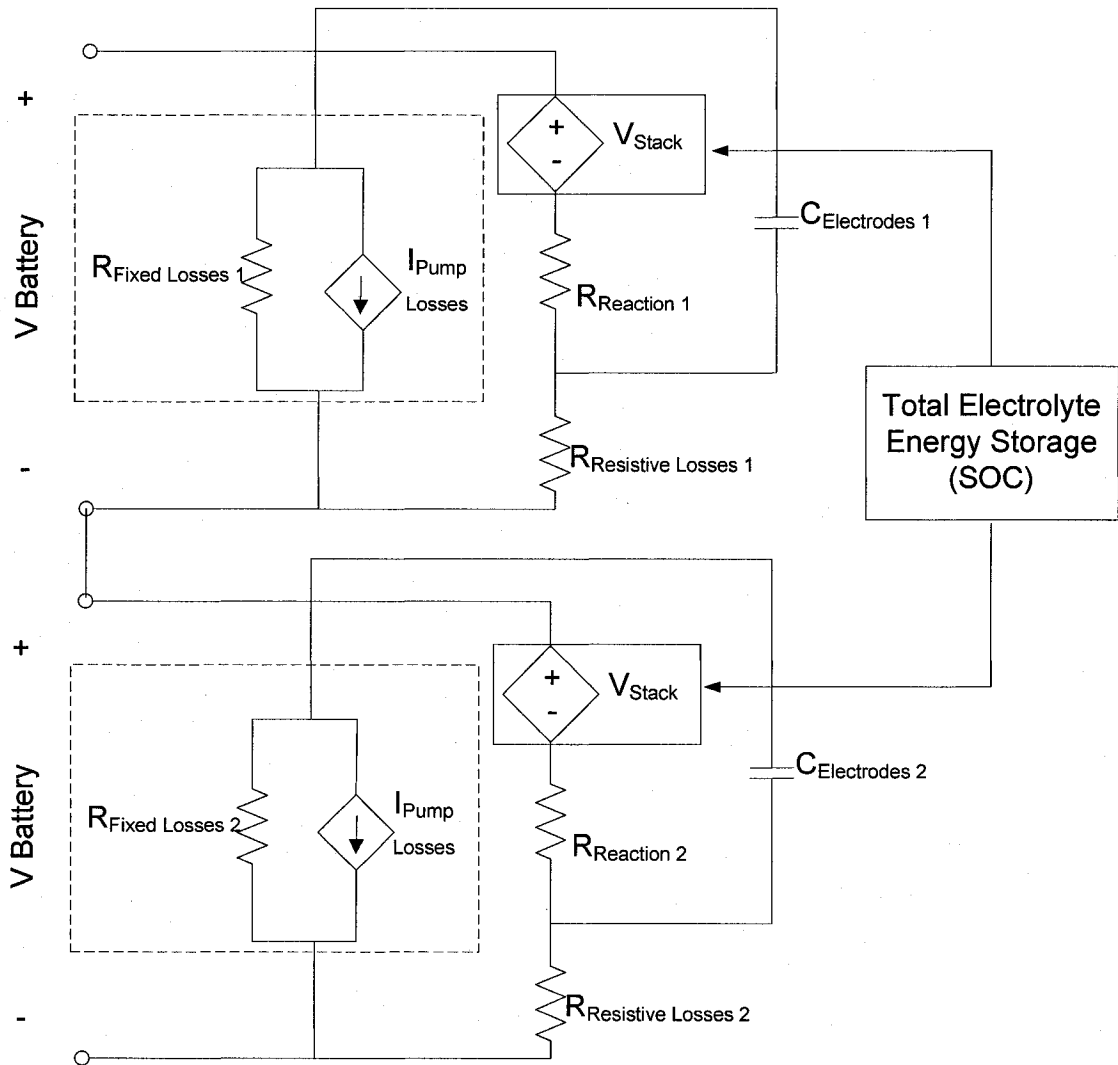


Fig. 4.2: Two VRB models in series

The varying efficiency of each stack can be considered by deriving separate parameter values for the parasitic fixed losses ($R_{\text{fixed losses}}$), the reaction losses (R_{reaction}) as well as the resistive losses ($R_{\text{resistive losses}}$). The associated pump losses (I_{pump}) will produce the same parasitic current in each sub-model; however the resulting parasitic losses will vary due to the difference in voltage across the parasitic branch. The internal stack voltages of each stack will be the same.

While there may be several physical pumps and tanks in such a system, the developed model represents these components in the following way:

- **Stack modelling:** The developed battery model is primarily a stack model, which represents the stack voltage and the associated operating losses. The voltage of each stack is dependent on the SOC, while the operating losses are modelled through various circuit parameters. A stack model is used for every battery.
- **Tank modelling:** The tank physical characteristics are not modelled in detail, because they do not have a major impact on the battery operation. It is assumed that the tanks are optimized to favour a satisfactory electrolyte flow to the stacks. The tanks are simply represented by a common variable which represents the overall SOC, shared by the various stack models.
- **Pump losses:** The pump losses are directly dependent on the operating conditions (SOC, current amplitude and battery voltage). For higher power flow, the pump losses will be greater. While physically, the pumps are associated with the tanks, each stack sub-model will represent its associated operating pump losses.

4.3.5 252 kW VRB System

The 252 kW VRB model system is shown in figure 4.3 below. Six sub-models are used. Individual stack efficiency can vary by up to 3%. This can be taken into account by modifying the individual sub-model parameters ($R_{\text{fixed losses}}$, R_{reaction} , $R_{\text{res losses}}$) accordingly.

This battery bank can be operated at a maximum of 400 A. With a 1200 V dc bus, this would translate into an output power of 480 kW, which meets our needs. In terms of energy content, the VRB tanks should be sized based on economic factors, as well as the requirement to operate the battery between 20% and 80% SOC at all times.

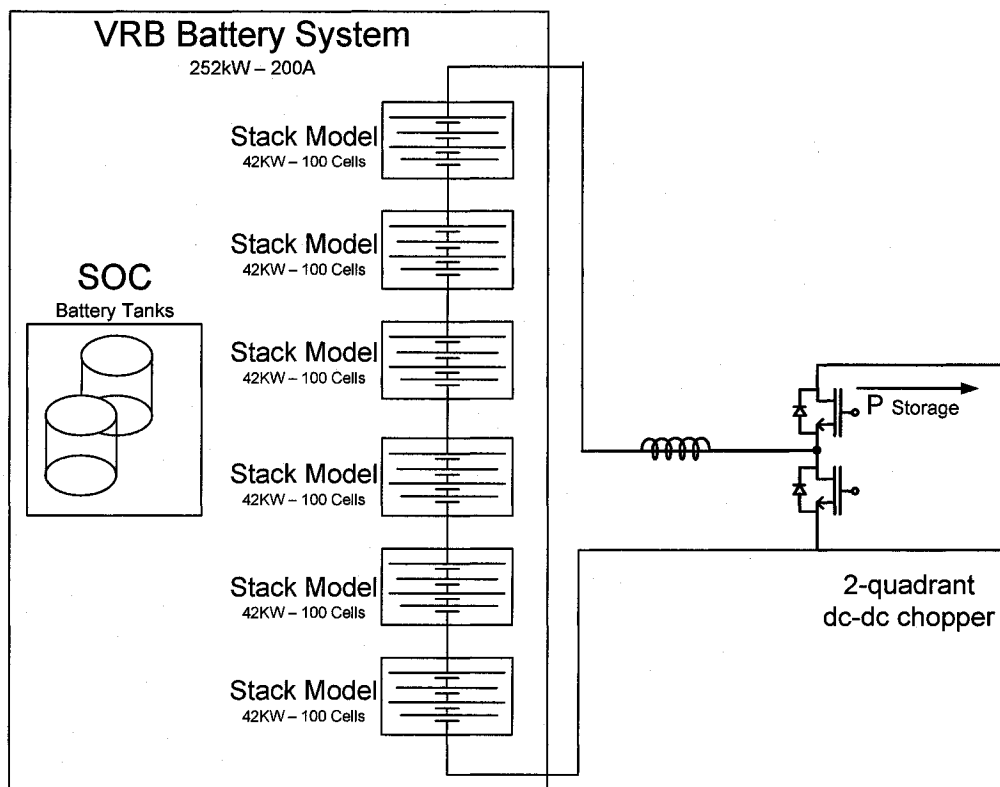


Fig. 4.3: 252 kW battery bank

4.4 Battery Converter Interface

4.4.1 Buck-Boost dc-dc Converter

A dc chopper interface is used to control the current direction and amplitude through the battery. Figure 4.4 below shows the implementation of such a dc chopper in SIMULINK using the VRB model. The DFIG bus has been initially modeled as an ideal dc source. The dc chopper efficiency and controls will be examined for a 42 kW battery model.

4.4.2 Inductance Design

Part of the converter design involves determining an appropriate value for the battery side inductance. There will be a dc current ripple which will be dependent on the value of that inductance. This ripple will result in battery heating, as well as increased battery cycling, which can have a negative impact on the battery life.

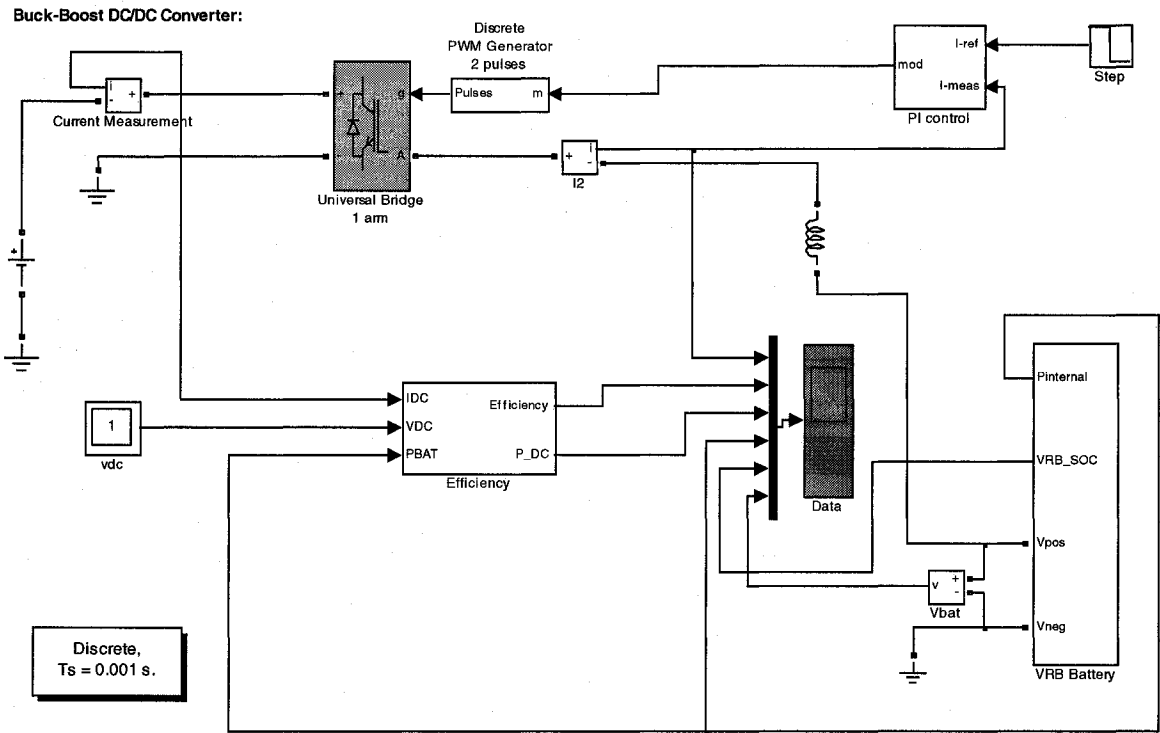


Fig. 4.4: Dc chopper implementation for VRB

A larger inductor value will result in a smaller current slope, and thus a smaller ripple. On the other hand, this results in a smaller response time for the controller. While the ripple can not be fully eliminated, a ripple of 10% or less of the dc current magnitude is deemed acceptable.

The dc bus voltage is 1200 V, and a current ripple of 10% or less for currents of up to 400 A is required. Thus the value of the inductance is obtained the following way:

$$\text{Switching Frequency} = 1080\text{Hz} \quad (26)$$

$$\Delta V = L \frac{\Delta i}{\Delta t} \quad (27)$$

$$L = \frac{\Delta V \times \Delta t}{\Delta i} = \frac{1200 \times 4.62e^{-4}}{40} = 14 \text{ mH} \quad (28)$$

An inductor of 14 mH provides the best trade-off between response speed and current ripple. It produces a ripple of 10% (figure 4.7), while generating an acceptable response time (figures 5.5 and 5.12).

4.4.3 Converter Controls

Figure 4.5 below shows that, by setting a reference current indirectly through the modulation index of the dc chopper, we are able to charge and discharge our battery at 400 A. The battery model used in this specific example is rated at 42 kW - 1 minute.

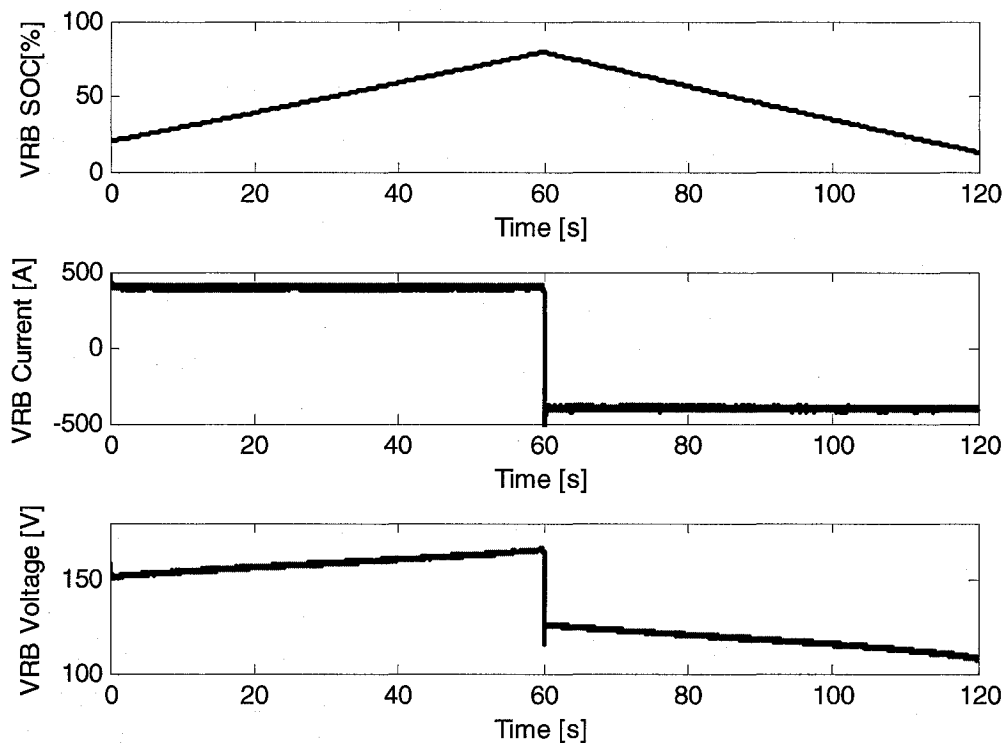


Fig. 4.5: Charging and discharging the 42 kW VRB using a dc chopper (400 A and -400 A respective current rates, 160 V, 1 min-42 kW VRB)

Since the current rate is dependent both on the modulation index, as well as the battery output voltage which varies with the SOC, a PI control scheme is used as shown in figure 4.6 below.

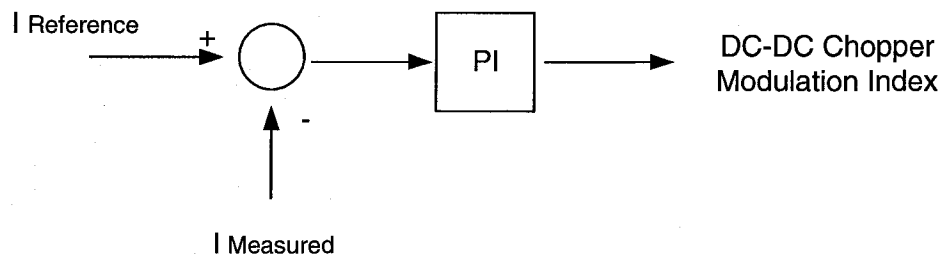


Fig. 4.6: Dc-dc chopper PI control

The response time of the controller can be observed to be negligible in figure 4.7, which shows the charge and discharge currents response to the reference. There is a ripple on the dc current of 30 A. This translates into about 10% for a 300 A current. This noise ripple depends on several factors including the PI controller settings and sample time, as well as the inductance used between the chopper and the battery.

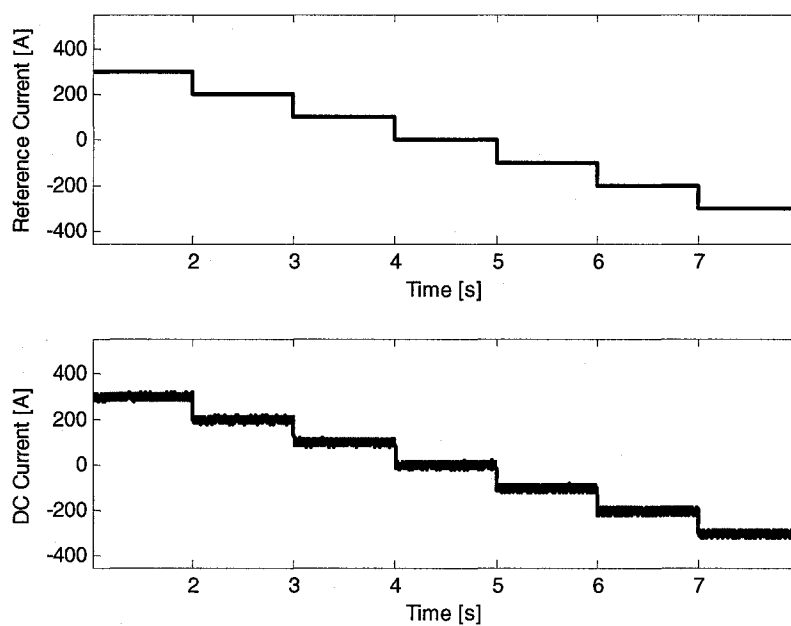


Fig. 4.7: 42 kW VRB current control using the dc chopper (180 V dc bus, varying current reference)

4.4.4 VRB dc efficiency

The system dc efficiency during charge and discharge, including chopper losses, will be examined in this section. As was shown in chapter 2, the battery is more efficient for higher SOC. The SOC will be arbitrarily fixed at 50% as the reference current is

varied in order to determine the system efficiency at various operating points. The charge and discharge efficiencies are defined as follows:

$$\eta_{Discharge} = \frac{P_{DC_BUS}}{P_{Battery_Internal}} \quad (29)$$

$$\eta_{Charge} = \frac{P_{Battery_Internal}}{P_{DC_BUS}} \quad (30)$$

The discharge is found to be most efficient at currents between 175 and 215 A, close to the rated current (200A). The battery system efficiency reaches 82.5 % in this region. It drops considerably for currents below 100 A and above 400 A. This can be seen in figure 4.8. In figures 4.9, charging operation is found to be most efficient at currents between 120 A and 170 A. The battery system efficiency also reaches 82.5% in that region.

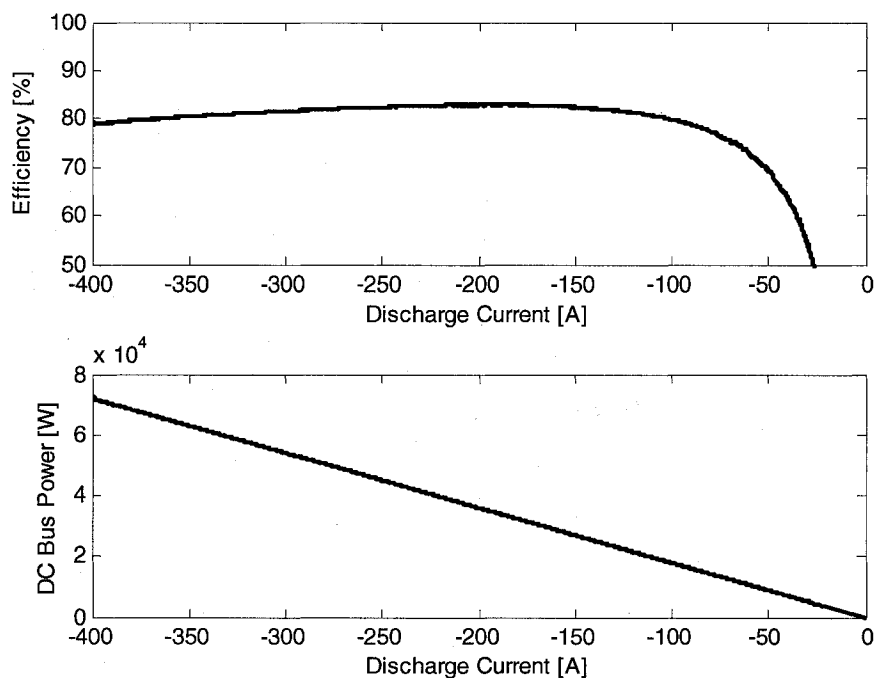


**Fig. 4.8: Discharge efficiency versus current for VRB-Chopper
160 V dc bus, 50% SOC, 42 kW VRB**

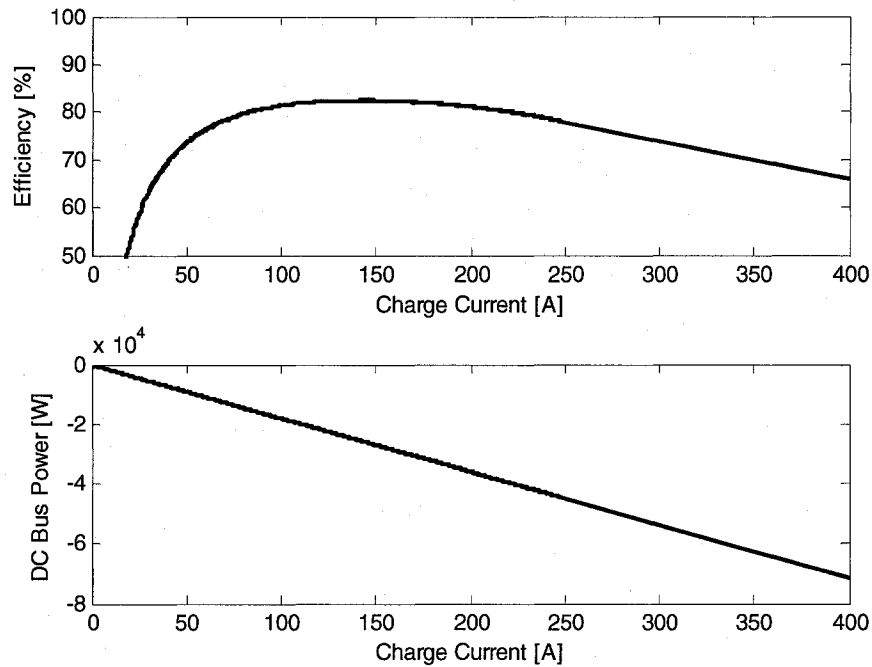


**Fig. 4.9: Charge efficiency versus current for VRB-Chopper
160 V dc bus, 50% SOC, 42 kW VRB**

The VRB efficiency values agree with the ones presented in [17]. In field trials, overall dc battery efficiencies were found to be between 82% and 85%.

In comparison with the battery efficiency prior to the dc chopper implementation, the efficiencies have dropped slightly. The charge efficiency was found to be around 86% in chapter 3 in the best operating regions. This translates into a drop in efficiency of 3.5% during charge and discharge. Typically converter losses vary around 5%, and thus the results found are satisfactory. This brings the overall system round-trip efficiency to 68%.

4.5 Conclusions

In this chapter, a dc-dc chopper interface was developed for the VRB model, in order to control the power flow in and out from a dc bus. VRB design and sizing issues were discussed, and a 42 kW battery model was developed for larger wind turbine

Chapter 4: Wind Energy Storage System Design

applications. Multiple models were used in series to represent a 252 kW multiple-stack VRB system.

The system performance was evaluated including the transient response and system efficiency. The VI transfer characteristic was obtained for various SOC, and the model Thevenin equivalent was derived. The converter losses were found to reduce the system dc efficiency by 3.5% during charge and discharge. The VRB-chopper system can now be integrated in various DFIG systems in order to smooth out turbine power output under fluctuating wind conditions.

Chapter 5

Wind Energy Storage System Implementation

5.1 Introduction

In the previous chapter, a VRB storage system was designed for large DFIG wind turbines as a solution to storing and releasing energy as required. A dc-dc interface was developed to control the power flow. Its impact on system performance was also examined. This system will now be integrated in a DFIG system. The storage system will be used to level the turbine output power, by charging or discharging accordingly.

This will be done using various available DFIG models: the detailed DFIG system model, the average DFIG system model and the simple DFIG system model. These models provide varying accuracies and simulation speeds.

The detailed model is well suited for short-term simulations (seconds). The average model on the other hand is better suited for medium and long term simulations (minutes and hours), and provides a good tradeoff between accuracy and simulation speed. Finally, the simple model is best suited for real-time simulations. The first two cases will adopt a localized storage scheme, while the last case will use a centralized storage scheme.

5.2 Storage Schemes

There are two possible schemes to consider: local and centralized storage. In the local storage scheme shown in figures 5.1, the storage system is integrated on the dc bus of the DFIG system. The advantages include a dedicated storage device for each DFIG system. There is no need for an additional dc-ac converter to connect the storage system to the grid, as the ac side converter of the DFIG system is used for that purpose. The objective is to smooth the power delivered to the grid by the turbine. This can be summarized in the following equation:

$$P_{Wind} + P_{Storage} = P_{Grid} \quad (31)$$

P_{Grid} constant can be made constant by controlling the power flowing in and out of the storage device.

The centralized storage scheme is shown in figure 5.2 below. In this setup, the storage system is connected directly to the grid, independently of the DFIG. In that setup, the storage can be sized to accommodate several turbines simultaneously. However there is a cost disadvantage because an additional dc-ac inverter is required. This is thus better suited for larger wind farms, since the cost per kWh of a VRB drops as its capacity increases.

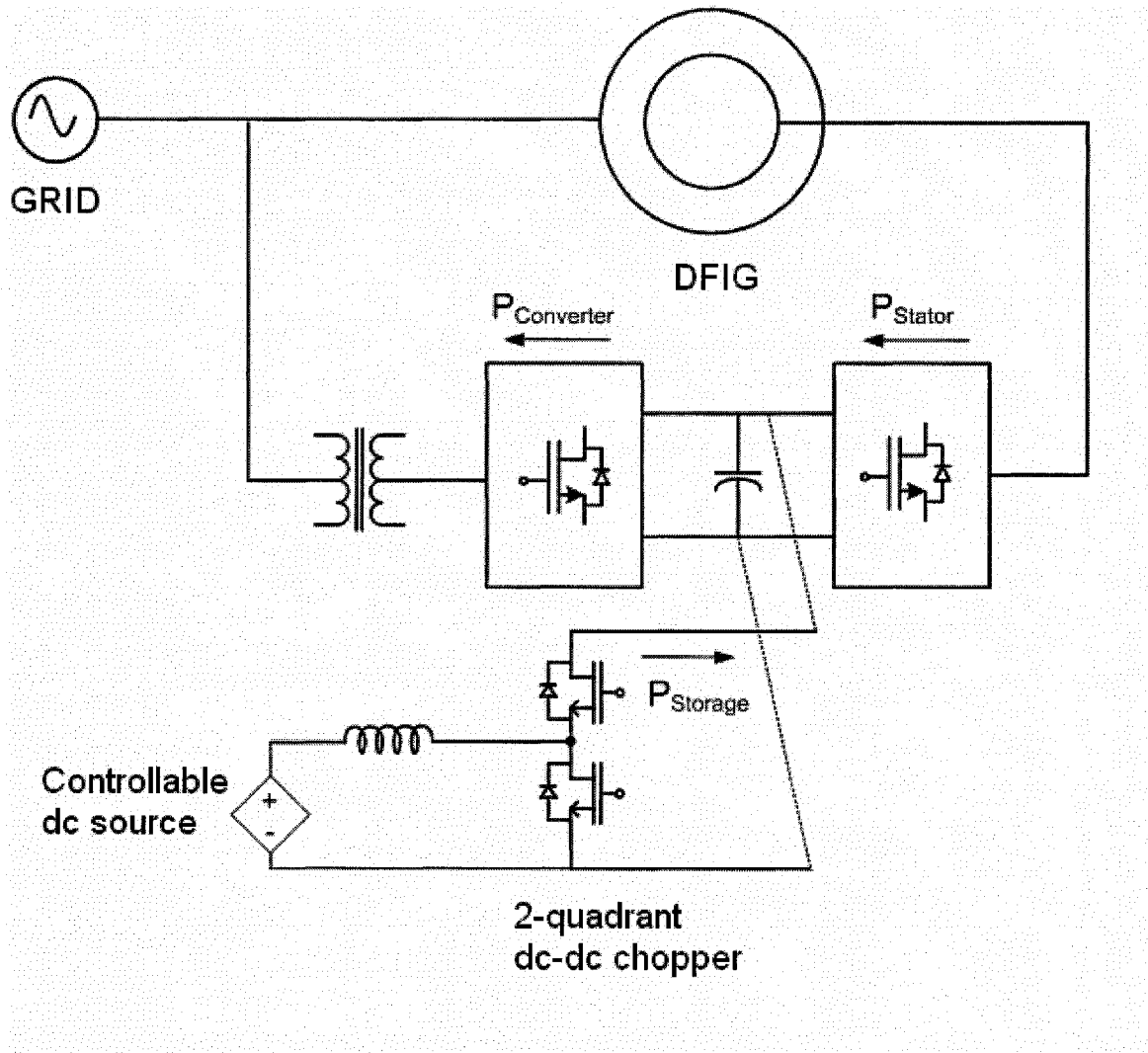


Fig. 5.1: Local DFIG storage system

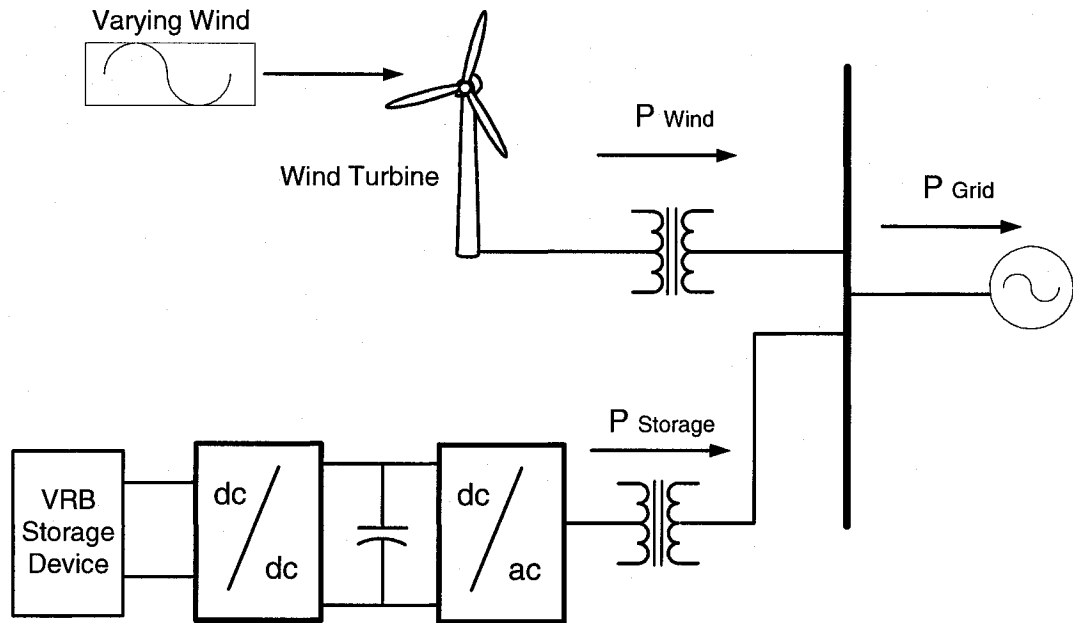


Fig. 5.2: Centralized storage system

5.3 DFIG Detailed System Model

5.3.1 Model Operation without Storage

The integration of a VRB storage system in the DFIG wind turbine will be examined. Since the battery output is a dc voltage, and the battery is controlled through a dc-dc chopper, there is an interest in placing the storage system on the dc bus of the DFIG. Injected currents will affect directly the line-side of the DFIG system without any negative impact on the DFIG operation.

The DFIG detailed model available in the SimPowerSystems SIMULINK toolbox is used. The model is adjusted to reflect the operation of a single 1.5 MW wind turbine. This DFIG system operates best at a rated wind speed of 10 m/s.

5.3.2 Controlling the Battery System

The battery is controlled through the dc-dc chopper, using a PI block, which sets the current in and out of the battery current to the desired reference, as discussed in section 4.4.

The VRB storage system will be used to regulate the line-side output power of the DFIG turbine. This will result in a smoother power output to the grid as the wind fluctuates over a short-term (seconds) and medium-term (minutes) time frame.

In order to achieve this, the system controls must be verified. A second PI controller is used in this case to control the power injected or extracted from the battery. The error signal is obtained by comparing the mean power output of the DFIG to the reference power, as shown in figure 5.3 below.

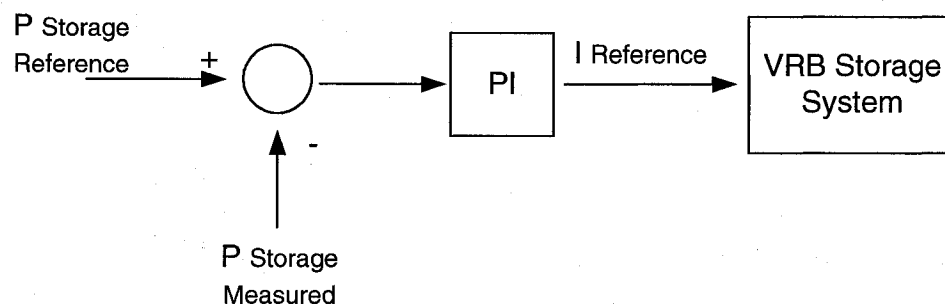
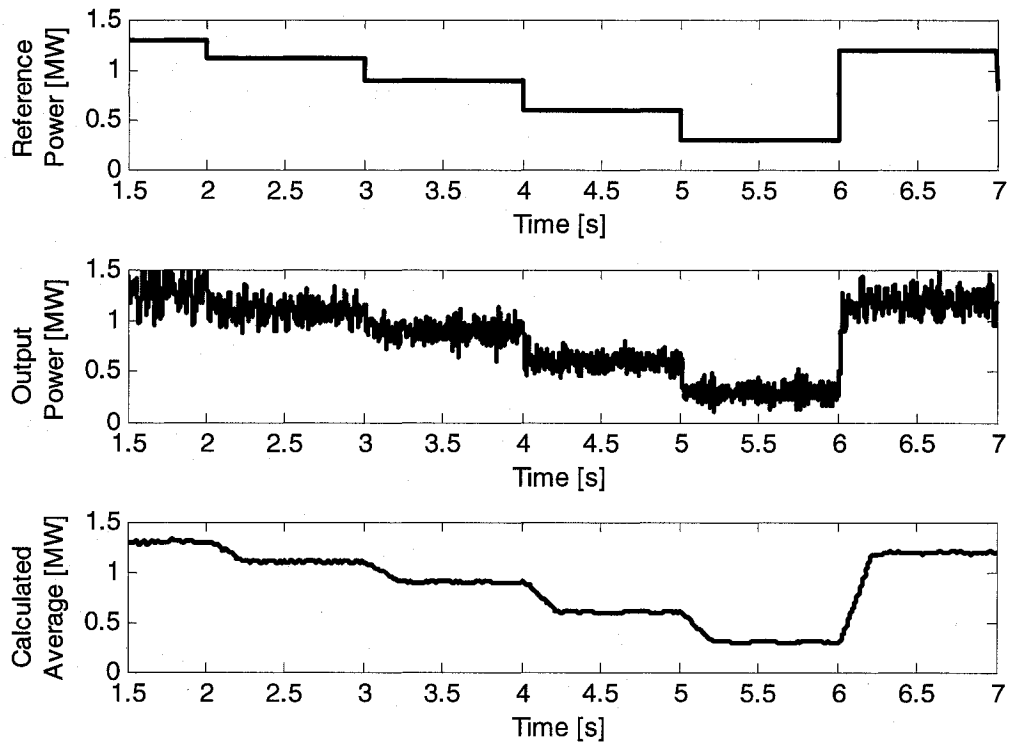


Fig. 5.3: DFIG system power reference controls

In order to test the controls, the system ability to respond to a varying reference power is verified in figure 5.4 below. The output power ripple was existent prior to VRB integration when using the detailed DFIG system model. It can partly be improved by increasing simulation time step.

The output power does a good job of following the reference power by injecting or absorbing power using the VRB as required. The response time of the control system is observed in figure 5.5 below.



**Fig. 5.4: Power output response (DFIG detailed model, 252 kW VRB)
50% SOC, 1200 V dc Bus, 252 kW VRB**

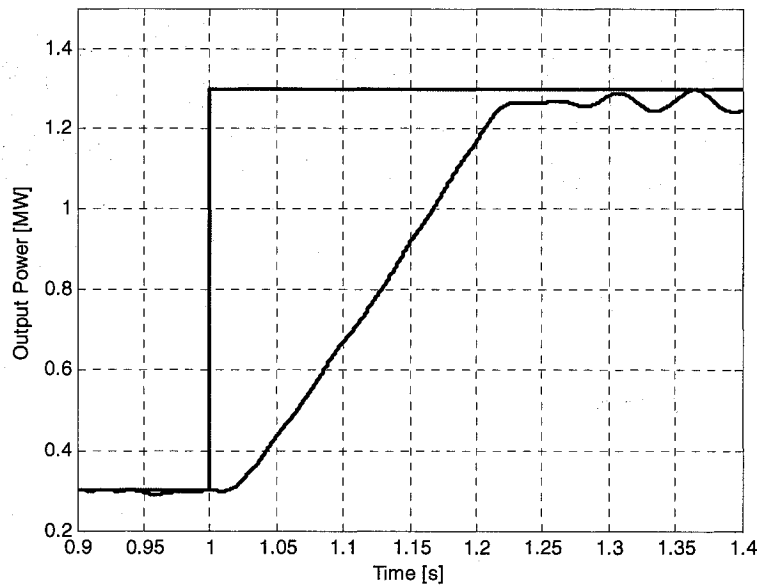


**Fig. 5.5: Power output response time (DFIG detailed model, 252kW VRB)
50% SOC, 1200 V dc Bus, 252 kW VRB**

The worse case transition response time was tuned down to 0.40 s. This is satisfactory for this application because, in the case of faster wind variations, the DFIG turbine will take care of filtering the high frequency wind oscillations.

The next step is to determine the value of the system output reference power during normal operation. The used DFIG turbine can output 0.85 MW at a rated wind speed of 10m/s, which will be used as the power reference. Thus the storage system will act to keep the output power at 0.85 MW, regardless of wind variations.

The storage system reference power will be determined as the difference between the actual DFIG power output, and the desired one. The overall controls are shown in figure 5.6 below.

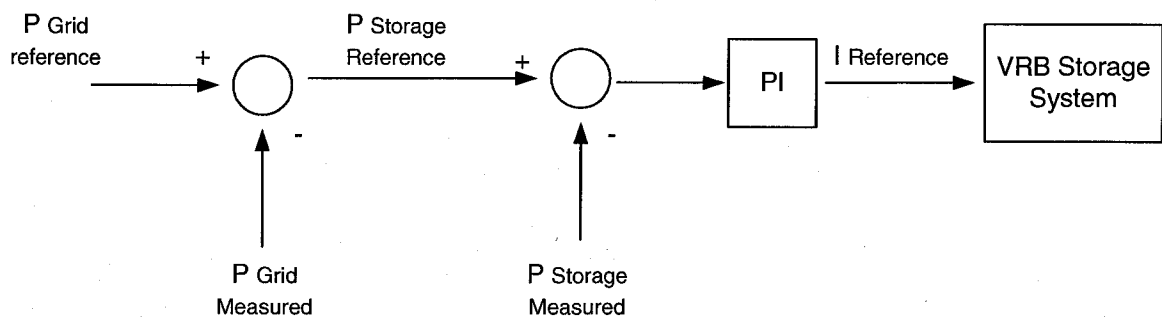


Fig. 5.6: Overall control system

5.3.3 Wind System Operation

In order to test the validity of the control system, two simple cases are observed. In the first case, the wind suddenly drops from its nominal value of 10 m/s, to 6 m/s. Figure 5.7 below shows the output power as well as mean output power with and without the VRB storage system on the dc bus.

There is a significant improvement: the power output will remain at an average of 0.85 MW when the battery storage is active. The injected current on the dc bus, the drop in the SOC as well as the Battery output voltage are shown in figure 5.8.

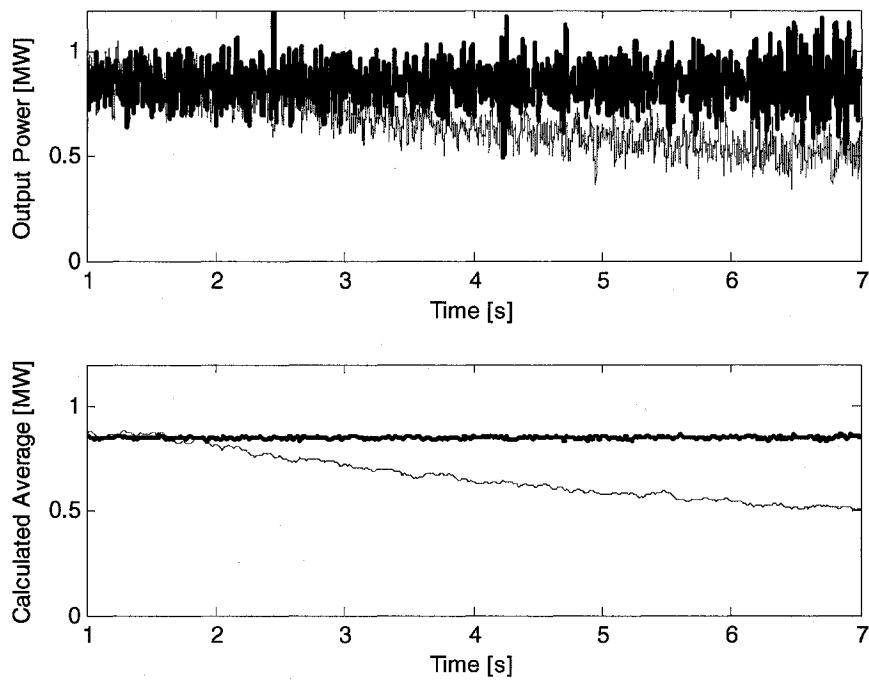


Fig. 5.7: Power output after sudden wind drop (DFIG detailed model, 252 kW VRB)
 From 10 to 6 m/s, 50% SOC, 252 kW-1 h VRB, 0.85 MW reference power

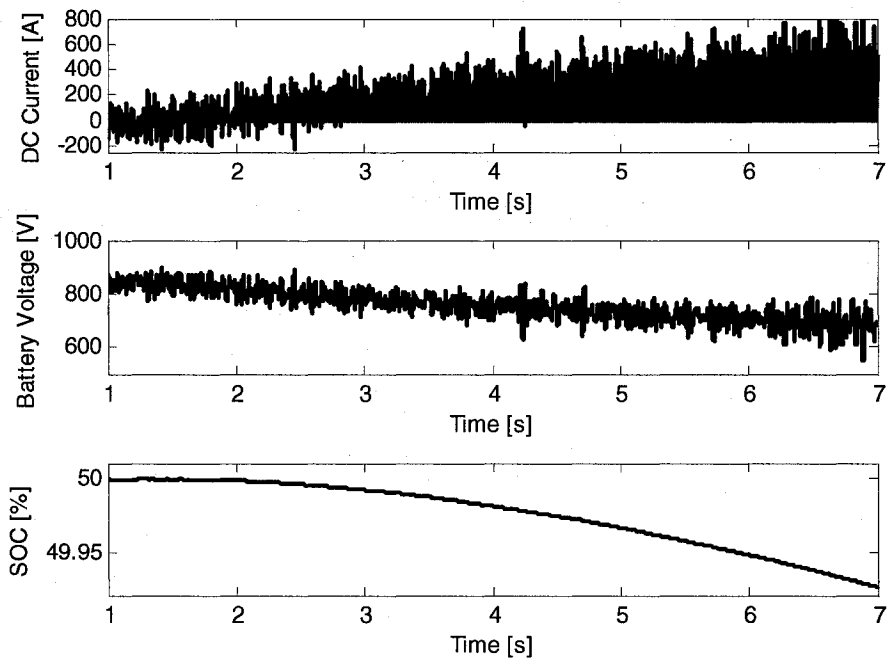


Fig. 5.8: VRB system after sudden wind drop (DFIG detailed model, 252 kW VRB)
 From 10 to 6 m/s, 50% SOC, 252 kW-1 h VRB, 0.85 MW reference power

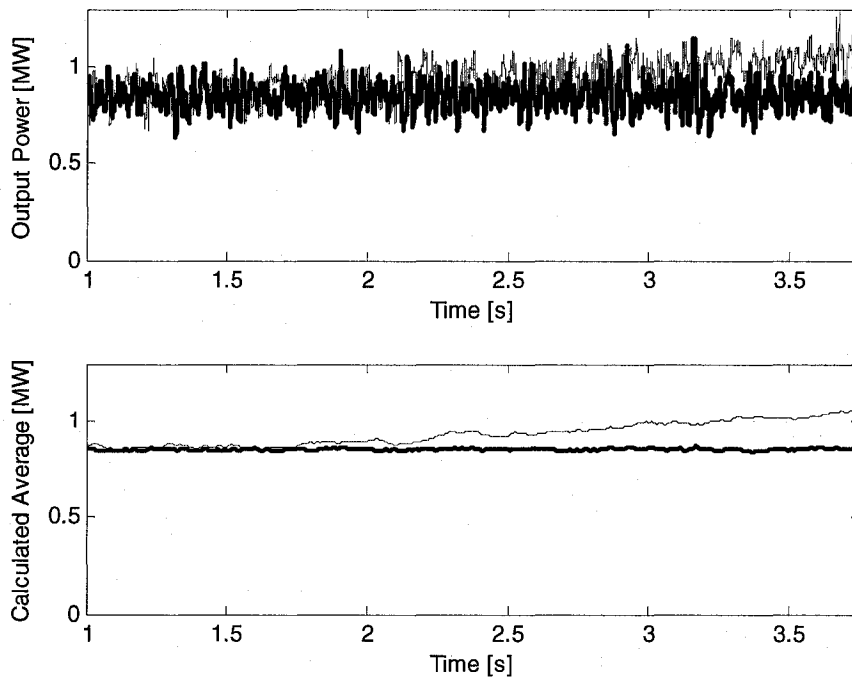


Fig. 5.9: Power output after sudden wind rise (DFIG detailed model, 252 kW VRB)
 From 10 to 13 m/s, 50% SOC, 252 kW-1 h VRB, 0.85 MW reference power

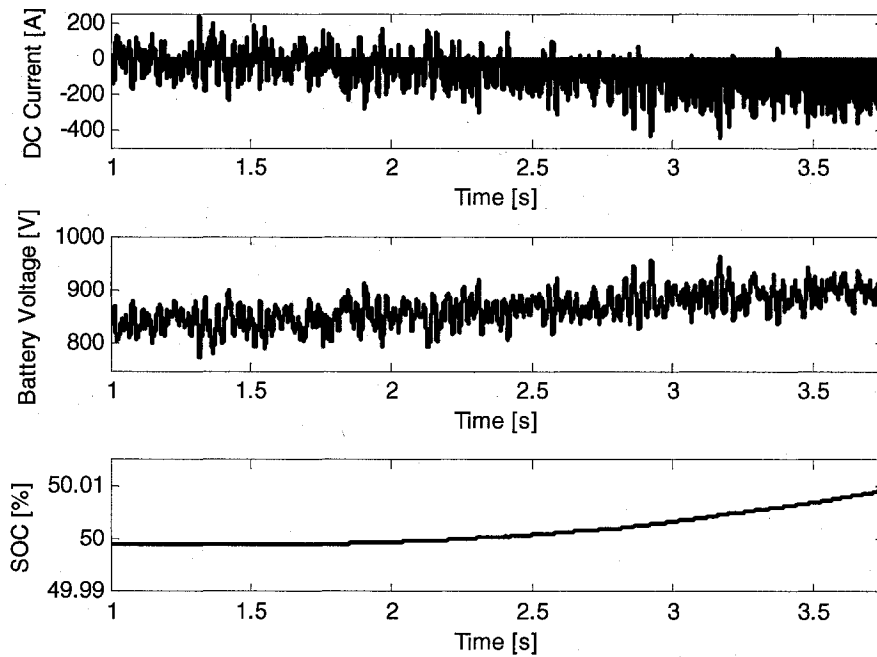


Fig. 5.10: VRB system after sudden wind rise (DFIG detailed model, 252 kW VRB)
 From 10 to 13 m/s, 50% SOC, 252 kW-1 h VRB, 0.85 MW reference power

The next case that is considered is a sudden wind rise from 10 to 13 m/s. Figure 5.9 shows that the output power is maintained at 0.85 MW when the VRB system is used. Figure 5.10 shows the operation of the VRB system.

In this section, the preliminary implementation of a VRB on the dc bus of a DFIG system was shown. The storage system was used to smooth out the power. This computationally heavy DFIG system model is mostly suited for short-term simulations (seconds). There is thus a need to examine other possible DFIG system models better suited for medium and long term simulations.

5.4 DFIG Average System Model

5.4.1 Operation without Storage

Another model available through the SimPowerSystem library is the DFIG system average model. This model is less computationally heavy since it does not consider converter switching losses and harmonics. It is ideal for medium-term (minutes) simulations.

The same wind storage scheme discussed in section 5.3 is used, which consists of integrating the VRB on the dc bus of the DFIG system, thus taking advantage of the line-side dc-ac converter.

5.4.2 Controlling the Battery System

In this section, the controls of the storage system are verified. They have been slightly modified from the detailed model controls. Figure 5.11 shows the response of the system to a varying output power reference.

Figure 5.12 below shows a worse case transition, where the reference output power is switched from 0.3 MW to 0.9 MW. The response time is of 0.17 seconds, which is satisfactory since higher frequency wind fluctuations would be filtered out through the DFIG mechanical inertia.

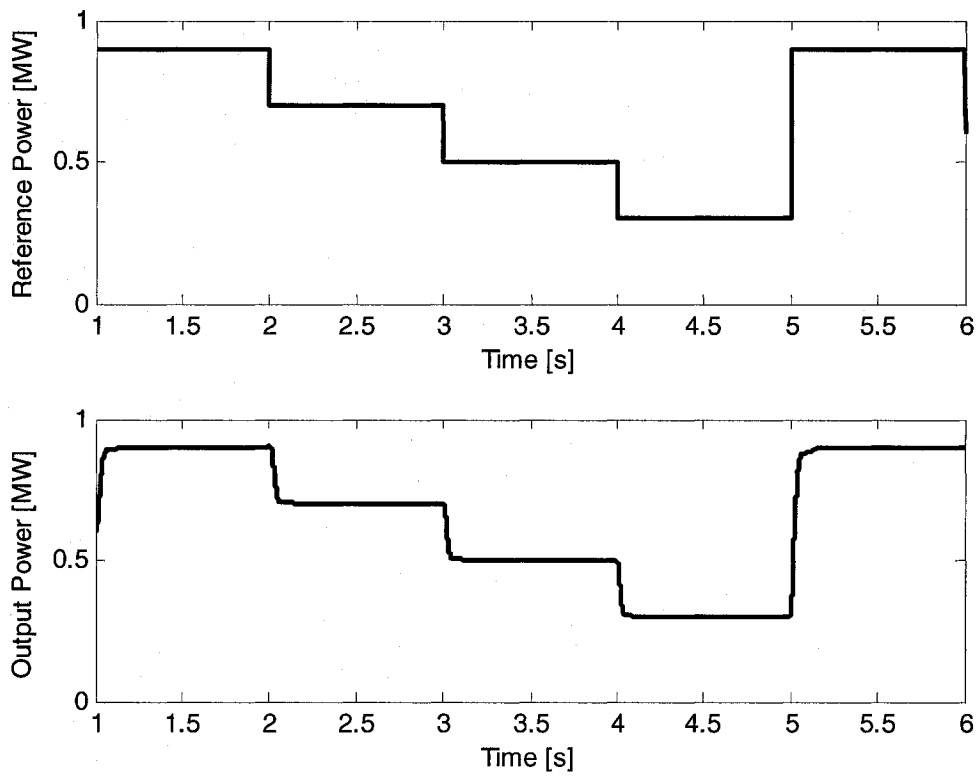
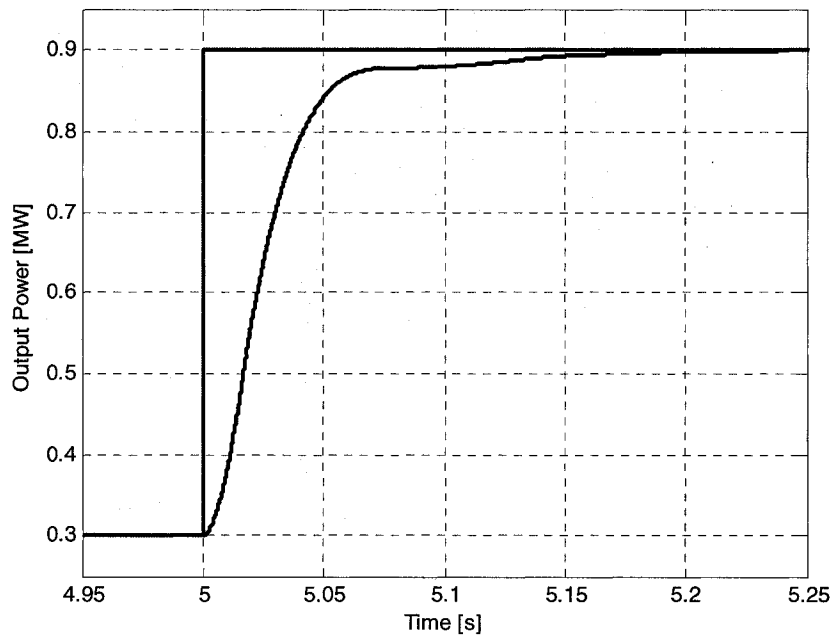


Fig. 5.11: Power output response (DFIG average model, 252 kW VRB)



**Fig. 5.12: Power output response time (DFIG average model, 252 kW VRB)
(Reference and output power traces)**

5.4.3 System Operation

In order to test the system, the wind profile shown in figure 5.13 below is used. Figure 5.14 shows the Average DFIG turbine model power output obtained from this wind profile, prior to the integration of the VRB storage system.

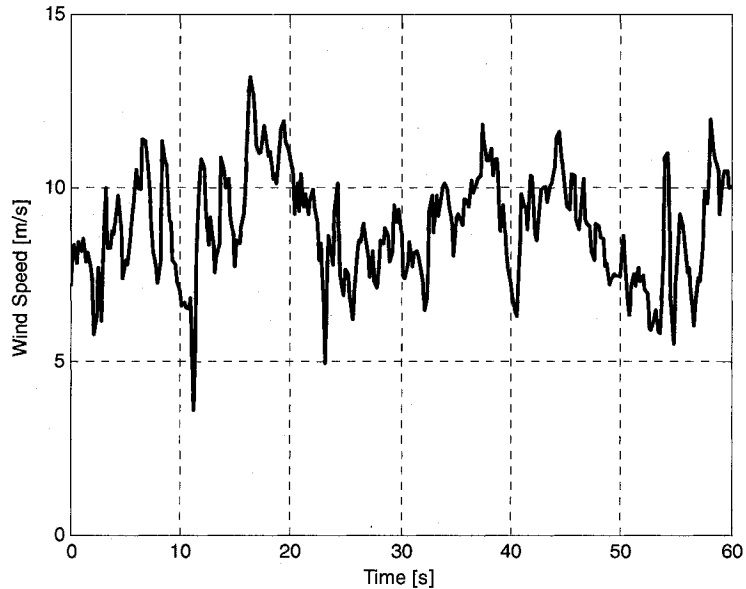


Fig. 5.13: Wind profile

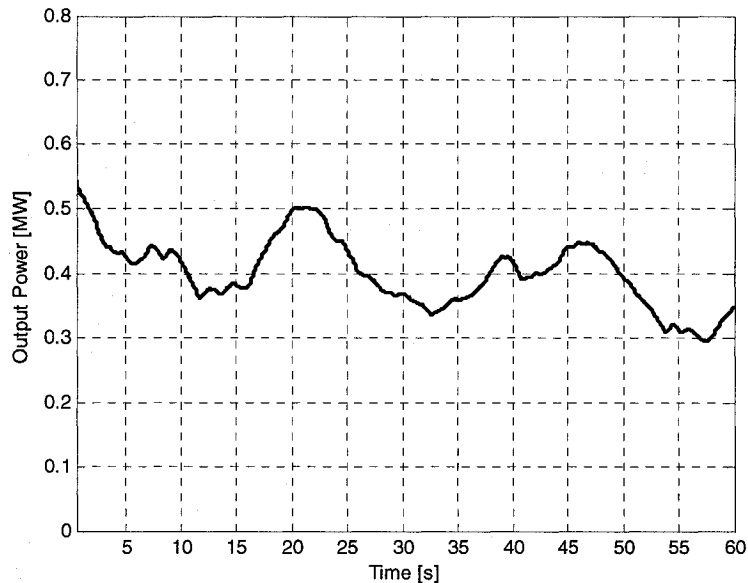


Fig. 5.14: Turbine output power without storage (DFIG average model, 252 kW VRB)

The turbine output fluctuates considerably, and thus the need for a VRB as a means to smooth out these variations is justified. Figure 5.15 below shows the results obtained when the VRB storage system and corresponding controls are added to the model. The power output is centered on the set reference of 0.4 MW.

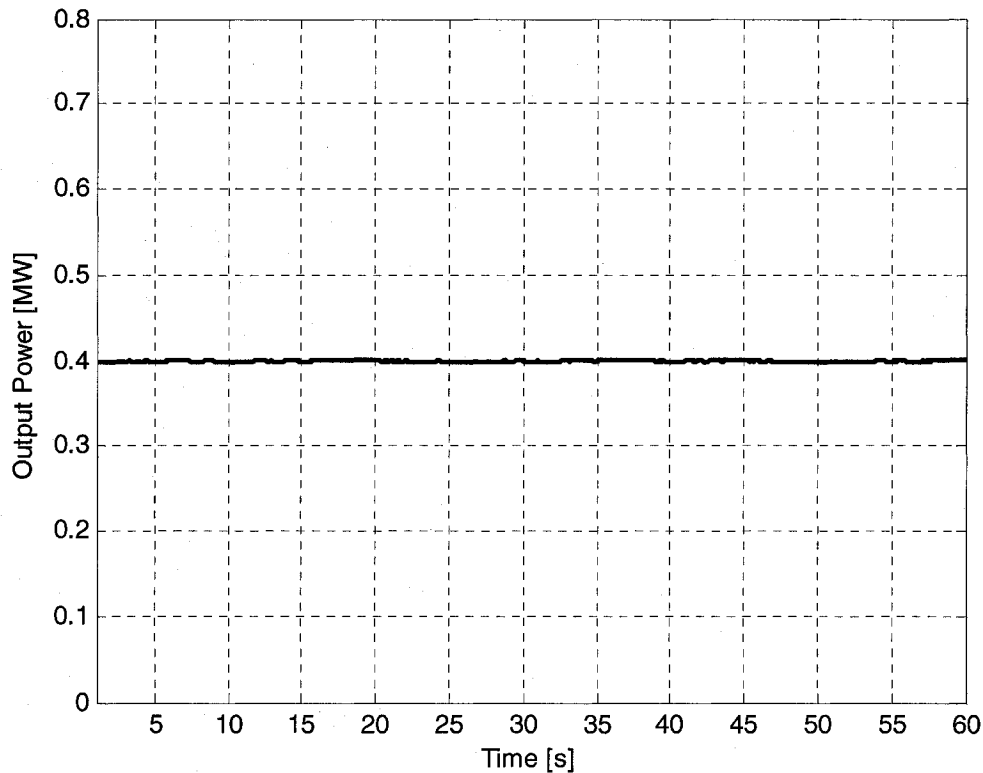


Fig. 5.15: Turbine output power with storage (DFIG average model, 252 kW VRB)

Figure 5.16 shows the SOC variations during this simulation, while figure 5.17 shows the battery output power. The SOC fluctuates around its initial value of 50%.

When a wind storage system is designed, the expected wind variations in a specific location should be analyzed. The wind and battery systems should subsequently be sized accordingly in order to ensure that the battery will not be under-charged or overcharged over a long-term period.

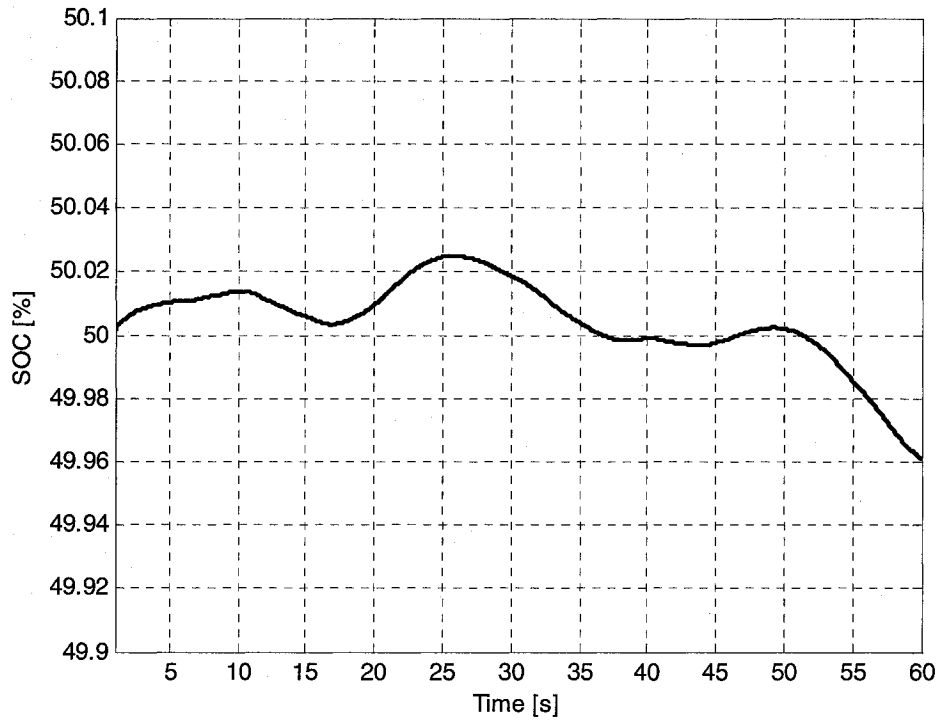


Fig. 5.16: Battery SOC (DFIG average model, 252 kW VRB)

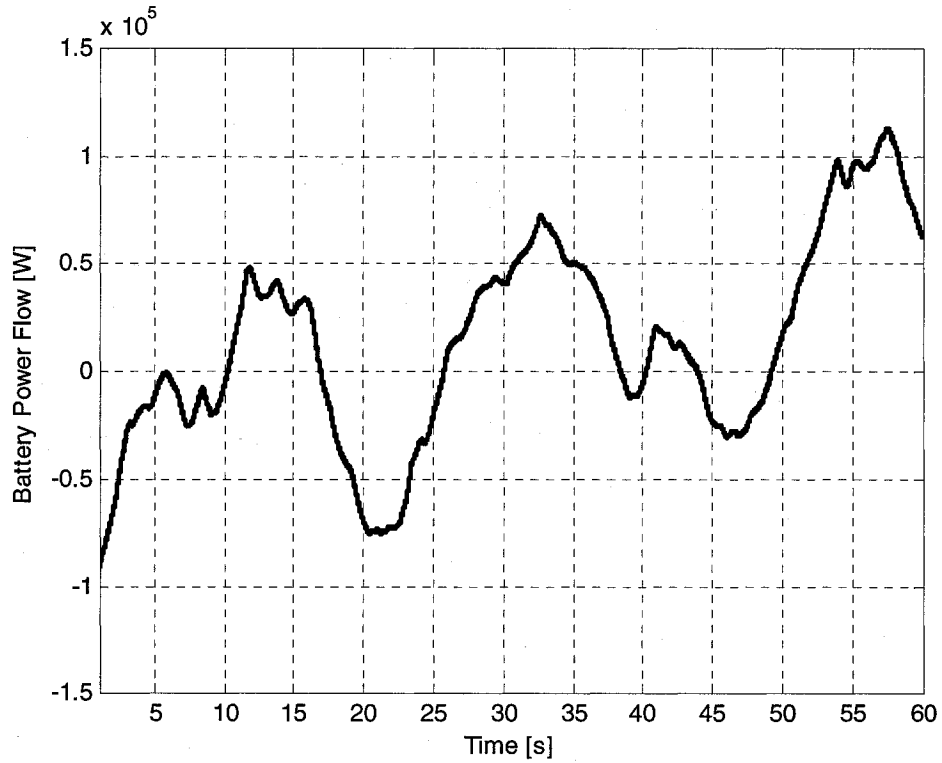


Fig. 5.17: Storage system power response (DFIG average model, 252 kW VRB)

The average DFIG wind storage model developed here is well suited for medium term simulations, and can be used in order to validate complex control schemes under various operating conditions.

In the next section, a real-time simulation of a similar system is considered, which mixes simulated and experimental circuit components.

5.5 DFIG Simple Model for Real-Time Simulation

5.5.1 Centralized storage

A centralized storage scheme consists of directly connecting the storage system to the grid bus, by using a dedicated ac-dc rectifier. In this case, the same storage system can then be used for several wind turbines. This design is not limited to DFIG systems.

Again, the objective here is to make P_{Grid} constant by controlling the power flowing in and out of the storage device. This setup will be implemented in a real-time simulation setup using a simplified DFIG model.

5.5.2 Real-Time System Implementation

Real-Time simulators can be used in various ways in order to help develop and validate battery models, as well as obtain experimental results. Various RT platforms exist, however the OPAL-RT simulator will be used, as it offers the best tradeoff between complexity, accuracy and accessibility for this project.

Through Opal-RT's I/O modules, the system will include a mix of real elements and simulated elements. The system will interface a simulated battery model, wind system and controller with real converters.

5.5.3 Experimental Setup

Figure 5.18 below shows the real-time experimental setup implemented. The Opal-RT I/O capabilities enable communication between the software and hardware. The

real parts of the circuit include a one-phase voltage source representing the grid, as well as an ac-dc converter, a dc-dc chopper and a controllable dc voltage source.

The role of the controllable dc voltage source is to act as the VRB in the real world. The voltage is dependent on the State of Charge and current, and is obtained from the VRB model which is loaded in the Opal-RT simulator. The same approach could be taken to represent various batteries in this way, simply by changing the model used.

Both converters are bidirectional. The dc-dc converter acts to set the current, based on the requirements to charge or discharge the battery. By loading the wind system circuit in the Opal-RT simulator, the response of the storage system can be simulated within a wind system. But first, the controls of the storage system need to be validated.

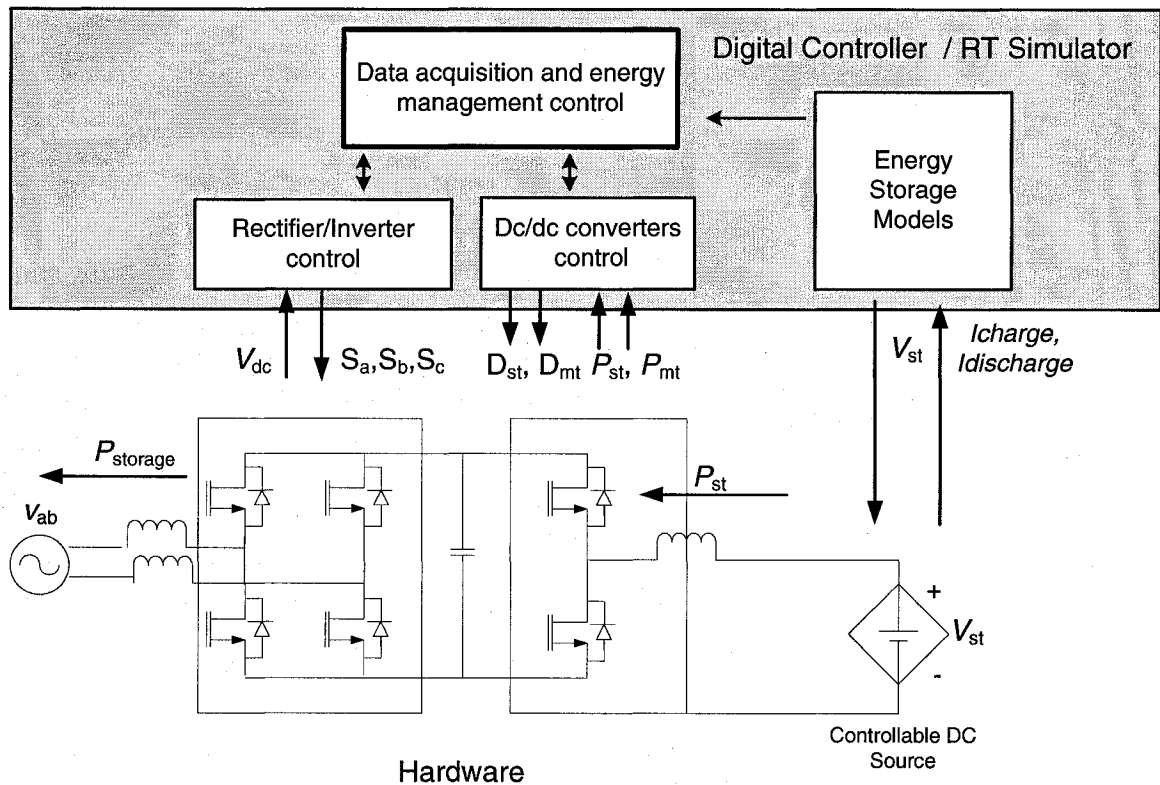


Fig. 5.18: RTS experimental setup

The real circuit elements used will be operated in the 150 W range. However, the simulated part of the circuit can be scaled up as needed, to represent the operation of wind turbines in the MW range.

5.5.4 Configuration and Validation of Control Systems

A simple PI control scheme is used, which sets the current based on a power reference. Figures 5.19 and 5.20 show how the battery dc power follows the reference closely.

5.5.5 Experimental Results

In this case study, the same wind profile from section 5.4 is used. The wind data is loaded into a 1MW DFIG wind turbine simple model. Since this power fluctuates with the wind, the purpose of the storage system is to smooth out the wind fluctuations. Figure 5.21 below shows the output of the wind turbine, without the storage device, and figure 5.22 shows the effect of the VRB system on the total output.

The power delivered to the grid is centered on 0.55MW. This is the scaled up simulated power, while the actual power delivered in the circuit is in the 150 W range. Figure 5.23 shows the power flow in and out of the battery model, and figure 5.24 shows the VRB State of Charge fluctuations.

Figures 5.25 and 5.26 show the dc voltages and the dc current; the controlled dc voltage source V_{dc} follows closely the battery model reference V_{bat} . The dc bus voltage is set at 300V. The dc current fluctuations correspond to the charge-discharge behaviour of the storage device, as it tries to maintain the total output power of the wind system at a constant value.

The developed RT system is well suited for battery model testing. In this case, it was used to demonstrate the role of a VRB in a wind energy system. The design and validation steps followed here can be repeated for various battery models as they become available, in order to assess their performance.

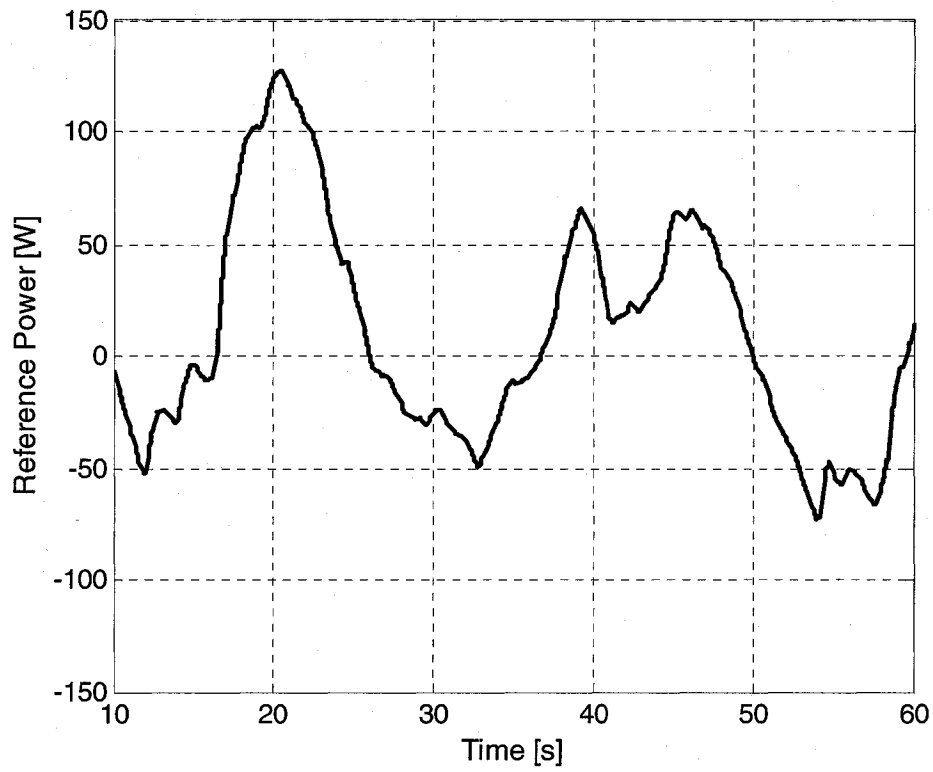


Fig. 5.19: Storage system power reference (Centralized storage, RTS)

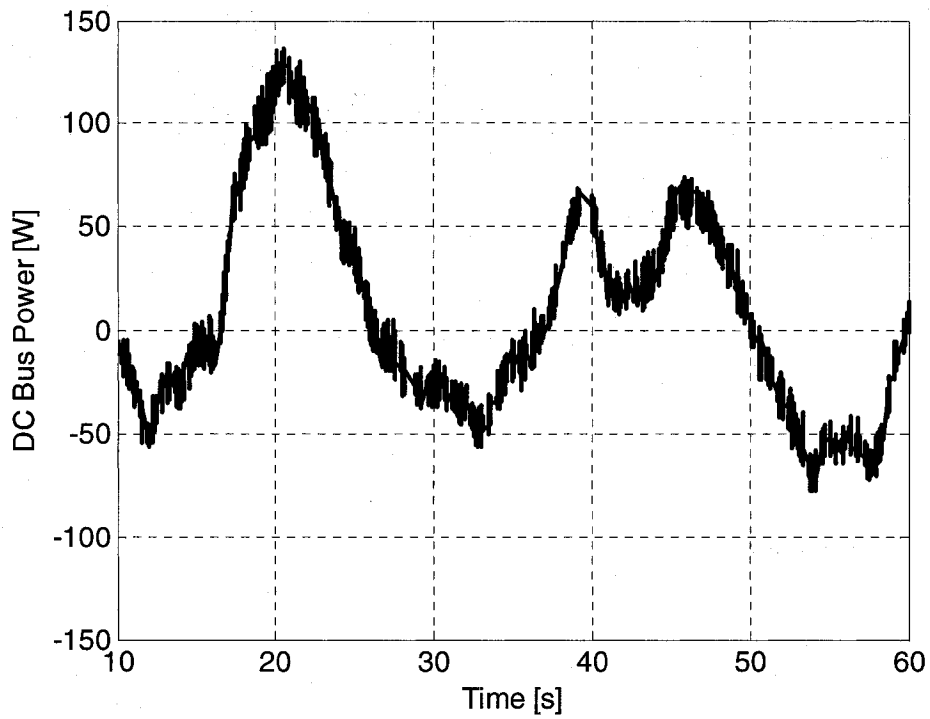


Fig. 5.20: Storage system response experimental results (Centralized storage, RTS)

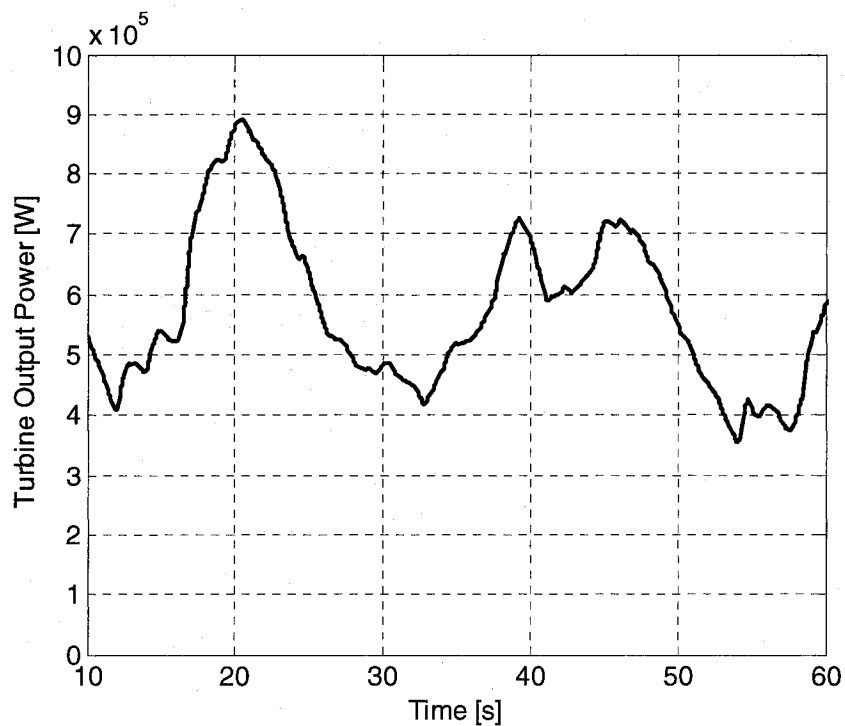


Fig. 5.21: Turbine output power without storage (Centralized storage, RTS)

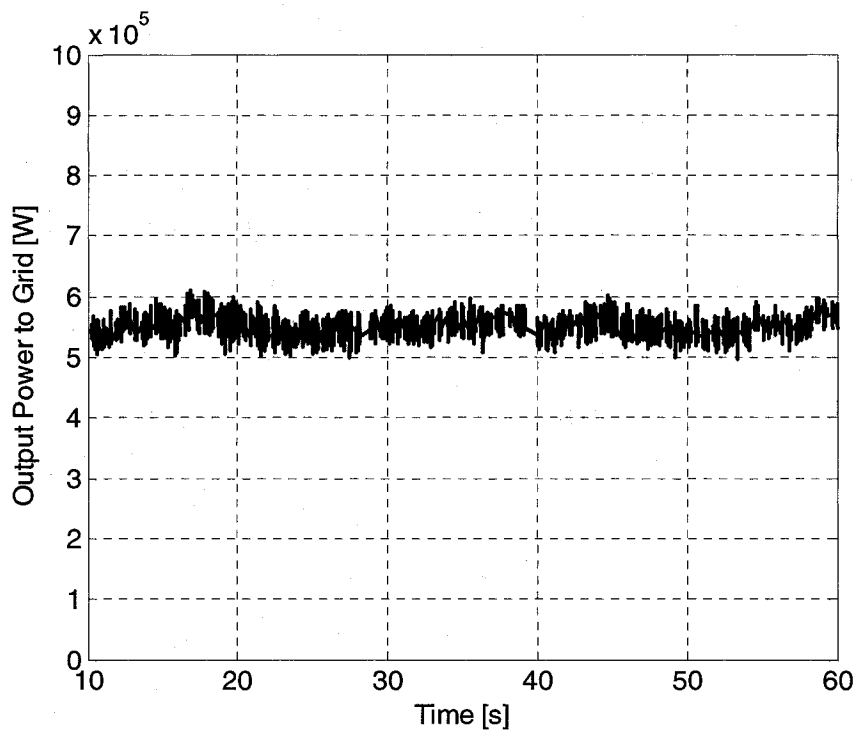


Fig. 5.22: Turbine output power with storage experimental results (Centralized storage, RTS)

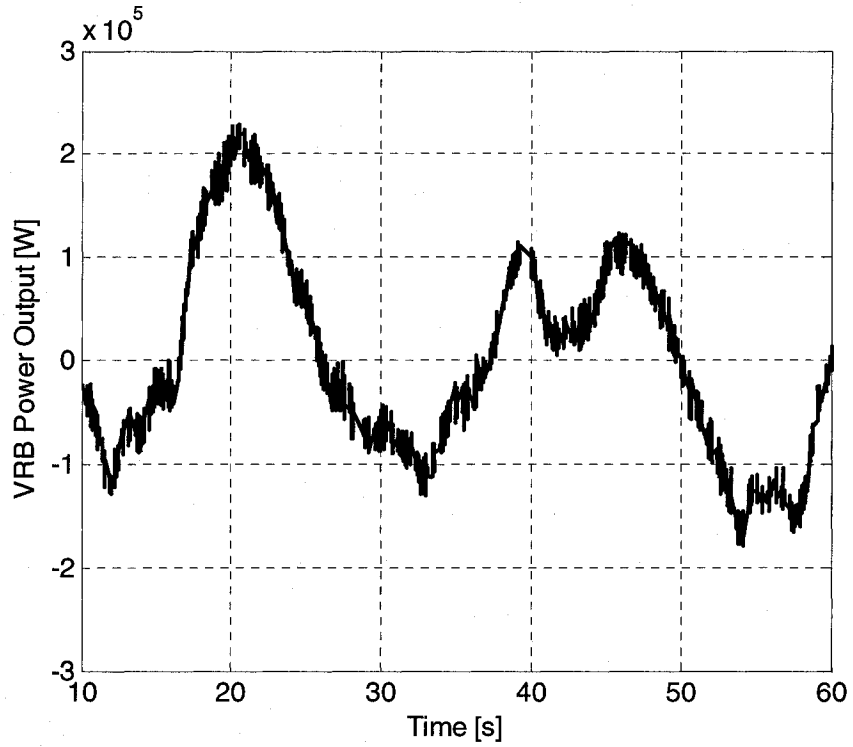


Fig. 5.23: Storage system power flow experimental results (Centralized storage, RTS)

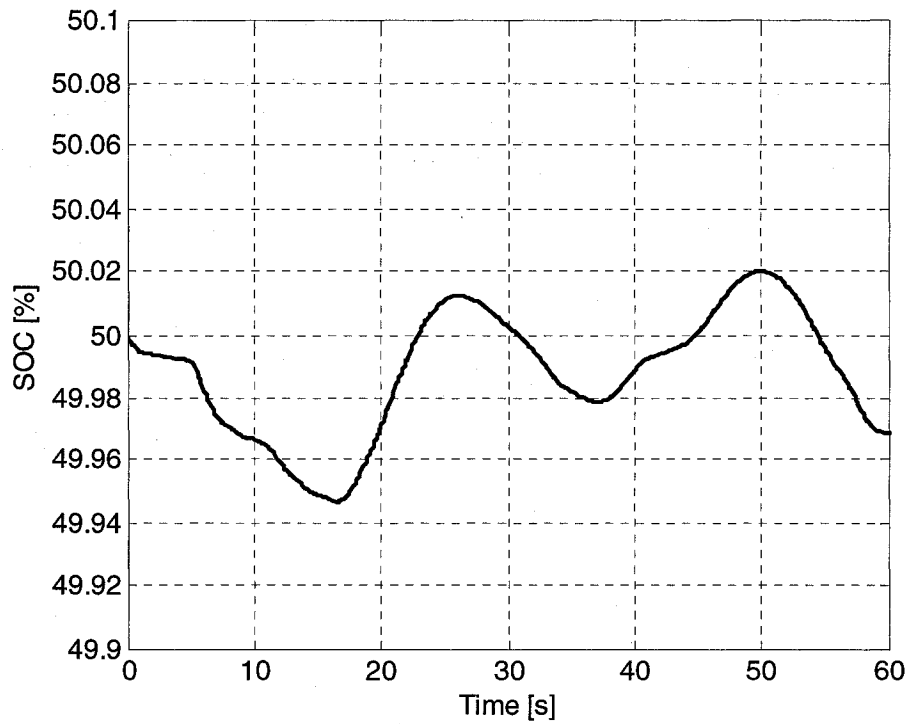


Fig. 5.24: Battery SOC (Centralized storage, RTS)

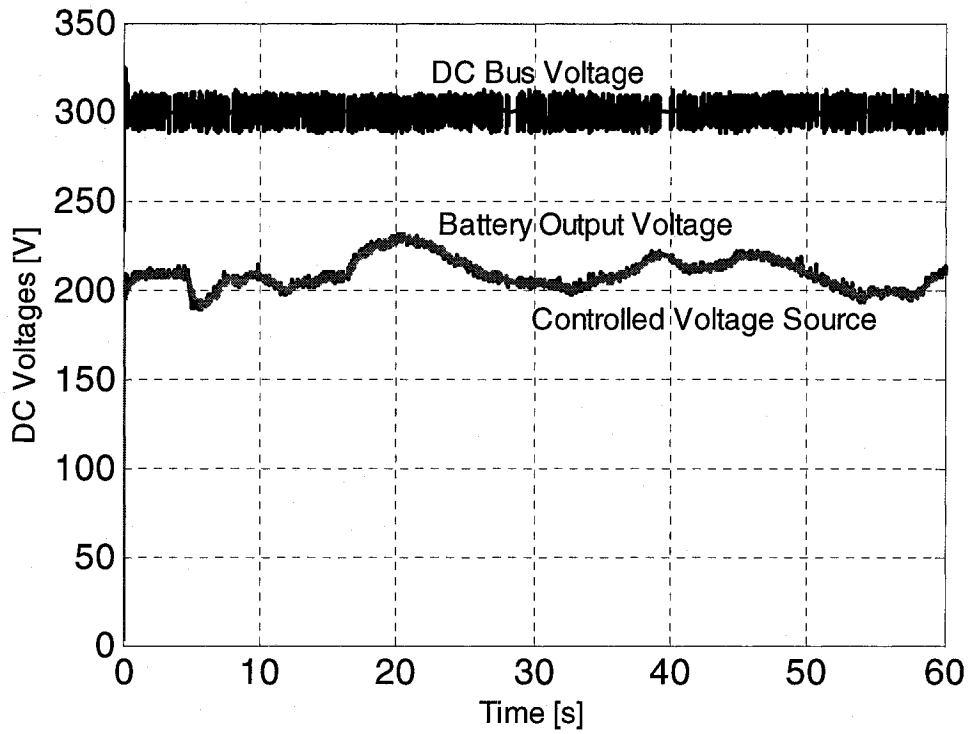


Fig. 5.25: Dc voltages experimental results (Centralized storage, RTS)

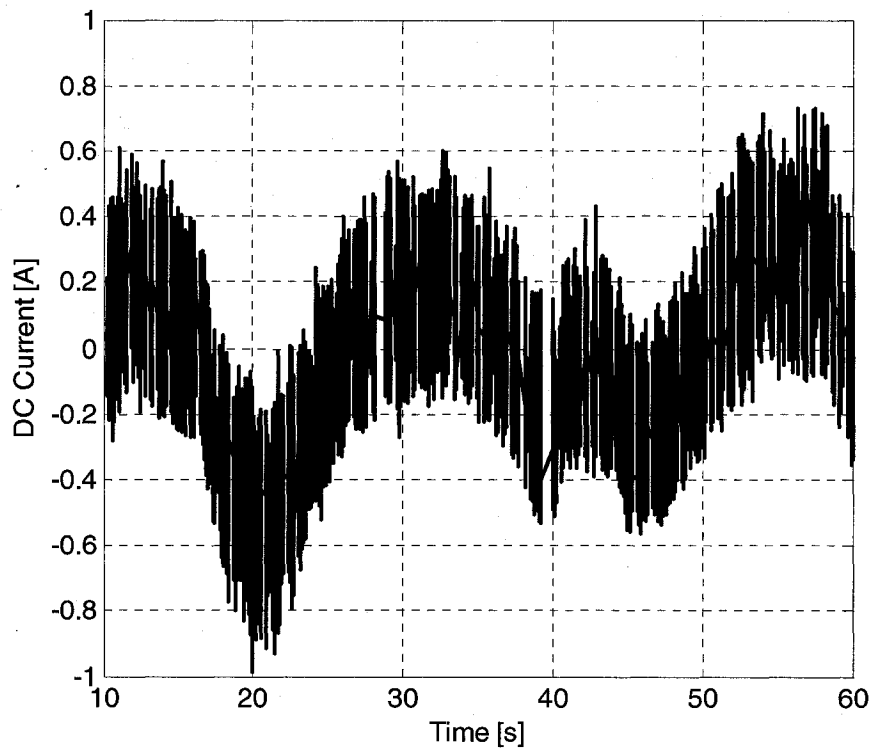


Fig. 5.26: Dc bus current experimental results (Centralized storage, RTS)

5.6 DFIG System Performance with VRB storage

5.6.1 Battery Energy Management

When a VRB is integrated in a power system, the controls must ensure that the battery is not undercharged or overcharged, and remains between 20% and 80% SOC at all times. However, additional factors have an impact on the battery energy management.

The power output reference of the wind system must be set appropriately so as to ensure the SOC net power flow is zero over a long period of time, as the VRB storage acts to smooth out the output. This was done in section 5.5 which resulted in acceptable SOC fluctuations, as shown in figures 5.16 and 5.24.

Additionally, the battery must be sized properly in order to guarantee energy availability for emergency situations. This requires the study of wind conditions on a specific wind site, in order to obtain accurate forecasts. The stored energy can then be managed accordingly.

The model implemented in the DFIG systems can be used to validate the sizing of a wind turbine as well as the control strategies used, over a desired period of time. The VRB system has proven to be well suited for this type of application, since the battery energy capacity parameter can be easily sized, independently of other design parameters.

5.6.2 System Overall Efficiency

The system overall efficiency is dependent on the VRB efficiency (sections 3.5.2, 3.6.2), as well as the converter efficiencies (section 4.4.4). The VRB system efficiency was determined to be a function of operating current, as well as of the SOC.

Converter losses are typically of 4%. The battery dc round-trip efficiency, including the dc-dc converter losses was found to be 68%. Additional converter losses will bring the VRB storage system ac roundtrip efficiency down to 62.5%.

This efficiency compares well with other storage system, and makes the VRB well suited for wind applications. However, the efficiency can drop considerably if the

control systems do not ensure optimized operation, which emphasizes the need for complex control algorithms.

5.6.3 Impact on Grid

In sections 5.2, 5.3 and 5.4, the storage system ability to smooth the power output of a wind turbine was demonstrated, using various DFIG system models, and on various scales. This resulted in reduced power fluctuations, which justify the use of VRB storage for DFIG systems, especially in weaker grids.

In remote hybrid diesel systems in particular, the storage system can be used to allow shutting down diesel generators when they are running at low capacity, and thus very low efficiency. If the wind suddenly drops, the VRB storage can then provide the required power in order to allow the diesel system start-up, without power interruption to the local grid, as was shown in section 5.3.3.

Battery storage is well suited for this type of application due to its quick response as was shown in sections 5.3.2 and 5.4.2. The VRB in particular is unique in the fact that it offers both a large energy capacity as well as a quick response.

5.7 Conclusions

In this chapter, the developed VRB model was used to demonstrate the integration of VRB storage in DFIG systems, considering both local and centralized storage schemes. This was done using three different DFIG models, each suited for a different time frame. The storage system controls were presented and validated, and the ability of the storage to smooth the output power of a turbine was demonstrated.

The VRB technology was shown to be an ideal choice for wind energy storage applications, due to its large energy capacity and quick response, which allow it to be used in both power smoothing (short-term) and load-levelling (long-term) applications. The overall storage ac round-trip efficiency was found to be 61.5% including converter losses, which is acceptable. However there is room for improvement. Efficiency was

Chapter 5: Wind Energy Storage System Implementation

found to drop considerably under certain operating conditions, which emphasizes the need for optimized control strategies.

The developed models can provide us insight on how to best operate the battery. Based on the obtained results, recommendations for the design and operation of a VRB will be presented in the next section.

Chapter 6

Conclusions and Future Work

6.1 Summary

6.1.1 Battery Models

The thesis focussed on the development of accurate and properly validated generic models, for VRB and Li-Ion technology. The models took into account the various battery physical and mathematical properties.

Various steps towards the validation of the models were discussed. A standard charge-discharge profile for experimental battery testing, based on typical wind profiles, was also presented.

The models allowed battery performance testing under various operating conditions to determine:

- The VI transfer characteristic which provided the batteries operating ranges.
- The efficiency which was used to determine the best operating conditions.
- The transient response which enabled a better design of controller dynamics.

They were also used in:

- The design and validation of the storage size required.
- The design and validation of the PI control scheme used for power smoothing.
- The comparison of various integration schemes (centralized vs. local storage).

6.1.2 Integration into Wind Systems

The design steps for the sizing, control and integration of a VRB system in various DFIG systems were presented. The key elements that needed to be considered for

Chapter 6: Conclusions and Future Work

VRB sizing were identified, including the power rating and energy rating design. The VRB model scalability was also considered. The scaled model provided the necessary insight to test overall system designs.

The integration of the model in offline and real-time simulations of various complexities allowed the testing and validation of the wind energy system design. Various SIMULINK storage systems were developed including:

- Integration of battery on DFIG dc Bus, using DFIG detailed model obtained from SimPowerSystems Library.
- Integration of battery on DFIG dc bus, using DFIG Average model obtained from SimPowerSystems Library.
- Centralized storage scheme using battery model with a simplified DFIG model.

6.2 Conclusions

6.2.1 Modelling

The battery performance results matched the results obtained from alternative sources, with a difference of less than 5%. The different system models are easily modifiable and can be used as a basis for further studies related to VRB and Li-Ion batteries, as well as other battery models, with the following conclusions:

- The detailed model is best suited for short-term simulations.
- The average model is best suited for medium-term simulations.
- The simple model is best suited for long-term simulations as well as real-Time simulations.

The storage system power smoothing capacity in short-term (seconds) and medium term applications (minutes) was also demonstrated using the models.

6.2.2 Operating Considerations

Models such as the ones implemented and studied in this report provide us with insight on how to operate batteries in an optimal way. Based on the results obtained in the thesis, the following recommendations should be taken into account for operating battery systems in wind energy applications:

- The battery should be operated at near-rated power whenever possible. The control algorithm should take into account the efficiency data.
- For Vanadium-Redox batteries, the most efficient region of operation is between 0.7 and 1 p.u. charge or discharge power, at a State of Charge of 40% to 80%.
- A VRB should be operated between a SOC of 20% and 80%, where the voltage is linear. This avoids overcharge and undercharge issues. The battery energy capacity should thus be sized appropriately during the design.
- A Li-Ion battery should be operated at rated power or lower. Higher currents result in reduced efficiency. It should also be operated at SOC between 20% and 80%.

6.2.3 Design Considerations

The thesis demonstrated that batteries are suitable for wind energy storage in comparison to other storage technologies for the following reasons:

- High efficiency when operated properly compared to other technologies (Round trip dc efficiencies before converter losses: VRB: 73%, Li-Ion: 92%).
- Fast response for power smoothing and load levelling applications (Worse case response time: VRB: 52 ms, Li-Ion: 19 ms).
- Flexibility in terms of operating conditions: can be operated at a fraction of the rated current, rated current, as well as maximum current (up to 200% the rated current).

Chapter 6: Conclusions and Future Work

The Li-Ion battery showed better technical performance with a quicker response and better efficiency. However the VRB technology appeared to be more effective than Li-Ion for high-power applications for the following reasons:

- Quick response time (52 ms): suitable for power smoothing (short-term) applications (higher frequency wind fluctuations are filtered out by wind turbine).
- Energy capacity dependent on tank size and amount of electrolyte: well suited for load levelling (medium and long-term) applications.
- Power rating dependent on number of cell stacks: well suited for high power applications.
- High scalability: independence of power and energy ratings.

The following recommendations should be taken into account when designing storage systems in wind energy applications:

- The choice between centralized and local storage depends on the system. A localized scheme is justified for single turbines. A centralized scheme on the other hand is advantageous for a wind farm.
- The battery sizing should account for the amount of energy that needs to be displaced, the mean power at which the system should be operated, as well as the power needed in emergency situations.
- A typical wind profile should be used as a standard to testing various battery models, wind storage systems and control algorithms. Through having a standard wind profile which represents the various possible wind conditions, meaningful comparisons of various technologies can be obtained.

6.2.4 A Methodology for the Study of Wind Storage Systems

Throughout this project, the various steps towards the study of battery storage in wind energy applications were discussed. Figure 6.1 summarizes the various steps taken, as a methodology for future studies. The emphasis is put on the development of battery models and their use in these types of studies.

6.3 Future Research

This report has covered the modelling and validation of VRB and Li-Ion batteries for wind energy applications. Some properties, like capacity fading, battery cycling, heating and concentration depletion were not included in the models. These battery characteristics should be taken into account in worse case operation analysis. While they have no major impact on VRB performance, they should be integrated in improved Li-Ion models, as well as other battery models. The battery energy capacity design, which will impact the load leveling properties of the battery, should also be considered with more detail.

Battery models, such as the ones developed in this thesis, allow researchers to test systems in a fast and accurate matter, which reduces the need for on-site testing until the final stages of a design project. They provide the basis for developing smart battery operation management algorithms. These algorithms should maximize battery efficiency as well as battery life. The project economics, wind forecasts as well as application requirements need to also be taken into account.

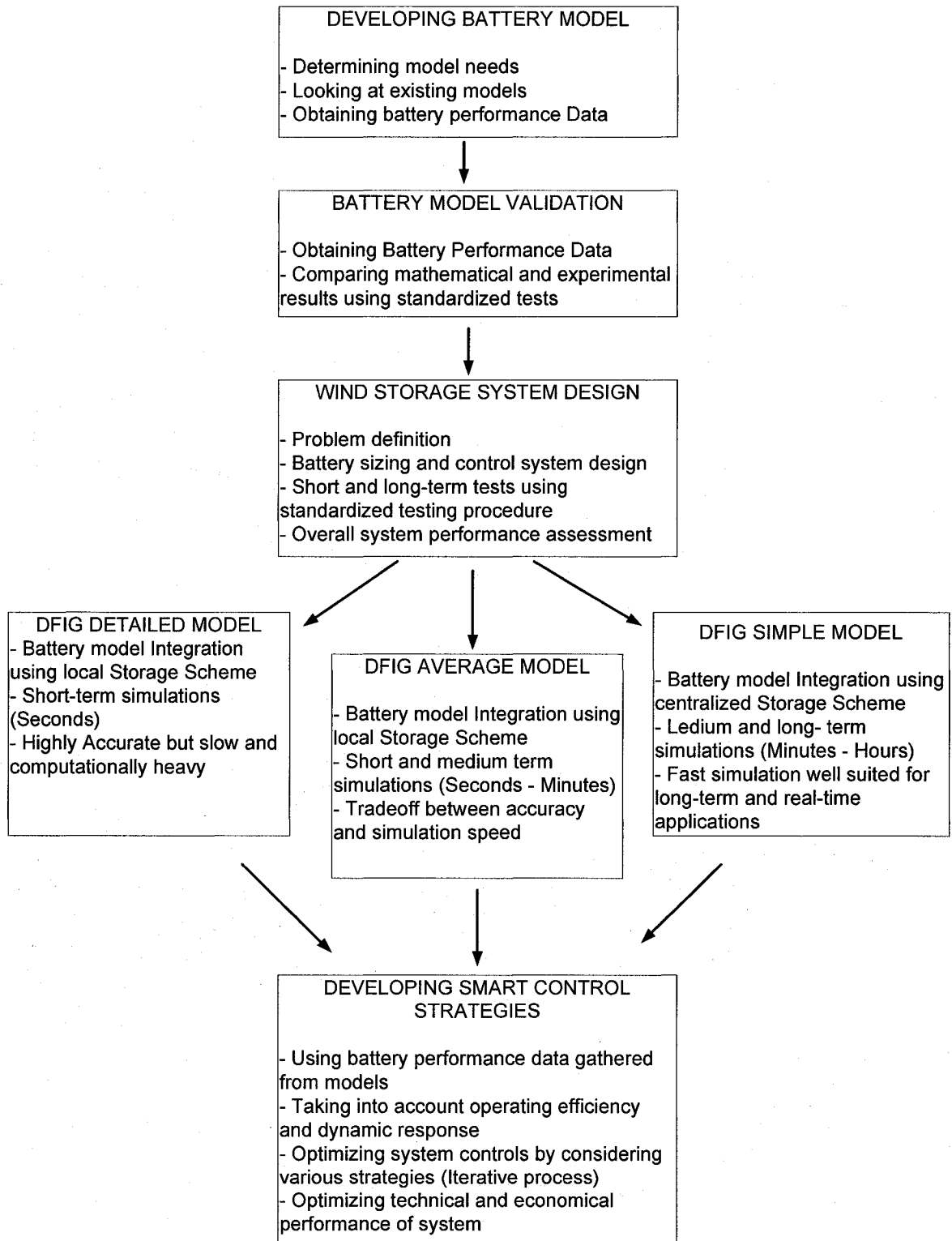


Fig. 6.1: Methodology for the study and design of wind storage systems

References

- [1] J. P. Barton and D. G. Infield, "Energy Storage and its use with intermittent renewable energy", IEEE Transactions on Energy Conversion, Volume: 19, Number: 2, June 2004, Page(s): 441-448.
- [2] M. Korpaas, A. Holen, and R. Hildrum, "Operation and sizing of energy storage for wind power plants in a market system", Journal of Electrical Power Energy Systems, Volume: 25, Page(s): 599-606, 2003.
- [3] J. Paatero and P. Lund, "Effect of energy storage on variations in wind power," Journal of Wind Energy, Volume 8, Page(s): 421-441, 2005.
- [4] L. Leclercq, C. Saudemont, B. Robyns, G. Cimuca, and M. Radulescu, "Flywheel energy storage system to improve the integration of wind generators into a grid", Journal of Electromotion, Volume 10, Number 3-4, 2003.
- [5] C. Abbey and G. Joos, "A Doubly-Fed Induction Machine and Energy Storage System for Wind Power Generation", Canadian Conference on Electrical and Computer Engineering, Volume: 2, Page(s): 1059-1062, May 2004.
- [6] C. Abbey and G. Joos, "Integration of Energy Storage with a Doubly-Fed Induction Machine for Wind Power Applications" Power Electronics Specialists Conference, IEEE 35th Annual, Volume: 3, Page(s): 1964-1968, June 2004.
- [7] E. Muljadi and J. T. Bialasiewicz, "Hybrid Power System with a Controlled Energy Storage", Industrial Electronics Society, The 29th Annual Conference of the IEEE, Volume: 2, Page(s): 1296-1301, November 2003.
- [8] F. Zhou, G. Joos et al. "Use of large Capacity SMES to improve the Power Quality and Stability of Wind Farms", IEEE Power Engineering Society General meeting, Volume: 2, Page(s): 2025-2030, June 2004.
- [9] Brad Roberts and Jim McDowall, "Commercial Successes in Power Storage: Advances in Power Electronics and Battery Application Yield New Opportunities", IEEE Power and Energy Magazine, Volume: 3, Number: 2, March 2005.
- [10] A. Shibata and K. Sato, "Development of a Vanadium Redox Flow Battery for Electricity Storage", IEEE Power Engineering Journal, Volume: 13, Issue: 3, Page(s): 130-135, June 1999.
- [11] G. Koshimizu and Tetsuo Numata, "Applications of Energy Storage for Stabilization of Wind Power in Power Systems", Subaru Project, ESA 2005 Annual Meeting Presentation, May 24, 2005.
- [12] J.M. Hawkins and T.P. Robbins, "A field trial of a Vanadium Energy Storage System", INTELEC 2001 Twenty-Third International Telecommunications Energy Conference, Page(s): 652 - 656, October 2001.

- [13] Chad Abbey and G. Joos., "Short-Term Energy Storage for Wind Energy Applications", Industry Applications Conference, Volume: 3, Page(s): 2035-2042, October 2005.
- [14] A. Joseph and M. Shahidehpour, "Battery Storage Systems in Electric Power Systems", IEEE Power Engineering Society General meeting, Page(s): 8, June 2006.
- [15] H. Takabayashi et al., "Development of valve-regulated lead-acid batteries for Power Storage", The Twenty-Fifth International Telecommunications Energy Conference, Page(s): 383-390, October 2003.
- [16] Z. M. Salameh, M. A. Casacca and W. A. Lynch, "A Mathematical Model for Lead-Acid Batteries", IEEE Transactions on Energy Conversion, Volume: 7, Number: 1, Page(s): 93-98, March 1992.
- [17] M. Gatrell and N. Gupta, "Developing a simple flow battery model - Initial concepts", Electricity Storage Systems Project, National Research Council Canada (NRC) document.
- [18] S Mikaye and N. Tokuda, "Vanadium-Redox Flow Battery for a Variety of Applications", IEEE Power Engineering Society Summer Meeting, Volume: 1, Page(s): 450-451, 2001.
- [19] N. Miyanaga, T. Inoue, et al., "Large-Scale Li-Ion Battery Cells for space use", The Twenty-Fifth International Telecommunications Energy Conference, Page(s): 241-248, October 2003.
- [20] I. Suzuki, T. Shizuki and K. Nishiyama, "High Power Li-Ion Battery for Backup Power Sources", The Twenty-Fifth International Telecommunications Energy Conference, Page(s): 317-322, October 2003.
- [21] Ken Mattern, "Controlling Power Flow of Wind Farms", Engineering Power Quality Products Division of S&C Electric Company, ESA 2005 Annual Meeting Presentation, May 24, 2005.
- [22] R. Rao, S. Vrudhula, D. N. Rakhmatov, "Battery Modeling for Energy-Aware System Design", IEEE Computer Magazine, Volume: 3, Page(s): 77-87, December 2003.
- [23] Marc Doyle, John Newman et al., "Comparison of Modeling Predictions with Experimental Data from Plastic Lithium Ion Cells" Journal of Electrochemical Society, Volume: 143, Issue 6, Page(s): 1890-1903, June 1996.
- [24] S. Gold, "A PSPICE Macromodel for Lithium-Ion Batteries", Twelfth Annual Battery Conference on Applications and Advances, Page(s): 215-222, January 1997.
- [25] S. Buller, M. Thele et al. "Impedance-Based Simulation Models of Supercapacitors and Li-Ion Batteries for Power Electronic Applications", IEEE Transactions on Industry Applications, Volume: 41, Number: 3, Page(s): 742-747, May 2005.
- [26] M. C. Glass, "Battery Electrochemical Nonlinear/Dynamic Spice Model", Proceedings of the 31st Intersociety Energy Conversion Engineering Conference, Volume: 1, Page(s): 292-297, August 1996.

- [27] L. Gao, S. Liu and R. Dougal, "Dynamic Lithium-Ion Battery Model for System Simulation", IEEE Transactions on Components and Packaging Technologies, Volume: 25, Number: 3, Page(s): 495-505, September 2002.
- [28] A. Shibata, S. Kanji et al., "Development of Vanadium Redox Flow Battery for Photovoltaic Generation System", Conference Record of the Twenty-Fourth IEEE Photovoltaic Specialists Conference, Volume: 1, Page(s): 950-953, December 1994.
- [29] M. -H. Li, T. Funaki and T. Hikiyama, "A Study of Output Terminal Voltage Modeling for Redox Flow Battery Based on Charge and Discharge Experiments", The Fourth Power Conversion Conference, April 2007.
- [30] N. Miyayama, T. Inoue, et al., "Large-Scale Li-Ion Battery Cells for space use", The Twenty-Fifth International Telecommunications Energy Conference, Page(s): 241-248, October 2003.
- [31] I. Suzuki, T. Shizuki and K. Nishiyama, "High Power Li-Ion Battery for Backup Power Sources", The Twenty-Fifth International Telecommunications Energy Conference, Page(s): 317-322, October 2003.